Aus der

Klinik und Poliklinik für Nuklearmedizin

Klinikum der Ludwig-Maximilians-Universität München

Messung von Tau Proteinablagerungen mittels PET bei primären Tauopathien

Dissertation

zum Erwerb des Doktorgrades der Humanbiologie

an der Medizinischen Fakultät der

Ludwig-Maximilians-Universität München

vorgelegt von

Matthias Brendel

aus

Marktoberdorf

Jahr
2024

Mit Genehmigung der Medizinischen Fakultät der

Ludwig-Maximilians-Universität München

Erstes Gutachten:	Prof. Dr. Peter Bartenstein
Zweites Gutachten:	Prof. Dr. Johannes Levin
Drittes Gutachten:	PD Dr. Georg Nübling

Dekan:	Prof. Dr. med. Thomas Gudermann

Tag der mündlichen Prüfung: 25.09.2024

Affidavit

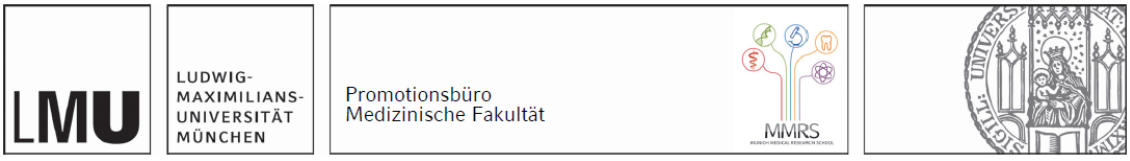

Eidesstattliche Versicherung

Brendel, Matthias

Name, Vorname

Ich erkläre hiermit an Eides statt, dass ich die vorliegende Dissertation mit dem Titel:

Messung von Tau Proteinablagerungen mittels PET bei primären Tauopathien

selbständig verfasst, mich außer der angegebenen keiner weiteren Hilfsmittel bedient und alle Erkenntnisse, die aus dem Schrifttum ganz oder annähernd übernommen sind, als solche kenntlich gemacht und nach ihrer Herkunft unter Bezeichnung der Fundstelle einzeln nachgewiesen habe.

Ich erkläre des Weiteren, dass die hier vorgelegte Dissertation nicht in gleicher oder in ähnlicher Form bei einer anderen Stelle zur Erlangung eines akademischen Grades eingereicht wurde.

München, 25.09.2024, Matthias Brendel

Ort, Datum
Doktorand

Matthias Brendel

Unterschrift Doktorandin bzw.

Inhaltsverzeichnis

Publikationsliste

Verzeichnis der Originalarbeiten (chronologisch)

1. Rominger, A.*; **Brendel, M.***; Burgold, S.; Keppler, K.; Baumann, K.; Xiong, G.; Mille, E.; Gildehaus, F.J.; Carlsen, J.; Schlichtiger, J.; Niedermoser, S.; Wangler, B.; Cumming, P.; Steiner, H.; Herms, J.; Haass, C.; Bartenstein, P. Longitudinal Assessment of Cerebral beta-Amyloid Deposition in Mice Overexpressing Swedish Mutant beta-Amyloid Precursor Protein Using 18F-Florbetaben PET. J Nucl Med. 2013, 54(7):1127-34. doi: 10.2967/jnumed.112.114660. (IF: 5.563)

2. **Brendel, M.**; Delker, A.; Rötzer, C.; Böning, G.; Carlsen, J.; Cyran, C.; Mille, E.; Gildehaus, FJ.; Cumming, P.; Baumann, K.; Steiner, H.; Haass, C.; Herms, J.; Bartenstein, P.; Rominger, A. Impact of Partial Volume Effect Correction on Cerebral ß-Amyloid Imaging in APP-Swe Mice using [18F]-Florbetaben PET. Neuroimage. 2014, 84:843-53. doi: 10.1016/j.neuroimage.2013.09.017. (IF: 6.357)

3. Ewers, M.; **Brendel, M.**; Rizk-Jackson, A.; Rominger, A.; Bartenstein, P.; Schuff, N.; Weiner, M.W. Reduced FDG-PET brain metabolism and executive function predict clinical progression in elderly healthy subjects. Neuroimage Clin. 2013, 4:45-52. doi: 10.1016/j.nicl.2013.10.018. (IF: 2.526)

4. **Brendel, M.**; Högenauer, M.; Delker, A.; Sauerbeck, J.; Bartenstein, P.; Seibyl, J.; Rominger, A. Improved Longitudinal [18F]-AV45 Amyloid PET by White Matter Reference and VOI-based Partial Volume Effect Correction. Neuroimage. 2015, 108:450-9. doi: 10.1016/j.neuroimage.2014.11.055. (IF: 5.463)

5. **Brendel, M.**; Reinisch, V.; Kalinowski, E.; Levin, J.; Delker, A.; Därr, S.; Pogarell, O.; Förster, S.; Bartenstein, P.; Rominger, A. Hypometabolism in Brain of Cognitively Normal Patients with Depressive Symptoms is Accompanied by Atrophy-Related Partial Volume Effects. Current Alzheimer Research. 2016, 13(5):475-86. (IF: 3.145)

6. **Brendel, M.**; Pogarell, O.; Xiong, G.; Delker, A.; Bartenstein, P.; Rominger, A. Depressive Symptoms Accelerate Cognitive Decline in Amyloid-Positive MCI Patients. Eur J Nucl Med Mol Imaging. 2015, 42(5):716-24. doi: 10.1007/s00259-014-2975-4. (IF: 5.537)

7. **Brendel, M.**; Jaworska, A.; Grießinger, E.; Rötzer, C.; Burgold, S.; Gildehaus, FJ.; Carlsen, J.; Cumming, P.; Baumann, K.; Haass, C.; Steiner, H.; Bartenstein, P.; Herms, J.; Rominger, A. Cross-sectional Comparison of Small Animal [18F]-Florbetaben Amyloid-PET Between Transgenic AD Mouse Models. Plos One. 2015, 10(2):e0116678. doi: 10.1371/journal.pone.0116678. (IF: 3.057)

8. Rominger, A.; Cumming, P.; **Brendel, M.**; Xiong, G.; Tatsch, K.; Bartenstein, P.; la Fougère, C.; Koch, W.; Pogarell, O. Altered serotonin and dopamine transporter availabilities in brain of depressed patients upon treatment with escitalopram: a [123I]β-CIT SPECT study. European Neuropsychopharmacology. 2015, 25(6):873-81. doi: 10.1016/j.euroneuro.2014.12.010. (IF: 4.409)

9. Högenauer, M.*; **Brendel, M.***; Delker, A.; Weiss, M.; Bartenstein, P.; Rominger, A. Impact of MRI-based Segmentation Artifacts on Amyloid- and FDG-PET Quantitation. Current Alzheimer Research. 2016, 13(5):597-607. (IF: 3.145)

10. **Brendel, M.***; Jaworska, A.*; Herms, J.*; Trambauer, J.*; Rotzer, C.; Gildehaus, F. J.; Carlsen, J.; Cumming, P.; Bylund, J.; Luebbers, T.; Bartenstein, P.; Steiner, H.; Haass, C.; Baumann, K.; Rominger, A. Amyloid-PET predicts inhibition of de novo plaque formation upon chronic gamma-secretase modulator treatment. Molecular Psychiatry. 2015, 20(10):1179-87. doi: 10.1038/mp.2015.74. (IF: 13.314)

11. Caballero, M.; **Brendel, M.**; Delker, A.; Ren, J.; Rominger, A.; Bartenstein, P.; Dichgans, M.; Weiner, M.; Ewers, M. Mapping three-year changes in gray matter and metabolism in Aß-positive nondemented subjects. Neurobiology of Aging. 2015, 36(11):2913-24. doi: 10.1016/j.neurobiolaging.2015.08.007. (IF: 5.153)

12. Albert, N.; Winkelmann, I.; Suchorska, B.; Wenter, V.; Schmid-Tannwald, C.; Mille, E.; Todica, A.; **Brendel, M.**; Tonn, JC.; Bartenstein, P. Early static 18F-FET-PET scans have a higher accuracy for glioma grading than the standard 20-40 minutes scans. Eur J Nucl Med Mol Imaging. 2016, 43(6):1105-14. doi: 10.1007/s00259-015-3276-2. (IF: 5.537)

13. **Brendel, M.***; Jaworska, A.*; Probst, F.; Overhoff, F.; Korzhova V.; Lindner, S.; Carlsen, J.; Bartenstein, P.; Harada R.; Kudo, Y.; Haass C.; Van Leuven F.; Okamura N.; Herms J.; Rominger A. MicroPET Imaging of Tau Pathology with 18F-THK5117 in two Transgenic Mouse Models. JNM. 2016, 57(5):792-8. doi: 10.2967/jnumed.115.163493. (IF: 6.646)

14. Suárez-Calvet, M.; Kleinberger, G.; Caballero, M.A.; **Brendel, M.**; Rominger, A.; Alcolea, D.; Fortea, J.; Lleó, A.; Blesa, R.; Gispert, J.D.; Sánchez-Valle, R.; Antonell, A.; Rami, L.; Molinuevo, J.L.; Brosseron, F.; Traschütz, A.; Heneka, M.T.; Struyfs, H.; Engelborghs, S.; Sleegers, K.; Van Broeckhoven, C.; Zetterberg, H.; Nellgård, B.; Blennow, K.; Crispin, A.; Ewers, M.*; Haass, C.* CSF sTREM2 is increased in early symptomatic stages of Alzheimer's disease and associates with neuronal injury markers. EMBO Mol. Med. 2016, 8(5):466-76. doi: 10.15252/emmm.201506123. (IF: 9.249)

15. Overhoff, F.*; **Brendel, M.***; Jaworska, A.; Korzhova, V.; Delker, A.; Probst, F.; Focke, C.; Gildehaus, F-J.; Carlsen, J.; Baumann, K.; Haass C.; Bartenstein, P.; Herms, J.; Rominger, A. Automated spatial brain normalization and hindbrain white matter reference tissue give improved [18F]-florbetaben PET quantitation in Alzheimer´s model mice. Frontiers in Neuroscience. 2016, 10:45. doi: 10.3389/fnins.2016.00045. (IF: 3.566)

16. **Brendel, M.***; Probst, F.*; Jaworska, A.; Overhoff, F.; Korzhova, V.; Albert, N.L.; Beck, R.; Lindner, S.; Gildehaus, F.J.; Baumann, K.; Bartenstein, P.; Kleinberger, G.; Haass, C.; Herms, J.; Rominger, A. Glial Activation and Glucose Metabolism in a Transgenic Amyloid Mouse Model: A Triple Tracer PET Study. J Nucl Medicine. 2016, 57(6):954-60. doi: 10.2967/jnumed.115.167858. (IF: 6.646)

17. Holzgreve, A.*; **Brendel, M.***; Gu, S.; Carlsen, J.; Mille, E.; Böning, G.; Mastrella, G.; Unterrainer, M.; Gildehaus, F.J; Rominger, A; Bartenstein, P.; Kälin, R.E.; Glass, R.; Albert, N.L. Monitoring of Tumor Growth with [18F]-FET PET in a Mouse Model of Glioblastoma: SUV Measurements and Volumetric Approaches. Frontiers in Neuroscience. 2016, 10:260. doi: 10.3389/fnins.2016.00260. (IF: 3.566)

18. Wollenweber, F.A.; Därr, S.; Müller, C.; Duering, M.; Buerger, K.; Zietemann, V.; Malik, R.; **Brendel, M.**; Ertl-Wagner, B.; Bartenstein, P.; Rominger, A.; Dichgans, M. Prevalence of Amyloid Pathology in Post-Stroke Mild Cognitive Impairment. Stroke. 2016, 47(10):2645-8. doi: 10.1161/STROKEAHA.116.013778. (IF: 6.032)

19. Mille, E.; Levin, J.; **Brendel, M.**; Zach, C.; Barthel, H.; Sabri, O.; Bartenstein, P.; Bötzel, K.; Danek, A.; Rominger, A. Cerebral Glucose Metabolism and Dopaminergic Function in Patients with Corticobasal Syndrome. J Neuroimaging. 2017, 27(2):255-261. doi: 10.1111/jon.12391. (IF: 1.953)

20. Guo, T.*; **Brendel, M.***; Grimmer, T.; Rominger, A.; Yakushev, I. Predicting regional pattern of longitudinal beta-amyloid accumulation by baseline positron emission tomography. J Nucl Medicine. 2017, 58(4):639-645. doi: 10.2967/jnumed.116.176115. (IF: 7.439)

21. Schönecker, S.; Prix, C.; Raiser, T.; Ackl, N.; Wlasich, E.; Stenglein-Krapf, G.; Mille, E.; **Brendel, M.**; Bartenstein, P.; Patt, M.; Sabri, O.; Levin, L.; Rominger, A.; Danek, A. Amyloid positron-emission-tomography with [18F]Florbetaben in the diagnostic workup of dementia patients. Der Nervenarzt. 2017, 88(2):156-161. doi: 10.1007/s00115-016-0249-z. (IF: 0.738)

22. Därr, S.; **Brendel, M.**; Zach, C.; Mille, E.; Schilling, D.; Zacherl, M.; Bürger, K.; Danek, A.; Pogarell, O.; Schildan, A.; Patt, M.; Barthel, H.; Sabri, O.; Bartenstein, P.; Rominger, A. Evaluation of Early-Phase [18F]-Florbetaben PET Acquisition in Clinical Routine Cases. Neuroimage Clinical. 2016, 14:77-86. doi: 10.1016/j.nicl.2016.10.005. (IF: 4.348)

23. Romagna, A.; Unterrainer, M.; Schmid-Tannwald, C.; **Brendel, M.**; Tonn, C.J.; Nachbichler, S.B.; Muacevic, A.; Bartenstein, P.; Kreth, F.W.; Albert, N.L. Suspected recurrence of brain metastases after focused high dose radiotherapy: can [18F]FET-PET overcome diagnostic uncertainties? Radiation Oncology. 2016, 11(1):139. doi: 10.1186/s13014-016-0713-8. (IF: 2.568)

24. Wenter, V.; Albert, N.L.; **Brendel, M.**; Fendler, W.P.; Cyran, C.C.; Bartenstein, P.; Friederichs, J.; Müller, J.P.; Militz M.; Hacker, M.; Hungerer, S. [18F]FDG PET accurately differentiates infected and non-infected non-unions after fracture fixation. Eur J Nucl Med Mol Imaging. 2017, 44(3):432-440. doi: 10.1007/s00259-016-3528-9. (IF: 7.704)

25. Kazmierczak, P.M., Todica, A.; Gildehaus, F-J.; Hirner-Eppeneder, H.; **Brendel, M.**; Eschbach, R.S.; Hellmann, M.; Nikolaou, K.; Reiser, M.F.; Wester, H-J.; Kropf, S.; Rominger, A.; Cyran, C.C. 68Ga-TRAP-(RGD)3 hybrid imaging for the in vivo monitoring of αvß3-integrin expression as biomarker of anti-angiogenic therapy effects in experimental breast cancer. Plos One. 2016, 11(12):e0168248. doi: 10.1371/journal.pone.0168248. (IF: 2.806)

26. **Brendel, M.**; Kleinberger, G.; Probst, F.; Jaworska, A.; Overhoff, F.; Blume, T.; Albert, N.L.; Carlsen, J.; Lindner, S.; Gildehaus, F.J.; Ozmen, L.; Suarez-Calvet, M.; Bartenstein, P.; Baumann, K.; Ewers, M.; Herms, J.; Haass, C.; Rominger, A. Increase of TREM2 during ageing of an Alzheimer's disease mouse model is paralleled by microglial activation and amyloidosis. Frontiers in Aging Neuroscience. 2017, 9:8. doi: 10.3389/fnagi.2017.00008. (IF: 3.582)

27. Blautzik, J.; **Brendel, M.**; Sauerbeck, J.; Kotz, S.; Scheiwein, F.; Bartenstein, P.; Seibyl, J.; Rominger, A. Reference region selection and the association between the rate of amyloid accumulation over time and the baseline amyloid burden. EJNMMI. 2017, 44(8):1364-1374. doi: 10.1007/s00259-017-3666-8. (IF: 7.704)

28. Segovia, F.; Gorriz, J.M.; Ramírez, J.; Martínez-Murcia, F.J.; Levin, J.; Schuberth, M.; **Brendel, M.**; Rominger, A.; Boetzel, K.; Garraux, G.; Phillips, C. Multivariate analysis of 18F-DMFP PET data to assist the diagnosis of parkinsonism. Frontiers in Neuroinformatics. 2017, 11:23. doi: 10.3389/fninf.2017.00023. (IF: 3.074)

29. Scheiwein, F.T.; Ishii, K.; Hosokawa, C.; Kaida, H.; Hyodo, T.; Hanaoka, K.; **Brendel, M.**; Bartenstein, P.; Rominger, A.; Murakami, T. Regional differences in amyloid deposition between 11C-PiB PET positive patients with and without elevated striatal amyloid uptake. Alzheimer's Disease & Parkinsonism. 2017, 7(317):2161-0460. doi: 10.4172/2161-0460.1000317. (IF: 3.030)

30. Russmann, V.; **Brendel, M.**; Mille, E.; Helm-Vicidomini, A.; Beck, R.; Günther, L.; Lindner, S.; Rominger, A.; Keck, M.; Salvamoser, J.D.; Albert, N.L.; Bartenstein, P.; Potschka, H. Identification of brain regions predicting epileptogenesis by serial [18F]GE-180 positron emission tomography imaging of neuroinflammation in a rat model of temporal lobe epilepsy. Neuroimage Clinical. 2017, 15:35-44. doi: 10.1016/j.nicl.2017.04.003. (IF: 3.869)

31. Blautzik, J.; Kotz, S.; **Brendel, M.**; Sauerbeck, J.; Vettermann, F.; Winter, Y.; Bartenstein, P.; Ishii, K.; Rominger, A. Relationship between body-mass index, ApoE4 status, and PET-based amyloid and neurodegeneration markers in amyloid-positive subjects with normal cognition or MCI. Journal of Alzheimer's Disease. 2018, 65(3):781-791. doi: 10.3233/JAD-170064. (IF: 3.476)

32. Kleinberger, G.; **Brendel, M.**; Mracsko, E.; Wefers, B.; Groeneweg, L.; Xiang, X.; Focke, C.; Deußing, M.; Suárez-Calvet, M.; Mazaheri, F.; Parhizkar. S; Pettkus, N.; Wurst, W.; Feederle, R.; Bartenstein, P.; Mueggler, T.; Arzberger, T.; Knuesel, I.; Rominger, A.; Haass, C. The FTD-like syndrome causing TREM2 T66M mutation impairs microglia function, brain perfusion and glucose metabolism. The EMBO Journal. 2017, 36(13):1837-1853. doi: 10.15252/embj.201796516. (IF: 10.557)

33. Unterrainer, M.; Vettermann, F.; **Brendel, M.**; Holzgreve, A.; Lifschitz, M.; Zähringer, M.; Suchorska, B.; Wenter, V.; Illigens, B.M.; Bartenstein, P.; Albert, N.L. Towards standardization of 18F-FET PET imaging: do we need a consistent method of background activity assessment? EJNMMI Research. 2017, 7(1):48. doi: 10.1186/s13550-017-0295-y. (IF: 2.630)

34. **Brendel, M.***; Focke, C.*; Blume, T.; Peters, F.; Deussing, M.; Probst, F.; Overhoff, F.; Albert, NL.; Lindner, S.; von Ungern-Sternberg, B.; Bartenstein, P.; Haass, C.; Kleinberger, G.; Herms, J.; Rominger, A. Time Courses of Cortical Glucose Metabolism and Microglial Activity Across the Life-Span of Wild-Type Mice: A PET Study. Journal of Nuclear Medicine. 2017, 58(12):1984-1990. doi: 10.2967/jnumed.117.195107. (IF: 7.439)

35. Albert, NL.; Unterrainer, M.; Fleischmann, D.; Lindner, S.; Vettermann, F.; Brunegraf, A.; Vomacka, L.; **Brendel, M.**; Wenter, V.; Wetzel, C.; Rupprecht, R.; Tonn, J.-C.; Belka, C.; Bartenstein, P.; Niyazi, M. TSPO PET for glioma imaging using the novel ligand 18F-GE-180 – first results in patients with glioblastoma. EJNMMI. 2017, 44(13):2230-2238. doi: 10.1007/s00259-017-3799-9. (IF: 7.704)

36. **Brendel, M.**; Wagner, L.; Levin, J.; Zach, C.; Lindner, S.; Bartenstein, P.; Okamura, N.; Rominger, A. Perfusion-phase [18F]THK5351 tau-PET Imaging as a Surrogate Marker for Neurodegeneration. JAD Reports. 2017, 1(1):109-113. doi: 10.3233/ADR-170023. (IF: 3.476)

37. **Brendel, M.***; Schnabel, J.*; Schönecker, S.; Wagner, L.; Brendel, E.; Meyer-Wilmes, J.; Unterrainer, M.; Schildan, A.; Patt, M.; Prix, C.; Ackl, N.; Catak, C.; Pogarell, O.; Levin, J.; Danek, A.; Buerger, K.; Bartenstein, P.; Barthel, H.; Sabri, O.; Rominger, A. Additive Value of Amyloid-PET in Routine Cases of Clinical Dementia Work-up after FDG-PET. EJNMMI. 2017, 44(13):2239-2248. doi: 10.1007/s00259-017-3832-z. (IF: 7.704)

38. Deussing, M.; Blume, T.; Vomacka, L.; Mahler, C.; Focke, C.; Todica, A.; Unterrainer, M.; Albert, N.L.; Lindner, S.; von Ungern-Sternberg, B.; Baumann, K.; Zwergal, A.; Bartenstein, P.; Herms, J.; Rominger, A.; **Brendel, M.** Coupling Between Physiological TSPO Expression in Brain and Myocardium Allows Stabilization of Late-Phase Cerebral [18F]GE180 PET Quantification. Neuroimage. 2018, 165:83-91. doi: 10.1016/j.neuroimage.2017.10.006. (IF: 5.426)

39. Vomacka, L.; Albert, N.L.; Lindner, S.; Unterrainer, M.; Mahler, C.; **Brendel, M.**; Ermoschkin, L.; Gosewisch, A.; Brunegraf, A.; Buckley, C.; Kümpfel, T.; Rupprecht, R.; Ziegler, S.; Kerschensteiner, M.; Bartenstein, P.; Böning, G. TSPO imaging using the novel PET ligand [18F]GE-180: Quantification approaches in patients with multiple sclerosis. EJNMMI Research. 2017, 7(1):89. doi: 10.1186/s13550-017-0340-x. (IF: 2.630)

40. Zwergal, A.; Günther, L.; **Brendel, M.**; Beck, R.; Lindner, S.; Xiong, G.; Eilles, E.; Unterrainer, M.; Albert, NL.; Becker-Bense, S.; Brandt, T.; Ziegler, S.; la Fougère, C.; Dieterich, M.; Bartenstein, P. In vivo imaging of glial activation after unilateral labyrinthectomy in the rat: a [18F]GE180-PET study. Frontiers in Neurology. 2017, 8:665. doi: 10.3389/fneur.2017.00665. (IF: 3.508)

41. **Brendel, M.***; Schönecker, S.*; Höglinger, G.; Lindner, S.; Havla, J.; Blautzik, J.; Sauerbeck, J.; Rohrer, G.; Zach, C.; Vettermann, F.; Lang, A.; Golbe, L.; Nübling, G.; Bartenstein, P.; Furukawa, K.; Ishiki, A.; Bötzel, K.; Danek, A.; Okamura, N.; Levin, J.; Rominger, A. [18F]-THK5351 PET Correlates with Topology and Symptom Severity in Progressive Supranuclear Palsy. Frontiers in Aging Neuroscience. 2018, 17;9:440. doi: 10.3389/fnagi.2017.00440. (IF: 3.633)

42. **Brendel, M.***; Sauerbeck, J.*; Greven, S.; Kotz, S.; Scheiwein, F.; Blautzik, J.; Delker, A.; Pogarell, O.; Ishii, K.; Bartenstein, P.; Rominger A. SSRI Treatment Improves Cognition and Grey Matter Atrophy but not Amyloid Burden during Two-Year Follow-Up in MCI and AD Patients with Depressive Symptoms. Journal of Alzheimer's Disease. 2018, 65(3):793-806. doi: 10.3233/JAD-170387. (IF: 3.517)

43. Unterrainer, M.; Mahler, C.; Vomacka, L.; Lindner, S.; Havla, J.; **Brendel, M.**; Böning, G.; Ertl-Wagner, B.; Kümpfel, T.; Milenkovic, V.; Rupprecht, R.; Kerschensteiner, M; Bartenstein, P.; Albert N.L. TSPO PET with [18F]GE-180 sensitively detects focal neuro-inflammation in patients with relapsing-remitting multiple sclerosis. EJNMMI. 2018, 45(8):1423-1431. doi: 10.1007/s00259-018-3974-7. (IF: 7.182)

44. Vettermann, F.; Rullmann, M.; Becker, G.; Luthardt, J.; Zientek, F.; Patt, M.; Meyer, M.; McLeod, A.; **Brendel, M.**; Blüher, M.; Sturmvoll, M.; Hilbert, A.; Ding, Y.; Sabri, O.; Hesse, S. Noradrenaline transporter availability in [11C]MRB PET predicts weight loss success in highly obese adults. EJNMMI. 2018, 45(9):1618-1625. doi: 10.1007/s00259-018-4002-7. (IF: 7.182)

45. Sauerbeck, J.; Ishii, K.; Hosokawa, C.; Kaida, H.; Scheiwein, F.T.; Hanaoka, K.; Rominger, A.; **Brendel, M.**; Bartenstein, P.; Murakami, T. The correlation between striatal and cortical binding ratio of 11C-PiB-PET in amyloid-uptake-positive patients. Annals of Nuclear Medicine. 2018, 32(6):398-403. doi: 10.1007/s12149-018-1258-8. (IF: 1.648)

46. **Brendel, M.**; Yousefi, B.; Blume, T.; Herz, M.; Focke, C.; Deussing, M.; Peters, F.; Lindner, S.; von Ungern-Sternberg, B.; Drzezga, A.; Bartenstein, P.; Haass, C.; Okamura, N.; Herms, J.; Yakushev, I.; Rominger, A. Comparison of 18F-T807 and 18F-THK5117 PET in a mouse model of tau pathology. Frontiers in Aging Neuroscience. 2018, 10:174. doi: 10.3389/fnagi.2018.00174. (IF: 3.633)

47. Guo, T.; Dukart, J.; **Brendel, M.**; Rominger, A.; Grimmer, T.; Yakushev, I. Rate of beta-amyloid accumulation varies with baseline amyloid burden: implications for anti-amyloid drug trials. Alzheimer's & Dementia. 2018, 14(11):1387-1396. doi: 10.1016/j.jalz.2018.05.013. (IF: 14.423)

48. Beyer, L.; Meyer-Wilmes, J.; Schoenecker, S.; Schnabel, J.; Brendel, E.; Prix, C.; Nübling, G.; Unterrainer, M.; Albert, N.L.; Pogarell, O.; Perneczky, R.; Catak, C.; Bürger, K.; Bartenstein, P.; Bötzel, K.; Levin, J.; Rominger, A.; **Brendel, M.** Clinical Routine FDG-PET Imaging of Suspected Progressive Supranuclear Palsy and Corticobasal Degeneration: A Gatekeeper for Subsequent Tau-PET Imaging? Frontiers in Neurology. 2018, 9:483. doi: 10.3389/fneur.2018.00483. (IF: 2.635)

49. Di Liberto, V.; van Dijk, M.; **Brendel, M.**; Waldron, A.M.; Moeller, C.; Koska, I.; Seiffert, I.; Gualtieri, F.; Gildehaus, F.J.; von Ungern-Sternberg, B.; Lindner, M.; Ziegler, S.; Palme, R.; Hellweg, R.; Gass, P.; Bartenstein, P.; Potschka, H. Imaging correlates of behavioral impairments: an experimental PET study in the rat pilocarpine epilepsy model. Neurobiology of Disease. 2018, 118:9-21. doi: 10.1016/j.nbd.2018.06.010. (IF: 5.160)

50. Irving, S.; Schöberl, F.; Pradhan, C.; **Brendel, M.**; Bartenstein, P.; Dieterich, M.; Brandt, T.; Zwergal, A. A novel real-space navigation paradigm reveals age- and gender dependent

changes of navigational strategies and hippocampal Activation. Journal of Neurology. 2018, 265(Suppl 1): 113-126. doi: 10.1007/s00415-018-8987-4. (IF: 4.204)

51. **Brendel, M.**; Jaworska, A.; Overhoff, F.; Blume, T.; Probst, F.; Gildehaus, F-J.; Bartenstein, P.; Haass, C.; Bohrmann, B.; Herms, J.; Willem, M.; Rominger, A. Efficacy of Chronic BACE1 Inhibition in PS2APP Mice Depends on the Regional Aβ Deposition Rate and Plaque Burden at Treatment Initiation. Theranostics. 2018, 8(18):4957-4968. doi: 10.7150/thno.27868. (IF: 8.063)

52. Focke, C.; Blume, T.; Zott, B.; Shi, Y.; Deussing, M.; Peters, F.; Schmidt, C.; Kleinberger, G.; Lindner, S.; Gildehaus, F.J.; Beyer, L.; von Ungern-Sternberg, B.; Bartenstein, P.; Ozmen, L.; Baumann, K.; Dorostkar, M.M.; Haass, C.; Adelsberger, H.; Herms, J.; Rominger, A.; **Brendel, M.** Early and longitudinal microglial activation but not amyloid accumulation predict cognitive outcome in PS2APP mice. Journal of Nuclear Medicine. 2019, 60(4):548-554. doi: 10.2967/jnumed.118.217703. (IF: 7.887)

53. Unterrainer, M.; Fleischmann, D.F.; Diekmann, C.; Vomacka, L.; Lindner, S.; Vettermann, F.; **Brendel, M.**; Wenter, V.; Ertl-Wagner, B.; Herms, J.; Wetzel, C.; Rupprecht, R.; Tonn, J.C.; Belka, C.; Bartenstein, P.; Niyazi, M.; Albert N.L. Comparison of 18F-GE-180 and dynamic 18F-FET PET in high grade glioma: a double tracer pilot study. EJNMMI. 2019, 46(3):580-590. doi: 10.1007/s00259-018-4166-1. (IF: 7.081)

54. van Dijk, R.M.; Di Liberto, V.; **Brendel, M.**; Waldron, A.-M.; Möller, C.; Gildehaus, F.J.; von Ungern-Sternberg, B.; Lindner, M.; Ziegler, S.; Palme, R.; Hellweg, R.; Gass, P.; Bartenstein, P.; Potschka, H. PET imaging biomarkers of behavioral impairments: a pilot µPET study in a rat electrical post-status epilepticus model. Epilepsia. 2018, 59(12):2194-2205. doi: 10.1111/epi.14586. (IF: 5.562)

55. Parhizkar, S.; Arzberger, T.; **Brendel, M.**; Kleinberger, G.; Deussing, M.; Focke, C.; Nuscher, B.; Xiong, M.; Ghasemigharagoz, A.; Katzmarski, N.; Krasemann, S.; Lichtenthaler, S.F.; Müller, S.A.; Colombo, A.; Monasor, L.S.; Tahirovic, S.; Herms, J.; Willem, M.; Pettkus, N.; Butovsky, O.; Bartenstein, P.; Edbauer, D.; Rominger, A.; Ertürk, A.; Grathwohl, S.A.; Neher, J.J.; Holtzman, D.M.; Meyer-Luehmann, M.; Haass, C. Loss of TREM2 function increases amyloid seeding but reduces plaque associated ApoE. Nature Neuroscience. 2019, 22(2):191-204. doi: 10.1038/s41593-018-0296-9. (IF: 20.071)

56. Blume, T.; Focke, C.; Peters, F.; Deussing, M.; Albert, N.L.; Lindner, S.; Gildehaus, F.J.; von Ungern-Sternberg, B.; Ozmen, L.; Baumann, K.; Bartenstein, P.; Rominger, A.; Herms, J.; **Brendel, M.** Microglial response to increasing amyloid load saturates with ageing: A longitudinal dual tracer in vivo µPet-Study. Journal of Neuroinflammation. 2018, 15(1):307. doi: 10.1186/s12974-018-1347-6. (IF: 5.700)

57. Nack, A.*; **Brendel, M.***; Nedelcu, J.; Daerr, M.; Nyamoya, S.; Beyer, C.; Focke, C.; Deussing, M.; Hoornaert, C.; Ponsaerts, P.; Schmitz, C.; Bartenstein, P.; Rominger, A.; Kipp, M. Expression of Translocator Protein and [18F]-GE180 Ligand Uptake in Multiple Sclerosis Animal Models. Cells. 2019, 8(2): E94. doi: 10.3390/cells8020094. (IF: 4.366)

58. Morbelli, S.; Chincarini, A.; **Brendel, M.**; Rominger, A.; Bruffaerts, R.; Vandenberghe, R.; Kramberger, M.G.; Trost, M.; Garibotto, V.; Nicastro, N.; Frisoni, G.B.; Lemstra, A.F.; van der Zande, J.; Pilotto, A.; Padovani, A.; Garcia-Ptacek, S.; Savitcheva, I.; Ochoa-Figueroa, M.A.; Davidsson A.; Camacho, V.; Peira, E.; Arnaldi, D.; Bauckneht, M.; Pardini, M.; Sambuceti, G.; Aarsland, D.; Nobili, F. Metabolic Patterns across clinical core features in patients with Dementia with Lewy Bodies: a project of the European Consortium for Dementia with Lewy Bodies (E-DLB). Annals of Neurology. 2019, 85(5):715-725. doi: 10.1002/ana.25453. (IF: 9.037)

59. Götzl, J.K.*; **Brendel, M.***; Werner, G.*; Parhizkar, S.; Monasor, L.S.; Kleinberger, G.; Colombo, A-V.; Deussing, M.; Wagner, M.; Winkelmann, J.; Diehl-Schmid, J.; Levin, J.; Fellerer,

K.; Reifschneider, A.; Bultmann, S.; Bartenstein, P.; Rominger, A.; Tahirovic, S.; Smith, S.T.; Madore, C.; Butovsky, O.; Capell, A.; Haass, C. Opposite microglial activation stages upon loss of PGRN or TREM2 result in reduced cerebral glucose metabolism. EMBO Molecular Medicine. 2019, 11(6):e9711. doi: 10.15252/emmm.201809711. (IF: 8.821)

60. Sacher, C.*; Blume, T.*; Beyer, L.*; Peters, F.; Eckenweber, F.; Sgobio, C.; Deussing, M.; Albert, NL.; Unterrainer, M.; Lindner, S.; Gildehaus, F-J.; von Ungern-Sternberg, B.; Brzak, I.; Neumann, U.; Saito, T.; Saido, TC.; Bartenstein, P.; Rominger, A.; Herms, J.*; Brendel M.*. Longitudinal PET Monitoring of Amyloidosis and Microglial Activation in a Second Generation Amyloid-beta Mouse Model. Journal of Nuclear Medicine. 2019, 60(12):1787-1793. doi: 10.2967/jnumed.119.227322. (IF: 7.887)

61. Beyer, L.*; Schnabel, J.*; Kazmierczak, P.; Ewers, M.; Schönecker, S.; Prix, C.; Meyer-Wilmes, J.; Unterrainer, M.; Catak, C.; Pogarell, O.; Perneczky, P.; Albert, N.L.; Bartenstein, P.; Danek, A.; Buerger, K.; Levin, J.; Rominger, A.*; **Brendel, M.***. Neuronal Injury Biomarkers for Assessment of the Individual Cognitive Reserve in Clinically Suspected Alzheimer's Disease. Neuroimage Clinical. 2019, 24:101949. doi: 10.1016/j.nicl.2019.101949. (IF: 4.350)

62. **Brendel, M.***; Deussing, M.*; Blume, T.*; Kaiser, L.; Probst, F.; Overhoff, F.; Peters, F.; von Ungern-Sternberg, B.; Ryazanov, S.; Leonov, A.; Griesinger, C.; Zwergal, A.; Levin, J.; Bartenstein, P.; Yakushev, I.; Cumming, P.; Boening, G.; Ziegler, S.; Herms, J.; Giese, A.; Rominger, A. Late-Stage Anle138b Treatment Ameliorates Tau Pathology and Metabolic Decline in a Mouse Model of Human Alzheimer's Disease Tau. Alzheimer's Research & Therapy. 2019, 11(1):67. doi: 10.1186/s13195-019-0522-z. (IF: 6.116)

63. Schönecker, S.*; **Brendel, M.***; Palleis, C.; Beyer, L.; Höglinger, G.U.; Schuh, E.; Rauchmann, B.S.; Sauerbeck, J.; Rohrer, G.; Sonnenfeld, S.; Furukawa, K.; Ishiki, A.; Okamura, N.; Bartenstein, P.; Dieterich, M.; Bötzel, K.; Danek, A.; Rominger, A.*; Levin, J*. PET imaging of astrogliosis and tau facilitates diagnosis of parkinsonian syndromes. Frontiers in Aging Neuroscience. 2019, 11:249. doi: 10.3389/fnagi.2019.00249. eCollection 2019. (IF: 4.362)

64. Unterrainer, M.; Fleischmann, D.F.; Vettermann, F.; Ruf, V.; Vomacka, L.; Nelwan, D.; Lindner, S.; **Brendel, M.**; Wenter, V.; Stöcklein, S.; Herms, J.; Milenkovic, V.; Rupprecht, R.; Tonn, J.C.; Belka, C.; Bartenstein, P.; Niyazi, M.; Albert N.L. TSPO PET, tumour grading and molecular genetics in histologically verified glioma: a correlative 18F-GE-180 PET study. EJNMMI. 2020, 47(6):1368-1380. doi: 10.1007/s00259-019-04491-5. (IF: 9.236)

65. Hochstrasser, T.; Rühling, S.; Hecher, K.; Fabisch, K.H.; Chrzanowski, U.; **Brendel, M.**; Eckenweber, F.; Sacher, C.; Schmitz, C.; Kipp, M. Stereological investigation of regional brain volumes after acute and chronic cuprizone-induced demyelination. Cells 2019, 8(9):E1024. doi: 10.3390/cells8091024. (IF: 4.366)

66. Schoeberl, F.; Pradhan, C.; Irving, S.; Buerger, K.; Xiong, G.; Kugler, G.; Kohlbecher, S.; Engmann, J.; Werner, P.; **Brendel, M.**; Schneider, E.; Perneczky, R.; Jahn, K.; la Fougère, C.; Bartenstein, P.; Brandt, T.; Dieterich, M.; Zwergal, A. Real-space navigation testing differentiates betw.een amyloid-positive and -negative aMCI. Neurology. 2020, 94(8):e861-e873. doi: 10.1212/WNL.0000000000008758. (IF: 9.910)

67. Huber, M.; Beyer, L.; Prix, C.; Schoenecker, S.; Palleis, C.; Rauchmann, B.S.; Morbelli, S.; Chincarini, A.; Bruffaerts, R.; Vandenberghe, R.; Van Laere, K.; Kramberger, M.G.; Trost, M.; Grmek, M.; Garibotto, V.; Nicastro, N.; Frisoni, G.B.; Lemstra, A.W.; van der Zande, J.; Pilotto, A.; Padovani, A.; Garcia-Ptacek, S.; Savitcheva, I.; Ochoa-Figueroa, M.A.; Davidsson, A.; Camacho, V.; Peira, E.; Arnaldi, D.; Bauckneht, M.; Pardini, M.; Sambuceti, G.; Voeglein, J.; Schnabel, J.; Unterrainer, M.; Perneczky, R.; Pogarell, O.; Buerger, K.; Catak, C.; Bartenstein, P.; Cumming, P.; Ewers, M.; Danek, A.; Levin, J.; Aarsland, D.; Nobili, F.; Rominger, A.; **Brendel, M.** Metabolic Correlates of Dopaminergic Loss in Dementia with Lewy bodies. Movement Disorders. 2020, 35(4):595-605. doi: 10.1002/mds.27945. (IF: 10.338)

68. Bremova-Ertl, T.; Sztatecsny, C.; **Brendel, M.**; Moser, M.; Moeller, B.; Clevert, D.; Beck-Woedl, S.; Kun-Rodrigues, C.; Bras, J.; Rominger, A.; Ninov, D.; Strupp, M.; Schneider, S. The clinical, ocular motor and imaging profile of Niemann Pick type C heterozygosity. Neurology. 2020, 94(16):e1702-e1715. doi: 10.1212/WNL.0000000000009290. (IF: 9.910)

69. Nedelcu, J.; Reinbach, C.; Riedler, P.; **Brendel, M.**; Rominger, A.; Kaye, J.; Behrangi, N.; Jiangshan, Z.; Schmitz, C.; Kipp, M. Laquinimod ameliorates secondary brain inflammation. Neurobiology of Disease. 2020, 134:104675. doi: 10.1016/j.nbd.2019.104675. (IF: 5.996)

70. Beyer, L.; **Brendel, M.**; Scheiwein, F.; Sauerbeck, J.; Hosakawa, C.; Alberts, I.; Shi, K.; Bartenstein, P.; Ishii, K.; Seibyl, J.; Cumming, P.; Rominger, A. Improved Risk Stratification for Progression from Mild Cognitive Impairment to Alzheimer's Disease with a Multi-Analytical Evaluation of Amyloid-Positron Emission Tomography. JAD. 2020, 74(1):101-112. doi: 10.3233/JAD-190818. (IF: 4.472)

71. Beyer, L.; Nitschmann, A.; Barthel, H.; van Eimeren, T.; Unterrainer, M.; Sauerbeck, J.; Marek, K.; Song, M.; Palleis, C.; Respondek, G.; Hammes, J.; Barbe, M.T.; Onur, O.; Jessen, F.; Saur, D.; Schroeter, M.L.; Rumpf, J.; Rullmann, M.; Schildan, A.; Patt, M.; Neumaier, B.; Barret, O.; Madonia, J.; Russell, D.S.; Stephens, A.W.; Roeber, S.; Herms, J.; Bötzel, K.; Levin, J.; Classen, J.; Höglinger, G.U.; Bartenstein, P.; Villemagne, V.L.; Drzezga, A.; Seibyl. J; Sabri, O.; **Brendel, M.** Early-Phase [18F]PI-2620 Tau-PET Imaging as a Surrogate Marker of Neuronal Injury. EJNMMI. 2020, 47(12). doi: 10.1007/s00259-020-04788-w. (IF: 9.326)

72. Sacher, C.; Blume, T.; Beyer, L.; Biechele, G.; Sauerbeck, J.; Eckenweber, F.; Deussing, M.; Focke, C.; Parhizkar, S.; Lindner, S.; Gildehaus, FJ.; von Ungern-Sternberg, B.; Baumann, K.; Tahirovic, S.; Kleinberger, G.; Willem, M.; Haass, C.; Bartenstein, P.; Cumming, P.; Rominger, A.; Herms, J.; **Brendel, M.** Asymmetry of fibrillar plaque burden in amyloid mouse models. Journal of Nuclear Medicine. 2020, 61(12). doi: 10.2967/jnumed.120.242750. (IF: 10.057)

73. **Brendel, M.***; Barthel, H.*; van Eimeren, T.*; Marek, K.; Beyer, L.; Song, M.; Palleis, C.; Gehmeyr, M.; Fietzek, U.; Respondek, G.; Sauerbeck, J.; Nitschmann, A.; Zach, C.; Hammes, J.; Barbe, M.T.; Onur, O.; Jessen, F.; Saur, D.; Schroeter, M.L.; Rumpf, J.; Rullmann, M.; Schildan, A.; Patt, M.; Neumaier, B.; Barret, O.; Madonia, J.; Russell, D.S.; Stephens, A.; Roeber, S.; Herms, J.; Bötzel, K.; Classen, J.; Bartenstein, P.; Villemagne, V.L.; Levin, J.; Höglinger, G.U.; Drzezga, A.; Seibyl, J.; Sabri, O. Assessment of 18F-PI-2620 as a Biomarker in Progressive Supranuclear Palsy. JAMA Neurology. 2020, 77(11). doi: 10.1001/jamaneurol.2020.2526. (IF: 18.302)

74. Becker-Bense, S.; Willoch, F.; Stephan, T.; **Brendel, M.**; Yakushev, I.; Habs, M.; Ziegler, S.; Herz, M.; Schwaiger, M.; Dieterich, M.; Bartenstein, P. Direct comparison of activation maps during galvanic vestibular stimulation: A hybrid H2[15 O] PET – BOLD MRI activation study. Plos One. 2020, 15(5). doi: 10.1371/journal.pone.0233262. (IF: 3.240)

75. Lu, J.; Bao, W.; Li, M.; Li, L.; Zhang, Z.; Alberts, I.; **Brendel, M.**; Cumming, P.; Lu, H.; Xiao, Z.; Zuo, C.; Guan, Y.; Zhao, Q.; Rominger, A. Associations of [18F]-APN-1607 Tau PET Binding in the Brain of Alzheimer`s Disease Patients with Cognition and Glucose Metabolism. Frontiers in Neuroscience. 2020, 14. doi: 10.3389/fnins.2020.00604. (IF: 4.677)

76. Zacherl, M.J.; Todica, A.; Wängler, C.; Schirrmacher, R.; Hajebrahimi, M.A.; Pircher, J.; Li, X.; Lindner, S.; **Brendel, M.**; Bartenstein, P.; Massberg, S.; Brunner, S.; Lehner, S.; Hacker, M.; Huber, B.C. Molecular imaging of cardiac CXCR4 expression in a mouse model of acute myocardial infarction using a novel 68Ga-mCXCL12 PET tracer. Journal of Nuclear Cardiology. 2020. doi.org/10.1007/s12350-020-02262-6. (IF: 5.952)

77. Ewers, M.; Biechele, G.; Suárez-Calvet, M.; Sacher, C.; Blume, T.; Morenas-Rodriguez, E.; Deming, Y.; Piccio, L.; Cruchaga, C.; Kleinberger, G.; Shaw, L.; Trojanowski, J.Q.; Herms, J.; Dichgans, M.; the Alzheimer's Disease Neuroimaging Initiative (ADNI), **Brendel, M.**; Haass, C.; Franzmeier, N. Higher CSF sTREM2 and microglia activation associate with slower rate of beta-amyloid accumulation. EMBO Molecular Medicine. 2020, 12(9). doi: 10.15252/emmm.202012308. (IF: 12.137)

78. Eckenweber, F.; Luque, J.M.; Blume, T.; Sacher, C.; Biechele, G.; Wind, K.; Deussing, M.; Briel, N.; Lindner, S.; Boening, G.; von Ungern-Sternberg, B.; Unterrainer, M.; Albert, N.L.; Zwergal, A.; Levin, J.; Bartenstein, P.; Cumming, P.; Rominger, A.; Höglinger, G.U.; Herms, J.; **Brendel, M.** Longitudinal TSPO expression in Tau Transgenic P301S Mice Predicts Increased Tau Accumulation and Deteriorated Spatial Learning. Journal of Neuroinflammation. 2020. doi.org/10.1186/s12974-020-01883-5. (IF: 8.322)

79. Henkel, R.; **Brendel, M.**; Paolini, M.; Brendel, E.; Grelich, L.; Beyer, L.; Gutzeit, A.; Pogarell, O.; Ricke, J.; Rominger, A.; Blautzik, J. FDG PET data is associated with cognitive performance in patients from a memory clinic. JAD. 2020, 78(1). doi: 10.3233/JAD-200826. (IF: 4.472)

80. Werner, G.; Damme, M.; Schludi, M.; Gnörich, J.; Wind, K.; Fellerer, K.; Wefers, B.; Wurst, W.; Edbauer, D.; **Brendel, M.**; Haass, C.; Capell, A. Loss of TMEM106B potentiates lysosomal and FTLD-like pathology in progranulin deficient mice. EMBO Reports. 2020, 21(10). doi: 10.15252/embr.202050241. (IF: 8.807)

81. Buchecker, V.; Waldron, A.; van Dijk, R.M.; Koska, I.; **Brendel, M.**; von Ungern-Sternberg, B.; Lindner, S.; Gildehaus, F.J.; Ziegler, S.; Bartenstein, P.; Potschka, H. [18F]MPPF and [18F]FDG µPET imaging in rats: impact of transport and restraint stress. EJNMMI Research. 2020, 10(1). doi: 10.1186/s13550-020-00693-3. (IF: 3.138)

82. Palleis, C.; Sauerbeck, J.; Beyer, L.; Harris, S.; Schmitt, J.; Morenas-Rodriguez, E.; Finze, A.; Nitschmann, A.; Ruch-Rubinstein, F.; Eckenweber, F.; Biechele, G.; Blume, T.; Shi, Y.; Weidinger, E.; Prix, C.; Bötzel, K.; Danek, A.; Rauchmann, B-S.; Stöcklein, S.; Lindner, S.; Unterrainer, M.; Albert, N.L.; Wetzel, C.; Rupprecht, R.; Rominger, A.; Bartenstein, P.; Herms, J.; Perneczky, R.; Haass, C.; Levin, J.*; Höglinger, G.U.*; **Brendel, M.***; In vivo Assessment of Neuroinflammation in 4-Repeat Tauopathies. Movement Disorders. 2021, 36(4). doi: 10.1002/mds.28395. (IF: 9.698)

83. Biechele, G.; Franzmeier, N.; Blume, T.; Ewers, M.; Medina Luque, J.; Eckenweber, F.; Sacher, C.; Beyer, L.; Ruch-Rubinstein, F.; Lindner, S.; Gildehaus, F.J.; von Ungern-Sternberg, B.; Cumming, P.; Bartenstein, P.; Rominger, A.; Höglinger, G.U.; Herms, J.; **Brendel, M.** Glial activation is moderated by sex in response to amyloidosis but not to tau pathology in mouse models of neurodegenerative diseases. Journal of Neuroinflammation. 2020, 17(1). doi: 10.1186/s12974-020-02046-2. (IF: 8.322)

84. Beyer, L.; Meyer-Wilmes, J.; Schönecker, S.; Schnabel, J.; Sauerbeck, J.; Scheifele, M.; Prix, C.; Unterrainer, M.; Catak, C.; Pogarell, O.; Palleis, C.; Perneczky, R.; Danek, A.; Buerger, K.; Bartenstein, P.; Levin, J.; Rominger, A.; Ewers, M.; **Brendel, M.** Cognitive reserve hypothesis in frontotemporal dementia: A FDG-PET study. Neuroimage: Clinical. 2021, 29:102535. doi: 10.1016/j.nicl.2020.102535. (IF: 4.881)

85. Bauckneht, M.; Chincarini, A.; **Brendel, M.**; Rominger, A.; Beyer, L.; Bruffaerts, R.; Vandenberghe, R.; Kramberger, M.G.; Trost, M.; Garibotto, V.; Nicastro, N.; Frisoni, G.B.; Lemstra, A.W.; van Berckel, B.N.M; Pilotto, A.; Padovani, A.; Ochoa-Figueroa, M.A.; Davidsson, A.; Camacho, V.; Peira, E.; Arnaldi, D.; Pardini, M.; Donegani, M.I.; Raffa, S.; Miceli, A.; o Sambuceti, G.; Aarsland, D.; Nobili, F.; Morbelli, S. Associations between education, age and the Dementia with Lewy Bodies (DLB) metabolic pattern: a European-DLB consortium project. Alzheimer's & Dementia. 2021, 17(8):1277-1286. doi: 10.1002/alz.12294. (IF: 16.655)

86. Biechele, G.; Wind, K.; Blume, T.; Sacher, C.; Beyer, L.; Eckenweber, F.; Franzmeier, N.; Ewers, M.; Zott, B.; Lindner, S.; Gildehaus, F-J..; von Ungern-Sternberg, B.; Tahirovic, S.; Willem, M.; Bartenstein, P.; Cumming, P.; Rominger, A.; Herms, J.; **Brendel, M.** Microglial Activation in the Right Amygdala-Entorhinal-Hippocampal Complex is Associated with Preserved Spatial Learning in AppNL-G-F mice. Neuroimage. 2021, 230:117707. doi: 10.1016/j.neuroimage.2020.117707. (IF: 7.024)

87. Kreuzer, A.; Sauerbeck, J.; Scheifele, M.; Stockbauer, A.; Schoenecker, S.; Prix, C.; Wlasich, E.; Loosli, S.V.; Kazmierczak, P.; Unterrainer, M.; Catak, C.; Janowitz, D.; Pogarell, O.; Palleis, C.; Perneczky, R.; Albert, N.L.; Bartenstein, P.; Danek, A.; Buerger, K.; Levin, J.; Zwergal, A.; Rominger, A.; **Brendel, M.**; Beyer, L. Detection gap of right-asymmetric neuronal degeneration by CERAD test battery in Alzheimer's disease. Frontiers in Aging Neuroscience. 2021, 13:611595. doi: 10.3389/fnagi.2021.611595. (IF: 5.702)

88. Schöberl, F.; Pradhan, C.; Grosch, M.; **Brendel, M.**; Jostes, F.; Obermaier, K.; Sowa, C.; Jahn, K.; Bartenstein, P.; Brandt, T.; Dieterich, M.; Zwergal, A. Bilateral vestibulopathy causes selective deficits in recombining novel routes in real space. Scientific Reports. 2021, 11(1):2695. doi: 10.1038/s41598-021-82427-6. (IF: 4.997)

89. Safaiyan, S.; Besson-Girard, S.; Kaya, T.; Cantuti-Castelvetri, L.; Liu, L.; Ji, H.; Schifferer, M.; Gouna, G.; Usifo, F.; Kannaiyan, N.; Fitzner, D.; Xiang, X.; Rossner, M.J.; **Brendel, M.**; Gokce, O.; Simons, M. White matter aging drives microglial diversity. Neuron. 2021, 109(7):1100-1117.e10. doi: 10.1016/j.neuron.2021.01.027. (IF: 18.688)

90. Song, M.; Beyer, L.; Kaiser, L.; Barthel, H.; van Eimeren, T.; Marek, K.; Nitschmann, A.; Scheifele, M.; Palleis, C.; Respondek, G.; Kern, M.; Biechele, G.; Hammes, J.; Bischof, G.; Barbe, M.; Onur, O.; Jessen, F.; Saur, D.; Schroeter, M.; Rumpf, J.; Rullmann, M.; Schildan, A.; Patt, M.; Neumaier, B.; Barret, O.; Madonia, J.; Russell, D.; Stephens, A.; Mueller, A.; Roeber, S.; Herms, J.; Boetzel, K.; Danek, A.; Levin, J.; Classen, J.; Höglinger, G.; Bartenstein, P.; Villemagne, V.; Drzezga, A.; Seibyl, J.; Sabri, O.; Böning, G.; Ziegler, S.; **Brendel, M.** Binding characteristics of [18F]PI-2620 distinguish the clinically predicted tau isoform in different tauopathies by PET. Journal of Cerebral Blood Flow Metabolism. 2021, 41(11):2957-2972. doi: 10.1177/0271678X211018904. (IF: 6.597)

91. Grosch M.; Beyer, L.; Lindner, M.; Kaiser, L.; Ahmadi, S.; Stockbauer, A.; Bartenstein, P.; Dieterich, M.; **Brendel, M.**; Zwergal, A.; Ziegler, S. Metabolic connectivity-based single subject classification by multi-regional linear approximation in the rat. Neuroimage. 2021, 235:118007. doi: 10.1016/j.neuroimage.2021.118007. (IF: 7.400)

92. Unterrainer, M.; Ruf, V.; von Rohr, K.; Suchorska, B.; Mittlmeier, L.M.; Beyer, L.; **Brendel, M.**; Wenter, W.; Kunz, W.G.; Bartenstein, P.; Herms, J.; Niyazi, M.; Tonn, J.C.; Albert, N.L. TERT-promoter mutational status in glioblastoma – is there an association with amino acid uptake on dynamic 18F-FET PET? Frontiers in Oncology. 2021, 11:645316. doi: 10.3389/fonc.2021.645316. (IF: 5.738)

93. Palleis, C.*; **Brendel, M.***; Finze, A.; Weidinger, E.; Bötzel, K.; Danek, A.; Beyer, B.; Nitschmann, A.; Kern, M.; Biechele, G.; Rauchmann, B.S.; Häckert, J.; Höllerhage, M.; Stephens, A.W.; Drzezga, A.; van Eimeren, T.; Villemagne, V.L.; Schildan, A.; Barthel, H.; Patt, M.; Sabri, O.; German Imaging Initiative for Tauopathies (GII4T); Bartenstein, P.; Perneczky, R.; Haass, C.; Levin, J.; Höglinger, G.U. Cortical [18F]PI-2620 binding differentiates Corticobasal Syndrome subtypes. Movement Disorders. 2021, 36(9):2104-2115. doi: 10.1002/mds.28624. (IF: 9.698)

94. Schmitt, J.; Palleis, C.; Sauerbeck, J.; Unterrainer, M.; Harris, S.; Prix, C.; Weidinger, E.; Katzdobler, S.; Wagemann, O.; Danek, A.; Beyer, L.; Rauchmann, B.S.; Rominger, A.; Simons, M.; Bartenstein, P.; Perneczky, R.; Haass, C.; Levin, J.; Höglinger, G.U.; **Brendel, M.**

Dual-phase β-Amyloid PET Captures Neuronal Injury and Amyloidosis in Corticobasal Syndrome. Frontiers in Aging Neuroscience. 2021, 13:661284. doi: 10.3389/fnagi.2021.661284. (IF: 5.702)

95. Beyer, L.; Gosewisch, A.; Lindner, S.; Völter, F.; Mittlmeier, L.; Tiling, R.; **Brendel, M.**; Cyran, C.C.; Unterrainer, M.; Rübenthaler, J.; Auernhammer, C.J.; Spitzweg, C.; Böning, G.; Gildehaus, F.J.; Jurkschat, K.; Wängler, C.; Wängler, B.; Schirrmacher, R.; Wenter, V.; Todica, A.; Bartenstein, P.; Ilhan, H. Dosimetry and optimal scan time of [18F]SiTATE PET/CT in Patients with Neuroendocrine Tumours. EJNMMI. 2021, 48(11):3571-3581. doi: 10.1007/s00259-021-05351-x. (IF 9.236)

96. Biechele, G.; Sebastian Monasor, L.; Wind, K.; Blume, T.; Parhizkar, S.; Arzberger, T.; Sacher, C.; Beyer, L.; Eckenweber, F.; Gildehaus, F.J.; von Ungern-Sternberg, B.; Willem, M.; Bartenstein, P.; Cumming, P.; Rominger, A.; Herms, J.; Lichtenthaler, S.F.; Haass, C.; Tahirovic, S.; **Brendel, M.** Glitter in the Darkness? Non-fibrillar β-amyloid Plaque Components Significantly Impact the β-amyloid PET Signal in Mouse Models of Alzheimer's Disease. JNM. 2022, 63(1):117-124. doi:10.2967/jnumed.120.261858. (IF: 9.300)

97. Franzmeier, N.; Ossenkoppele, R.; **Brendel, M.**; Rubinski, A.; Smith, R.; Kumar, A.; Mattsson-Carlgren, N.; Strandberg, O.; Duering, M.; Buerger, K.; Dichgans, M.; Hansson, O.; Ewers, M. The BIN1 rs744373 Alzheimer's disease risk SNP is associated with faster Aβ-associated tau accumulation and cognitive decline. Alzheimer's & Dementia. 2022, 18(1):103-115. doi: 10.1002/alz.12371 (IF: 14.000)

98. Mittlmeier, L.M.; **Brendel, M.**; Beyer, L.; Albert, N.L.; Todica, A.; Zacherl, M.J.; Wenter, V.; Herlemann, A.; Kretschmer, A.; Ledderrose, S.; Hegemann, N.S.; Kunz, W.G.; Ricke, J.; Bartenstein, P.; Ilhan, H.; Unterrainer, M. Feasibility of different tumor delineation approaches for 18F-PSMA-1007 PET/CT imaging in prostate cancer patients. Frontiers in Oncology. 2021, 11:663631. doi: 10.3389/fonc.2021.663631 (IF: 5.738)

99. Song, M.; Scheifele, M.; Barthel, H.; van Eimeren, T.; Beyer, L.; Marek, K.; Eckenweber, F.; Palleis, C.; Kaiser, L.; Finze, A.; Kern, M.; Nitschmann, A.; Biechele, G.; Katzdobler, S.; Bischof, G.; Hammes, J.; Jessen, F.; Saur, D.; Schroeter, M.L.; Rumpf, J.J.; Rullmann, M.; Schildan, A.; Patt, M.; Neumaier, B.; Stephens, A.; Rauchmann, B.S.; Perneczky, R.; Levin, L.; Classen, J.; Höglinger, G.U.; Bartenstein, P.; Boening, G.; Ziegler, S.; Villemagne, V.; Drzezga, A.; Seibyl, J.; Sabri, O.; **Brendel, M.** Feasibility of Short Imaging Protocols for [18F]PI-2620 Tau-PET in Progressive Supranuclear Palsy. EJNMMI. 2021, 48(12):3872-3885. doi: 10.1007/s00259-021-05391-3. (IF: 10.057)

100. Neitzel, J.; Franzmeier, N.; Rubinski, A.; Dichgans, M.; **Brendel, M.**; ADNI Alzheimer's Disease Neuroimaging Initiative, Malik, R.; Ewers, M. KL-VS heterozygosity is associated with lower amyloid-dependent tau accumulation and memory impairment in Alzheimer's disease. Nature Communications. 2021, 12(1):3825. doi: 10.1038/s41467-021-23755-z. (IF: 17.694)

101. Vettermann, F.J.; Harris, S.; Schmitt, J.; Unterrainer, M.; Lindner, S.; Rauchmann, B.; Palleis, C.; Weidinger, E.; Beyer, L.; Eckenweber, F.; Schuster, S.; Biechele, G.; Ferschmann, C.; Milenkovic, V.M.; Wetzel, C.H.; Rupprecht, R.; Janowitz, D.; Buerger, K.; Perneczky, R.; Höglinger, G.U.; Levin, J.; Haass, C.; Tonn, J.C.; Niyazi, M.; Bartenstein, P.; Albert, N.L.*; Brendel, M*. Impact of TSPO receptor polymorphism on [18F]GE-180 binding in healthy brain and pseudo-reference regions of neurooncological and neurodegenerative disorders. Life. 2021, 11(6):484. doi: 10.3390/life11060484. (IF: 3.253)

102. Willroider, M.; Roeber, S.; Horn, A.K.E.; Arzberger, T.; Scheifele, M.; Respondek, G.; Sabri, O.; Barthel, H.; Patt, M.; Mishchenko, O.; Schildan, A.; Mueller, A.; Koglin, N.; Stephens, A.W.; Levin, J.; Höglinger, G.U. Bartenstein, P.; Herms, J.; **Brendel, M.**; Beyer, L. Superiority of formalin-fixed paraffin-embedded brain tissue for in vitro assessment of progressive supranuclear palsy tau pathology with [18F]PI-2620. Frontiers in Neurology. 2021, 12:684523. doi: 10.3389/fneur.2021.684523. (IF: 4.086)

103. Mittlmeier, L.; Suchorska, B.; Ruf, V.; Holzgreve, A.; **Brendel, M.**; Herms, J.; Bartenstein, P.; Tonn, J.C.; Unterrainer, M.; Albert, N.L. 18F-FET PET uptake characteristics of long-term IDH-wildtype diffuse glioma survivors. Cancers. 2021, 13(13):3163. doi: 10.3390/cancers13133163. (IF: 6.575)

104. Xiang, X.; Wind, K.; Wiedemann, T.; Blume, T.; Shi, Y.; Briel, N.; Beyer, L.; Biechele, G.; Eckenweber, F.; Zatcepin, A.; Lammich, S.; Ribicic, S.; Tahirovic, S.; Willem, M.; Deussing, M.; Palleis, C.; Rauchmann, B.; Gildehaus, F.; Lindner, S.; Spitz, C.; Franzmeier, F.; Baumann, K.; Rominger, A.; Bartenstein, P.; Ziegler, S.; Drzezga, A.; Respondek, G.; Buerger, K.; Perneczky, R.; Levin, J.; Höglinger, G.; Herms, J.; Haass, C.; **Brendel, M.*** Microglial activation states drive glucose uptake and FDG-PET alterations in neurodegenerative diseases. Science Translational Medicine. 2021, 13(615):eabe5640. doi: 10.1126/scitranslmed.abe5640. (IF: 19.343)

105. Etminani, K.; Soliman, A.; Davidsson, A.; Chang, J.R.; Martínez-Sanchis, B.; Byttner, S.; Camacho, V.; Bauckneht, M.; Stegeran, R.; Ressner, M.; Agudelo-Cifuentes, M.; Chincarini, A.; **Brendel, M.**; Rominger, A.; Bruffaerts, R.; Vandenberghe, R.; Kramberger, M.G.; Trost, M.; Nicastro, N.; Frisoni, G.B.; Lemstra, A.W.; van Berckel, B.N.M.; Pilotto, A.; Padovani, A.; Morbelli, S.; Aarsland, D.; Nobili, F.; Garibotto, V.; Ochoa-Figueroa, M. A 3D deep learning model to predict the diagnosis of Dementia with Lewy Bodies, Alzheimer's Disease and Mild Cognitive Impairment using brain 18F-FDG PET. EJNMMI. 2022, 49(2):563-584. doi: 10.1007/s00259-021-05483-0. (IF: 9,100)

106. Biel, D.; **Brendel, M.**; Rubinski, A.; Buerger, K.; Janowitz, D.; Dichgans, M.; Franzmeier, N. Tau-PET and in vivo Braak-staging as prognostic markers of future cognitive decline in cognitively normal to demented individuals. Alzheimer's Research & Therapy. 2021, 13(1):137. doi: 10.1186/s13195-021-00880-x. (IF: 8.831)

107. Biechele, G.; Blume, T.; Deussing, M.; Zott, B.; Shi, Y.; Xiang, X.; Franzmeier, N.; Kleinberger, G.; Peters, F.; Ochs, K.; Focke, C.; Sacher, C.; Wind, K.; Schmidt, C.; Lindner, S.; Gildehaus, F.; Eckenweber, F.; Beyer, L.; von Ungern-Sternberg, B.; Bartenstein, P.; Baumann, K.; Dorostkar, M.; Rominger, A.; Cumming, P.; Willem, M.; Adelsberger, H.; Herms, J.; **Brendel, M.** Pre-therapeutic Microglia Activation and Sex Determine Therapy Effects of Chronic Immunomodulation. Theranostics. 2021, 11(18):8964-8976. doi: 10.7150/thno.64022. (IF: 11.600)

108. Todica, A.; Mittlmeier, L.M.; Gildehaus, F.; Unterrainer, M.; Beyer, L.; **Brendel, M.**; Ledderose, S.T.; Schott, M.; Rodler, S.; Rath, L.; Marcon, J.; Ilhan, H.; Cyran, C.C.; Stief, C.G.; Staehler M.; Bartenstein, P. 68Ga-EMP-100 PET/CT – a novel ligand for visualizing c-MET-expression in metastatic renal cell carcinoma – first in human biodistribution and imaging results. EJNMMI. 2022, 49(5):1711.1720. doi: 10.1007/s00259-021-05596-6. (IF: 9.100)

109. Kirchner, M.A.; Holzgreve, A.; **Brendel, M.**; Orth, M.; Ruf, V.C.; Steiger, K.; Pötter, D.; Gold, L.; Unterrainer, M.; Mittlmeier, L.M.; Lindner, S.; Kaiser, L.; Maas, J.; Von Baumgarten, L.; Ilhan, H.; Belka, C.; Notni, J.; Bartenstein, P.; Lauber, K.; Albert, N.L. PSMA PET imaging in glioblastoma: A preclinical evaluation and theranostic outlook. Frontiers in Oncology. 2021, 11:774017. doi: 10.3389/fonc.2021.774017. (IF: 5.738)

110. Reifschneider, A.; Robinson, S.; van Lengerich, B.; Gnörich, J.; Logan, T.; Heindl, S.; Vogt, M.A.; Weidinger, E.; Riedl, L.; Wind, K.; Zatcepin, A.; Pesämaa, I.; Haberl, S.; Nuscher, B.; Kleinberger, G.; Klimmt, J.; Götzl, J.K. Liesz, A.; Bürger, K.; **Brendel, M.**; Levin, J.; Diehl-Schmid, J.; Suh, Y.; Di Paolo, G.; Lewcock, J.W.; Monroe, K.M.; Paquet, D.; Capell, A.; Haass, C. Loss of TREM2 reduces hyperactivation of progranulin deficient microglia but not lysosomal pathology. EMBO Journal. 2022, 41(4):e109108. doi: 10.15252/embj.2021109108. (IF: 11.400)

111. Kaiser, L.; Holzgreve, A.; Quach, S.; Ingrisch, M.; Unterrainer, M.; Dekorsy, M.J.; Lindner, S.; Ruf, V.; Brosch-Lenz, J.; Delker, A.; Böning, G.; Suchorska, B.; Niyazi, M.; Riemenschneider, M.J.; Stöcklein, S.; **Brendel, M.**; Rupprecht, R.; Thon, N.; von Baumgarten, L.C.; Tonn, J.C.; Bartenstein, P.; Ziegler, S.L.; Albert, N.L. Differential Spatial Distribution of TSPO or Amino Acid PET Signal and MRI Contrast Enhancement in Gliomas. Cancers. 2022, 14(3):53. doi: 10.3390/cancers14010053. (IF: 5.200)

112. Finze, A.; Wahl, H.; Janowitz, D.; Buerger, K.; Linn, J.; Rominger, A.; Stoecklein, S.; Bartenstein, P.; Wollenweber, F.A.; Catak, C.*; **Brendel, M.*** Regional associations of cortical superficial siderosis and β-amyloid-PET positivity in patients with cerebral amyloid angiopathy. Frontiers in Aging Neuroscience. 2022, 13:786143. doi: 10.3389/fnagi.2021.786143. (IF: 4.800)

113. Shi, Y.; Cui, M.; Ochs, K.; **Brendel, M.**; Strübing, F.; Briel, N.; Eckenweber, F.; Zou, C.; Banati, R.; Liu, G.; Middleton, R.; Rupprecht, R.; Rudolph, U.; Zeilhofer, H.U.; Rammes, G.; Herms, J.; Dorostkar, M. Long-term diazepam treatment enhances microglial spine engulfment and impairs cognitive performance via the mitochondrial 18 kDa translocator protein (TSPO). Nature Neuroscience. 2022, 25(3):317-329. doi: 10.1038/s41593-022-01013-9. (IF: 25.000)

114. Zatcepin, A.; Heindl, S.; Schillinger, U.; Kaiser, L.; Lindner, S.; Bartenstein, P.; Kopczak, A.; Liesz, A.; **Brendel, M.**; Ziegler, S.I.. Reduced acquisition time [18F]GE-180 PET scanning protocol replaces gold-standard dynamic acquisition in a mouse ischemic stroke model. Frontiers in Medicine. 2022, 9:830020. doi: 10.3389/fmed.2022.830020. (IF: 3.900)

115. Franzmeier, N.*; **Brendel, M.***; Beyer, L.; Sleman, L.; Kovacs, G.; Arzberger, T.; Kurz, C.; Respondek, G.; Lukic, M.J.; Biel, D.; Rubinski, A.; Frontzkowski, L.; Hummel, S.; Finze, A.; Palleis, C.; Joseph, E.; Weidinger, E.; Katzdobler, S.; Song, M.; Biechele, G.; Kern, M.; Scheifele, M.; Rauchmann, B-S.; Perneczky, R.; Rullman, M.; Patt, M.; Schildan, A.; Barthel, H.; Sabri, O.; Rumpf, J.J.; Schroeter, M.L.; Classen, J.; Villemagne, V.; Seybl, J.; Stephens, A.W.; Lee, E.B.; Coughlin, D.G.; Giese, A.; Grossman, M.; McMillan, C.T.; Gelpi, E.; Molina-Porcel, L.; Compta, Y.; van Swieten, J.C.; Laat, L.D.; Troakes, C.; Al-Sarraj, S.; Robinson, J.L.; Xie, S.X.; Irwin, D.J.; Roeber, S.; Herms, J.; Simons, M.; Bartenstein, P.; Lee, V.M.; Trojanowski, J.Q.; Levin, J.; Höglinger, G.U.; Ewers, M. Tau deposition patterns are associated with functional connectivity in primary tauopathies – evidence from tau-PET and histopathology. Nature Communications. 2022, 13(1):1362. doi: 10.1038/s41467-022-28896-3. (IF: 16.600)

116. Schuster, S.; Beyer, L.; Palleis, C.; Harris, S.; Schmitt, J.; Weidinger, E.; Prix, C.; Bötzel, K.; Danek, A.; Rauchmann, B-S.; Stöcklein, S.; Lindner, S.; Unterrainer, M.; Albert, N.L.; Mittlmeier, L.M.; Wetzel, C.H.; Rupprecht, R.; Rominger, A.; Bartenstein, P.; Perneczky, R.; Levin, J.; Höglinger, G.U.; **Brendel, M.;** Dekorsy, F.J.. Impact of partial volume correction on [18F]GE-180 PET quantification in subcortical brain regions of patients with corticobasal syndrome. Brain Sciences. 2022, 12(2):204. doi: 10.3390/brainsci12020204. (IF: 3.300)

117. Holzgreve , A.; Völter, F.; Delker, A.; Kunz, W.G.; Fabritius, M.P.; **Brendel, M.**; Albert, N.L.; Bartenstein, P.; Unterrainer, M.; Unterrainer L.M. Detection of splenic tissue using 99mTc-labelled denatured red blood cells scintigraphy – a quantitative single center analysis. Diagnostics. 2022, 12(2):486. doi: 10.3390/diagnostics12020486. (IF: 3.600)

118. Wu, P.; Zhao, Y.; Wu, J.; **Brendel, M.**; Ge, J.; Bernhardt, A.;Li, L.; Lu, J.; Alberts, I.; Katzdobler, S.; Yakushev, I.; Xu, Q.; Sun, Y.; Liu, F.; Levin, J.; Höglinger, G.U.; Bassetti, C.; Guan, Y.; Oertel, W.H.; Weber, W.; Rominger, A.; Wang, J.; Zuo, C.; Shi, K. Differential diagnosis of parkinsonism based on deep metabolic imaging indices. Journal of Nuclear Medicine. 2022, 63(11):1741-1747. doi: 10.2967/jnumed.121.263029. (IF: 9.300)

119. Blume, T.; Deussing, M.; Biechele, G.; Peters, F.; Zott, B.; Schmidt, C.; Franzmeier, N.; Wind, K.; Eckenweber, F.; Sacher, C.; Shi, Y.; Ochs, K.; Kleinberger, G.; Xiang, X.; Focke, C.; Lindner, S.; Gildehaus, F.J.; Beyer, L.; von Ungern-Sternberg, B.; Bartenstein, P.; Baumann, K.; Adelsberger, H.; Rominger, A.; Cumming, P.; Willem, M.; Dorostkar, M.M.; Herms, J.; **Brendel, M.** Chronic PPARγ Stimulation Shifts Amyloidosis to Higher Fibrillarity but Improves Cognition. Frontiers in Aging Neuroscience. 2022, 14:854031. doi: 10.3389/fnagi.2022.854031. (IF: 4.800)

120. Messerschmidt, K.*; Barthel, H.*; **Brendel, M.***; Scherlach, C.; Hoffmann, K.-T.; Rauchmann, B.S.; Rullmann, M.; Marek, K.; Villemagne, V.L.; Rumpf, J.; Saur, D.; Schroeter, M.L.; Schildan, A.; Patt, M.; Beyer, B.; Song, M.; Palleis, C.; Katzdobler, S.; Fietzek, U.M.; Respondek, G.; Scheifele, M.; Nitschmann, A.; Zach, C.; Barret, O.; Madonia, J.; Russell, D.; Stephens, A.; Roeber, S.; Herms, J.; Bötzel, K.; Bartenstein, P.; Levin, J.; Seibyl, J.; Hoeglinger, G.U.; Classen, J.; Sabri, O. 18F-PI-2620 Tau PET Improves the Imaging Diagnosis of Progressive Supranuclear Palsy. Journal of Nuclear Medicine. 2022, 63(11):1754-1760. doi: 10.2967/jnumed.121.262854. (IF: 9.300)

121. Unterrainer, L.M.; Lindner, S.; Eismann, L.; Casuscelli, J.; Gildehaus, F-J.; Ngoc Bui, V.; Albert, N.L.; Holzgreve, A.; Beyer, L.; Todica, A.; **Brendel, M.**; Cyran, C.C.; Karl, A.; Stief, C.G.; Ledderose, S.T.; Unterrainer, M.; Bartenstein, P.; Wenter, V.; Kretschmer, A. Feasibility of [68Ga]Ga-FAPI-46 PET/CT for detection of nodal and hematogenous spread in high-grade urothelial carcinoma. EJNMMI. 2022, 49(10):3571-3580. doi: 10.1007/s00259-022-05761-5. (IF: 9.100)

122. Rullmann, M.; **Brendel, M.**; Schroeter, M.L.; Saur, D.; Levin, J.; Perneczky, R.G.; Tiepolt, S.; Patt, M.; Mueller, A.; Villemagne, V.L.; Classen, J.; Stephens, A.W.; Sabri, O.; Barthel, H. Multicenter 18F-PI-2620 PET for in vivo Braak staging of tau pathology in Alzheimer's disease. Biomolecules. 2022, 12(3):458. doi: 10.3390/biom12030458. (IF: 5.500)

123. Holzgreve, A.; Pötter, D.; **Brendel, M.**; Orth, M.; Weidner, L.; Gold, L.; Kirchner, M.A.; Bartos, L.M.; Unterrainer, L.M.; Unterrainer, M.; Steiger, K.; von Baumgarten, L.; Niyazi, M.; Belka, C.; Bartenstein, P.; Riemenschneider, M.J.; Lauber, K.; Albert, N.L.. Longitudinal [18F]GE-180 PET imaging facilitates in vivo monitoring of TSPO expression in the GL261 glioblastoma mouse model. Biomedicines. 2022, 10(4):738. doi: 10.3390/biomedicines10040738. (IF: 4.700)

124. Antons, M.; Lindner, M.; Grosch, M.; Oos, R.; Palumbo, G.; **Brendel, M.**; Ziegler, S.; Bartenstein, P.; Dieterich, M.; Zwergal, A. Longitudinal [18]UCB-H/[18F]FDG imaging depicts complex patterns of structural and functional neuroplasticity following bilateral vestibular loss in the rat. Scientific Reports. 2022, 12(1):6049. doi: 10.1038/s41598-022-09936-w. (IF: 4.600)

125. Prearo, I.; Dekorsy, F.; **Brendel, M.**; Lottspeich, C.; Dechant, C.; Schulze-Koops, H.; Hoffmann, U.; Czihal, M. Diagnostic yield of axillary artery ultrasound in addition to temporal artery ultrasound for the diagnosis of giant cell arteritis. Clinical and Experimental Rheumatology. 2022, 40(4):819-825. doi: 10.55563/clinexprheumatol/v1bvfz. (IF: 3.700)

126. Unterrainer, L.M.; Beyer, L.; Zacherl, M.J.; Gildehaus, F.J.; Todica, A.; Kunte, S.C.; Holzgreve, A.; Sheikh, G.T.; Herlemann, A.; Casuscelli, J.; **Brendel, M.**; Albert, N.L.; Wenter, V.; Schmidt-Hegemann, N.; Kunz, W.G.; Cyran, C.C.; Ricke, J.; Stief, C.G.; Bartenstein, P.; Ilhan, I.; Unterrainer, M. Total tumor volume on 18F-PSMA-1007 PET as additional imaging biomarker in mCRPC patients undergoing PSMA-targeted alpha therapy with 225Ac-PSMA-I&T. Biomedicines. 2022, 10(5):946. doi: 10.3390/biomedicines10050946. (IF: 4.700)

127. Zhao, Y.; Wu, P.; Wu, J.; **Brendel, M.**; Lu, J.; Ge, J.; Tang, C.; Hong, J.; Xu, Q.; Liu, F.; Sun, Y.; Ju, Z.; Lin, H.; Guan, Y.; Bassetti, C.; Schwaiger, M.; Huang, S.; Rominger, A.; Wang,

J.; Zuo, C.; Shi, K. Decoding the dopamine transporter imaging for the differential diagnosis of parkinsonism using deep learning. EJNMMI. 2022, 49(8):2798-2811. doi: 10.1007/s00259-022-05804-x. (IF: 9.100)

128. Krause, D.; Chrobok, A.; Karch, S.; Keeser, D.; Manz, K.M.; Koch, W.; **Brendel, M.;** Rominger, A.; Koller, G.; Behle, N.; Pogarell, O. Binding potential changes of SERT in patients with depression are associated with remission: A prospective [^{123}I]β-CIT-SPECT study. Exp Clin Psychopharmacol. 2023, 31(1):219-227. doi: 10.1037/pha0000566. (IF: 3.157)

129. Xia, D.; Lianoglou, S.; Sandmann, T.; Calvert, M.; Suh, J.H.; Thomsen, E.; Dugas, J.; Pizzo, M.E.; DeVos, S.L.; Earr, T.K.; Lin, C.; Davis, S.; Ha, C.; Leung, A.W.; Nguyen, H.; Chau, R.; Yulyaningsih, E.; Lopez, I.; Solanoy, H.; Masoud, S.T.; Liang, C.; Lin, K.; Astarita, G.; Khoury, N.; Zuchero, J.Y.; Thorne, R.G.; Shen, K.; Miller, S.; Palop, J.J.; Garceau, D.; Sasner, M.; Whitesell, J.D.; Harris, J.A; Hummel, S.; Gnörich, J.; Wind, K.; Kunze, L.; Zatcepin, A.; **Brendel, M.**; Willem, M.; Haass, C.; Barnett, D.; Zimmer, T.S.; Orr, A.G.; Scearce-Levie, K.; Lewcock, J.W.; Di Paolo, G. & Sanchez, P.E. Novel App knock-in mouse model shows key features of amyloid pathology and reveals profound metabolic dysregulation of microglia. Molecular Neurodegeneration. 2022, 17(1):41. doi: 10.1186/s13024-022-00547-7. (IF: 15.100)

130. Kuenze, G.; Kümpfel, R.; Rullmann, M.; Barthel, H.; **Brendel, M.**; Patt, M.; Sabri, O. Molecular simulations reveal distinct energetic and kinetic binding properties of 18F-]PI-2620 on tau filaments from 3R/4R and 4R tauopathies. ACS Chemical Neuroscience. 2022, 13(14):2222-2234. doi: 10.1021/acschemneuro.2c00291. (IF: 5.000)

131. Blume, T.; Filser, S.S.B.; Sgobio, C.; Peters, F.; Neumann, U.; Shimshek, D.R.; Saito, T.; Saido, T.; **Brendel, M.**; Herms, J. ß-secretase inhibition prevents structural spine plasticity deficits in App NL-G-F mice. Frontiers in Aging Neuroscience. 2022, 14:909586. doi: 10.3389/fnagi.2022.909586. (IF: 4.800)

132. Rauchmann, B.; **Brendel, M.**; Franzmeier, N.; Trappmann, L.; Zaganjori, M.; Morenas-Rodriguez, E.; Guersel, S.; Burow, L.; Kurz, C.; Haeckert, J.; Tatò, M.; Utecht, J.; Papazov, B.; Pogarell, O.; Janowitz, D.; Buerger, K.; Palleis, C.; Weidinger, E.; Biechele, G.; Schuster, S.; Finze, A.; Eckenweber, F.; Rupprecht, R.; Rominger, A.; Goldhardt, O.; Grimmer, T.; Keeser, D.; Stoecklein, S.; Dietrich, O.; Bartenstein, P.; Levin, J.; Hoeglinger, G.; Haass, C.; Perneczky, R. Microglial activation and connectivity in Alzheimer's disease and aging. Annals of Neurology. 2022, 92(5):768-781. doi: 10.1002/ana.26465. (IF: 11.200)

133. Frontzkowski, L.; Ewers, M.; **Brendel, M.**; Biel, D.; Ossenkoppele, R.; Hager, P.; Steward, A.; Dewenter, A.; Roemer, S.; Rubinski, A.; Buerger, K.; Janowitz, D.; Pichet Binette, A.; Smith, R.; Strandberg, O.; Mattsson-Carlgren, N.; Dichgans, M.; Hansson, O.; Franzmeier, N. Earlier Alzheimer's disease onset is associated with tau pathology in brain hub regions and facilitated tau spreading. Nature Communications. 2022, 13(1):4899. doi: 10.1038/s41467-022-32592-7 (IF: 16.600)

134. Aghakhanyan, G.; Rullmann, M.; Rumpf, J.; Schroeter, M.L.; Scherlach, C.; Patt, M.; **Brendel, M.**; Koglin, N.; Stephens, A.W.; Classen, J.; Hoffmann, K.T.; Sabri, O.; Barthel, H. Interplay of tau and functional network connectivity in progressive supranuclear palsy: a [18F]PI-2620 PET/MRI study. EJNMMI. 2022, 50(1):103-114. doi: 10.1007/s00259-022-05952-0. (IF: 9.100)

135. Katzdobler, S.; Nitschmann, A.; Barthel, H.; Bischof, G.; Beyer, L.; Marek, K.; Song, M.; Wagemann, O.; Palleis, C.; Weidinger, E.; Nack, A.; Fietzek, U.; Kurz, C.; Häckert, J.; Stapf, T.; Ferschmann, C.; Scheifele, M.; Eckenweber, F.; Biechele, G.; Franzmeier, N.; Dewenter, D.; Schönecker, S.; Saur, D.; Schroeter, M.L.; Rumpf, J.; Rullmann, M.; Schildan, A.; Patt, M.; Stephens, A.W.; van Eimeren, T.; Neumaier, B.; Drzezga, A.; Danek, A.; Classen, J.;

Bürger, K.; Janowitz, D.; Rauchmann, B.; Stöcklein, S.; Perneczky, R.; Schöberl, F.; Zwergal, A.; Höglinger, G.U.; Bartenstein, P.; Villemagne, V.; Seibyl, J.; Sabri, O.; Levin, J.*; **Brendel, M.***; for the German Imaging Initiative for Tauopathies (GII4T). Additive value of [18F]PI-2620 perfusion imaging in progressive supranuclear palsy and corticobasal syndrome. EJNMMI. 2023, 50(29):423-434. doi: 10.1007/s00259-022-05964-w. (IF: 10.057)

136. Bartos, L.M.; Kirchleitner, S.V.; Blobner, J.; Wind, K.; Kunze, L.; Holzgreve, A.; Gold, L.; Zatcepin, A.; Kolabas, Z.I.; Ulukaya, S.; Weidner, L.; Quach, S.; Messerer, D.; Bartenstein, P.; Tonn, J.C.; Riemenschneider, M.J.; Ziegler, S.; von Baumgarten, L.; Albert, N.L.*; **Brendel, M.*** 18 kDa translocator protein PET facilitates early and robust tumor detection in the immunocompetent SB28 glioblastoma mouse model. Frontiers in Medicine. 2022, 9:992993. doi: 10.3389/fmed.2022.992993. (IF 3.900)

137. Von Rohr, K.; Unterrainer, M.; Holzgreve, A.; Kirchner, M.A.; Li, Z.; Unterrainer, L.M.; Suchorska, B.; **Brendel, M.;** Tonn, J.C.; Bartenstein, P.; Ziegler, S.; Albert, N.L.; Kaiser, L. Can radiomics provide additional information in [18F]FET-negative glioma? Cancers. 2022, 14(19):4860. doi: 10.3390/cancers14194860. (IF 5.200)

138. Steward, A.; Biel, D.; **Brendel, M.;** Dewenter, A.; Roemer, S.; Rubinski, A.; Luan, Y.; Dichgans, M.; Ewers, M.; Franzmeier, N.. Functional Network Segregation is associated with attenuated tau spreading in Alzheimer's disease. Alzheimer's Dementia. 2023, 19(5):2034-2046. doi: 10.1002/alz.12867. (IF: 16.655)

139. Quach, S.; Holzgreve, A.; Kaiser, L.; Unterrainer, M.; Dekorsy, F.J.; Nelwan, D.V.; Bartos, L.M.; Kirchleitner, S.V.; Weller, J.; Weidner, L.; Niyazi, M.; Ruf, V.C.; Herms, J.; Stöcklein, S.; Wetzel, C.; Riemenschneider, M.J.; von Baumgarten, L.; Thon, N.; **Brendel, M.;** Rupprecht, R.; Bartenstein, P.; Tonn, J-C.; Albert, N.L. TSPO PET Signal using [18F]GE180 is Associated with Survival in Recurrent Gliomas. EJNMMI. 2023, 50(3):859-869. doi: 10.1007/s00259-022-06006-1. (IF: 10.057)

140. Biel, D.; Luan, Y.; **Brendel, M.**; Hager, P.; Dewenter, A.; Moscoso, A.; Otero Svaldi, D.; Higgins, I.A.; Pontecorvo, M.; Römer, S.; Steward, A.; Rubinski, A.; Zheng, L.; Schöll, M.; Shcherbinin, S.; Ewers, M.; Franzmeier, N. Combining tau-PET and fMRI meta-analyses for patient-centered prediction of cognitive decline in Alzheimer's disease. Alzheimer's Research & Therapy. 2022, 14(1):166. doi: 10.1186/s13195-022-01105-5. (IF: 9.000)

141. Soliman, A.; Chang, J.R.; Etminani, K.; Byttner, S.; Davidsson, A.; Martínez-Sanchis, B.; Camacho, V.; Bauckneht, M.; Stegeran, R.; Ressner, M.; Agudelo-Cifuentes, M.; Chincarini, A.; **Brendel, M.**; Rominger, A.; Bruffaerts, R.; Vandenberghe, R.; Kramberger, M.; Trost, M.; Nicastro, N; Frisoni, G.; Lemstra, A.; van Berckel, B.N.M.; Pilotto, A.; Padovani, A.; Morbelli, S.; Aarsland, D.; Nobili, F.; Garibotto, V.; Ochoa-Figueroa, M. Adopting Transfer Learning for Neuroimaging: a Comparative Analysis with a Custom 3D Convolution Neural Network Model. BMC Medical Informatics and Decision Making. 2022, 22(Suppl 6):318. doi: 10.1186/s12911-022-02054-7. (IF: 3.500)

142. van Lengerich, B.; Zhan, L.; Xia, D.; Chan, D.; Joy, D.; Park, J.; Tatarakis, D.; Calvert, M.; Hummel, S.; Lianoglou, S.; Pizzo, M.; Prorok, R.; Thomsen, E.; Bartos, L.; Beumers, P.; Capell, A.; Davis, S.; de Weerd, L.; Dugas, J.; Duque, J.; Earr, T.; Gadkar, K.; Giese, T.; Gill, A.; Gnoerich, J.; Ha, C.; Kannuswamy, M.; Kim, D.J.; Kunte, S.; Kunze, L.; Lac, D.; Lechtenberg, K.; Leung, A.; Liang, C.; Lopez, I.; McQuade, P.; Modi, A.; Torres, V.; Nguyen, H.; Pesämaa, I.; Propson, N.; Reich, M.; Robles-Colmenares, Y.; Schlepckow, K.; Slemann, L.; Solanoy, H.; Suh, J.; Thorne, R.; Vieira, C.; Wind, K.; Xiong, K.; Zuchero, D.Y.; Diaz, D.; Dennis, M.; Huang, F.; Scearce-Levie, K.; Watts, R.; Haass, C.; Lewcock, J.; Di Paolo, G.; **Brendel, M.**; Sanchez, P.; Monroe, K. A TREM2-activating antibody with a blood-brain barrier transport vehicle enhances microglial metabolism in Alzheimer's disease models. Nature Neuroscience. 2023, 26(3):416-429. doi: 10.1038/s41593-022-01240-0. (IF: 24.884)

143. Zatcepin, A.; Kopczak, A.; Holzgreve, A.; Hein, S.; Schindler, A.; Duering, M.; Kaiser, L.; Lindner, S.; Schidlowski, M.; Bartenstein, P.; Albert, N.L.; **Brendel, M.**; Ziegler, S.I. Machine learning-based approach reveals essential features for simplified TSPO PET quantification in ischemic stroke patients. Zeitschrift fuer Medizinische Physik. 2023, S0939-3889(22)00128-3. (IF: 7.215)

144. Völter, F.; Beyer, L.; Eckenweber, F.; Scheifele, M.; Bui, N.; Patt, M.; Barthel, H.; Katzdobler, S.; Palleis, C.; Franzmeier, N.; Levin, J.; Perneczky, R.; Rauchmann, B.; Sabri, O.; Hong, J.; Cumming, P.; Rominger, A.; Shi, K.; Bartenstein, P.; **Brendel, M.** Assessment of perfusion deficit with early-phases of [18F]PI-2620 tau-PET versus [18F]flutemetamol amyloid-PET recordings. EJNMMI. 2023, 50(5):1384-1394. doi: 10.1007/s00259-022-06087-y. (IF: 10.057)

145. Zounek, A.J.; Albert, N.L.; Holzgreve, A.; Unterrainer, M.; Brosch-Lenz, J.; Lindner, S.; Bollenbacher, A.; Boening, G.; Rupprecht, R.; **Brendel, M.**; von Baumgarten, L.; Tonn, J.C.; Bartenstein, P.; Ziegler, S.; Kaiser, L. Feasibility of radiomic feature harmonization for pooling of [18F]FET or [18F]GE-180 PET images of gliomas. Zeitschrift fuer Medizinische Physik. 2023, 33(1):91-102. doi: 10.1016/j.zemedi.2022.12.005. (IF: 7.215)

146. Biel, D.; Suárez-Calvet, M.; Hager, P.; Rubinski, A.; Dewenter, A.; Steward, A.; Roemer, S.; Ewers, M.; Haass, C.; **Brendel, M.***; Franzmeier, N.* sTREM2 is associated with amyloid-related p-tau increases and glucose hypermetabolism in Alzheimer's. EMBO Molecular Medicine. 2023, 15(2):e16987. doi: 10.15252/emmm.202216987. (IF: 14.260)

147. Eschbach, R.S.; Hofmann, M.; Späth, L.; Unterrainer, L.M.; Sheikh, G.T.; Delker, A.; Lindner, S.; Jurkschat, K.; Wängler, C.; Wängler, B.; Schirrmacher, R.; Tiling, R.; **Brendel, M.**; Wenter, V.; Dekorsy, F.J.; Zacherl, M.J.; Todica, A.; Ilhan, H.; Grawe, F.; Cyran, C.C.; Unterrainer, M.; Rübenthaler, J.; Knoesel, T.; Paul, T.; Boeck, S.; Westphalen, S.B.; Spitzweg, C.; Auernhammer, C.J.; Bartenstein, P.; Beyer, L. Comparison of somatostatin receptor expression in patients with neuroendocrine tumours with and without somatostatin analogue treatment imaged with [18F]SiTATE. Frontiers in Oncology. 2023, 13:992316. doi: 10.3389/fonc.2023.992316. (IF: 5.738)

148. Gnörich, J.; Reifschneider, A.; Wind, K.; Zatcepin, A.; Kunte, S.T.; Beumers, P.; Bartos, L.M.; Wiedemann, T.; Grosch, G.; Xiang, X.; Fard, M.K.; Ruch, F.; Werner, G.; Koehler, M.; Slemann, L.; Hummel, S.; Briel, N.; Blume, T.; Shi, Y.; Biechele, G.; Beyer, L.; Eckenweber, F.; Scheifele, M.; Bartenstein, P.; Albert, N.L.; Herms, J.; Tahirovic, S.; Haass, C.; Capell, C.; Ziegler, S.; **Brendel, M.** Depletion and activation of microglia impact metabolic connectivity of the mouse brain. Journal of Neuroinflammation. 2023, 20(1):47. doi: 10.1186/s12974-023-02735-8. (IF: 9.587)

149. Hong, J.; **Brendel, M.;** Erlandsson, K.; Sari, H.; Lu, J.; Clement, C.;Bui, N.V.; Meindl, M.; Ziegler, I.; Barthel, H.; Sabri, O.; Choi, H.; Sznitman, R.; Rominger, A.; Shi, K. Forecasting the Pharmacokinetics With Limited Early Frames in Dynamic Brain PET Imaging Using Neural Ordinary Differential Equation. IEEE Transactions on Radiation and Plasma Medical Sciences. 2023, 7(6):607-617. doi: 10.1109/TRPMS.2023.32532612023. (IF: 4.951)

150. Schönecker, S.; Palleis, C.; Franzmeier, N.; Katzdobler, S.; Ferschmann, C.; Schuster, S.; Finze, A.; Scheifele, M.; Prix, C.; Fietzek, U.; Weidinger, E.; Nübling, G.; Vöglein, J.; Patt, M.; Barthel, H.; Sabri, O.; Danek, A.; Höglinger, G.U.; **Brendel, M**.*; Levin, L.* Symptomatology in 4-repeat tauopathies is associated with data-driven topology of [18F]-PI-2620 tau-PET signal. NeuroImage: Clinical. 2023, 38:103402. doi: 10.1016/j.nicl.2023.103402. (IF: 4.891)

151. Palumbo, G.; Kunze, L.H.; Oos, R.; Wind-Mark, K.; Lindner, S.; Von Ungern-Sternberg, B.; Bartenstein, P.; Ziegler, S.; **Brendel, M.** Longitudinal Studies on Alzheimer Disease Mouse

Models with Multiple Tracer PET/CT: Application of Reduction and Refinement Principles in Daily Practice to Safeguard Animal Welfare during Progressive Aging. Animals. 2023, 13(11):1812. doi: 10.3390/ani13111812. (IF: 3.231)

152. Albert, N.L.; Nelwan, D.V.; Fleischmann, D.F.; Quach, S.; von Rohr, K.; Kaiser, L.; Teske, N.; Unterrainer, L.M.; Bartos, L.M.; Ruf, V.C.; **Brendel, M.**; Riemenschneider, M.J.; Wetzel, C.; Herms, J.; Rupprecht, R.; Thon, N.; Tonn, J.; Belka, C.; Bartenstein , P.; von Baumgarten, L.; Niyazi, M.; Unterrainer, M.; Holzgreve, A. Prognostic value of TSPO PET prior to radiotherapy in newly diagnosed IDH-wildtype glioblastoma. Journal of Nuclear Medicine. 2023, 64(10):1519-1525. doi: 10.2967/jnumed.122.265247. (IF: 11.082)

153. Kolabas, Z.I.; Kuemmerle, L.B.; Perneczky, R.; Förstera, B.; Ulukaya, S.; Ali, M.; Kapoor, S.; Bartos, L.M.; Büttner, M.; Caliskan, O.S.; Zhouyi Rong, Z.; Mai, H.; Höher, L.; Jeridi, D.; Molbay, M.; Khalin, I.; Deligiannis, I.K.; Negwer, M.; Roberts, K.; Simats, A.; Carofiglio, O.; Todorov, M.I.; Horvath, I.; Ozturk, F.; Hummel, S.; Biechele, G.; Zatcepin, A.; Unterrainer, M.; Gnörich, J.; Roodselaar, J.; Shrouder, J.; Khosravani, P.; Tast, B.; Richter, L.; Díaz-Marugan, L.; Kaltenecker, D.; Lux, L.; Chen, Y.; Zhao, S.; Rauchmann, B.; Sterr, M.; Kunze, I.; Stanic, K.; Besson-Girard, S.; Katzdobler, S.; Palleis, C.; Schädler, J.; Paetzold, J.C.; Hauser, A.E.; Gokce, O.; Lickert, H.; Steinke, H.; Benakis, C.; Braun, C.; Martinez-Jimenez, C.P.; Buerger, K.; Albert, N.L.; Levin, J.; Haass, C.; Kopczak, A.; Dichgans, M.; Havla, J.; Kümpfel, T.; Kerschensteiner, M.; Schifferer, M.; Simons, M.; Liesz, A.; Krahmer, N.; Bayraktar, O.A.; Franzmeier, N.; Plesnila, N.; Erener, S.; Puelles, V.G.; Delbridge, C.; Bhatia, H.S.; Hellal, F.; Elsner, M.; Bechmann, I.; Ondruschka, B.; **Brendel, M.**; Theis, F.J.; Erturk, A. Multi-omics and 3D-imaging reveal bone heterogeneity and unique calvaria cells in mice and humans. Cell. 2023, 186(17):3706-2725. doi: 10.1016/j.cell.2023.07.009. (IF: 66.850)

154. Kunze, L.H.; Ruch-Rubinstein, F.; Biechele, G.; Eckenweber, F.; Wind-Mark, K.; Dinkel, L.; Feyen, P.; Bartenstein, P.; Ziegler, S.; Paeger, L.; Tahirovic, S.; Herms, J.; **Brendel, M.** Long-term pioglitazone treatment has no significant impact on microglial activation and tau pathology in P301S mice. International Journal of Molecular Sciences. 2023, 24(12):10106. doi: 10.3390/ijms241210106. (IF: 6.208)

155. Unterrainer, M.; Kunte, S.C.; Unterrainer, L.M.; Holzgreve, A.; Delker, A.; Lindner, S.; Beyer, L.; **Brendel, M.**; Kunz, W.G.; Winkelmann, M.; Cyran, C.C.; Ricke, J.; Jurkschat, K.; Wängler, C.; Wängler, B.; Schirrmacher, R.; Belka, C.; Niyazi, M.; Tonn, J.C.; Bartenstein, P.; Albert, N.L. Next generation PET/CT imaging in meningioma – first clinical experiences using the novel SSTR-targeting peptide 18F-SiTATE. EJNMMI. 2023, 50(11):3390-3399. doi: 10.1007/s00259-023-06315-z. (IF: 10.057)

156. Wattjes, M.P.; Huppertz, H-J.; Mahmoudi, N.; Stöcklein, S.; Rogozinski, S.; Wegner, F.; Klietz, M.; Apostolova, I.; Levin, J.; Katzdobler, S.; Buhmann, C.; Berding, G.; **Brendel, M.**; Barthel, H.; Sabri, O.; Höglinger, G.; Buchert, R. Multi-Centre diagnostic performance of brain magnetic resonance imaging in the diagnosis of progressive supranuclear palsy with Richardson's syndrome and variant phenotypes. Movement Disorders. 2023. In press (IF: 9.698)

157. Finze, A.; Biechele, G.; Rauchmann, B-S.; Franzmeier, N.; Palleis, C.; Katzdobler, S.; Endy Weidinger, E.; Guersel, S.; Schuster, S.; Harris, S.; Schmitt, J.; Beyer, L.; Gnörich, J.; Lindner, S.; Albert, N.L.; Wetzel, C.; Rupprecht, R.; Rominger, A.; Danek, A.; Burow, L.; Kurz, C.; Tato, M.; Utecht, J.; Papazov, B.; Zaganjori, M.; Trappmann, L-K.; Goldhardt, O.; Grimmer, T.; Haeckert, J.; Janowitz, D.; Buerger, K.; Keeser, D.; Stoecklein, S.; Dietrich, O.; Morenas-Rodriguez, E., Barthel, H.; Sabri, O.; Bartenstein, P.; Simons, M.; Haass, C.; Höglinger, G.H.; Levin, J.; Perneczky, R.; **Brendel, M.** Individual regional associations between Aβ-, tau- and neurodegeneration (ATN) with microglial activation in patients with primary and secondary tauopathies. Molecular Psychiatry. 2023. In press. doi: 10.1038/s41380-023-02188-8. (IF: 13.437)

158. Vogler, L.C.; Ballweg, A.; Bohr, B.; Briel, N.; Wind, K.; Antons, M.; Kunze, L.; Gnörich, J.;Lindner, S.; Gildehaus, F-J.; Baumann, K.; Bartenstein, P.; Boening, G.; Ziegler, S.I.; Levin, J.; Zwergal, A.; Höglinger, G.U.; Herms, J.; **Brendel, M.** Assessment of synaptic loss in mouse models of β-amyloid and tau pathology using [18F]UCB-H PET imaging. Neuroimage Clinical. 2023, 39:103484. doi: 10.1016/j.nicl.2023.103484. (IF: 4.200)

159. Palleis, C.; Franzmeier, N.; Weidinger, E.; Bernhardt, A.M.; Katzdobler, S.; Wall, S.; Ferschmann, C.; Harris, S.; Julia Schmitt, J., Schuster, S.; Gnörich, J.; Finze, A.; Biechele, G.; Lindner, S.; Albert, N.L.; Bartenstein, P.; Sabri, O.; Barthel, H.; Rupprecht, R.; Nuscher, B.; Stephens, A.W.; Rauchmann, B-S.; Robert Perneczky, R.; Haass, C.; **Brendel, M.***; Levin, J.*; Höglinger, G.U.*. Association of Neurofilament light chain, [^{18}F]PI-2620 tau-PET, TSPO-PET and clinical progression in patients with amyloid-β-negative CBS. Neurology. 2023. In press. (IF: 9.900)

160. Buchert, R.; Wegner, F.; Huppertz, H-J.; Berding, G.; **Brendel, M.**; Apostolova, I.; Buhmann, C.; Dierks, A.; Katzdobler, S.; Klietz, M.; Levin, J.; Mahmoudi, N.; Rinscheid, A.; Rogozinski, S.; Rumpf, J-J.; Schneider, C.; Stöcklein, S.; Spetsieris, P.G.; Eidelberg, D.; Wattjes, M.P.; Sabri, O.; Barthel, H.; Höglinger, G.;. Automatic covariance pattern analysis outperforms visual reading of FDG-PET in variant PSP. Movement Disorders. 2023. In press (IF: 9.698)

161. Steward, A.; Biel, D.; Dewenter, A.; Roemer, S.; Wagner, F.; Dehsarvi, A.; Otero Svaldi, D.; Higgins, I.; **Brendel, M.**; Pontecorvo, M.; Dichgans, M.; Shcherbinin, S.; Ewers, M.; Franzmeier, N. The role of ApoE4 in the connectivity-mediated spreading of tau pathology at lower amyloid levels. JAMA Neurology. 2023. In press (IF: 29.000)

162. Weidner, L.; Lorenz, J.; Quach, S.; Braun, F.K.; Rothhammer-Hampl, T.; Ammer, L.; Vollmann-Zwerenz, A.; Bartos, L.M.; Dekorsy, F.J.; Holzgreve, A.; Kirchleitner, S.V.; Thon, N.; Greve, T.; Ruf, V.; Herms, J.; Bader, S.; Milenkovic, V.M.; von Baumgarten, L.; Menevse, A.N.; Hussein, A.; Sax, J.; Wetzel, C.H.; Rupprecht, R.; Proescholdt, M.; Schmidt, N.O.; Beckhove, P.; Hau, P.; Tonn, J.-C.; Bartenstein, P.; **Brendel, M.**; Albert, N.L.; Riemenschneider, M.J. Translocator protein (18kDA) (TSPO) marks mesenchymal glioblastoma cell populations characterized by elevated numbers of tumor-associated macrophages. Acta Neuropathologica Communications. 2023, 11(1):147. doi: 10.1186/s40478-023-01651-5. (IF: 7.100)

163. Wang, L.; Xu, H.; Min, W.; **Brendel, M.**; Rominger, A.; Shi, K.; Han, Y.; Jiang, J. A metabolism-functional connectome sparse coupling method to reveal imaging markers for Alzheimer's disease based on simultaneous PET / MRI scans. Human Brain Mapping. 2023, 44(17):6020-6030. doi: 10.1002/hbm.26493. (IF: 5.399)

164. Bartos, L.M.; Kirchleitner, S.V.; Kolabas, Z.I.; Quach, S.; Beck, A.; Lorenz, J.; Blobner, J.; Mueller, S.A.; Ulukaya, S.; Hoeher, L.; Horvath, I.; Wind-Mark, K.; Holzgreve, A.; Ruf, V.C.; Gold, L.; Kunze, L.H.; Kunte, S.T.; Beumers, P.; Park, H.; Antons, M.; Zatcepin, A.; Briel, N.; Hoermann, L.; Schaefer, R.; Messerer, D.; Bartenstein, P.; Riemenschneider, M.J.; Lindner, S.; Ziegler, S.; Herms, J.; Lichtenthaler, S.F.; Ertürk, A.; Tonn, J.C.; von Baumgarten, L.; Albert, N.L.*; **Brendel, M.*** Deciphering sources of PET signals in the tumor microenvironment of glioblastoma at cellular resolution. Science Advances. 2023, 9(43):eadi8986. doi: 10.1126/sciadv.adi8986. (IF: 13.600)

165. Blazhenets, G.; Soleimani-Meigooni, D.N.; Thomas, W.; Mundada, N.; **Brendel, M.**; Vento, S.; VandeVrede, L.; Heuer, H.W.; Ljubenkov, P.; Rojas, J.C.; Chen, M.K.; Amuiri, A.N.; Miller, Z.; Gorno-Tempini, M.L.; Miller, B.L.; Rosen, H.J.; Litvan, I.; Grossman, M.; Boeve, B.; Pantelyat, A.; Tartaglia, M.C.; Irwin, D.J.; Dickerson, B.C.; Baker, S.L.; Boxer, A.L.; Rabinovici, G.D.; La Joie, R. [18F]PI-2620 binding patterns in patients with suspected Alzheimer's disease and frontotemporal lobar degeneration. Journal of Nuclear Medicine. 2023, 64(12):1980-1989. doi: 10.2967/jnumed.123.265856. (IF: 9.300)

166. Ngoc Bui, V.; Unterrainer, L.M.; **Brendel, M.**; Kunte, S.C.; Holzgreve, A.; Allmendinger, F.; Bartenstein, P.; Klauschen, F.; Unterrainer, M.; Staehler, M.; Ledderose, S. PSMA-expression is highly associated with histological subtypes of renal cell carcinoma: Potential Implications for theranostic approaches. Biomedicines. 2023, 11(11):3095. doi: 10.3390/biomedicines11113095. (IF: 4.700)

167. Stockbauer, A.; Leonie Beyer, L.; Huber, M.; Kreuzer, A.; Palleis, C.; Katzdobler, S.; Rauchmann, B.-S.; Morbelli, S.; Chincarini, A.; Bruffaerts, R.; Vandenberghe, R.; Kramberger, M.G.; Trost, M.; Garibotto, V.; Nicastro, N.; Lathuilière, A.; Lemstra, A.W.; van Berckel, B.N.M.; Pilotto, A.; Padovani, A.; Ochoa-Figueroa, M.A.; Davidsson, A.; Camacho, V.; Peira, E.; Bauckneht, M.; Pardini, M.; Sambuceti, G.; Aarsland, D.; Nobili, F.; Gross, M.; Vöglein, J.; Perneczky, R.; Pogarell, O.; Buerger, K.; Franzmeier, N.; Danek, A.; Levin, J.; Höglinger, G.U.; Bartenstein, P.; Cumming, P.; Rominger, A.; **Brendel, M.** Metabolic network alterations as a supportive biomarker in Dementia with Lewy Bodies with preserved dopamine transmission. EJNMMI. 2023. In press. doi: 10.1007/s00259-023-06493-w. (IF: 9.100)

168. Franzmeier, N.; Dehsarvi, A.; Steward, A.; Biel, D.; Dewenter, A.; Roemer, S.; Wagner, F.; Groß, M.; **Brendel, M.**; Moscoso, A.; Arunachalam, P.; Blennow, K.; Zetterberg, H.; Ewers, M.; Schöll, M. Elevated CSF GAP-43 is associated with accelerated tau accumulation and spread in Alzheimer's disease. Nature Communications. 2023. In press. (IF: 16.600)

* Shared first/last authorship

Verzeichnis von Fallberichten

1. Schönecker, S.; **Brendel, M.**; van der Zee, J.; van Broeckhoven, C.; Rominger, A.; Danek, A.; Levin, J. Ein Geschwisterpaar mit frontotemporaler Lobärdegeneration und Amyotropher Lateralsklerose und einer neuen Mutation im TBK1-Gen (Thr462Lysfs). Fortschritte der Neurologie – Psychiatrie. 2016, 84(8):494-8. (IF: 0.714)

2. Schönecker, S.; **Brendel, M.**; Huber, M.; Vollmar, C.; Hans-Juergen Huppertz, HJ.; Teipel, S.; Okamura, N.; Levin, J.; Rominger, A.; Danek, A. Applied multimodal diagnostics in a case of presenile dementia. BMC Neurology 2016, 9(16):131. (IF: 2.006)

3. Feil, K.*; **Brendel, M.***; Hensler, M.; Bartenstein, P.; Seelos, K.; Dieterich, M.; Rominger, A.; Danek, A. FDG-PET in a case of very late-onset Huntington's disease. Movement Disorders Clinical Practice. 2018, 5(2):227-228. doi: 10.1002/mdc3.12601. (IF: 0.760)

4. Unterrainer, M.; Fleischmann, D.; Lindner, S.; **Brendel, M.**; Rupprecht, R.; Tonn, J.; Belka, C.; Bartenstein, P.; Niyazi, K.; Albert, N. Detection of cerebrospinal fluid dissemination of recurrent glioblastoma using TSPO-PET with 18F-GE-180. Clinical Nuclear Medicine. 2018, 43(7):518-519. doi: 10.1097/RLU.0000000000002113. (IF: 6.498)

5. Schöberl, F.; Levin, J.; Rémi, J.; Goldschagg, N.; Eren, O.; Okamura, N.; Unterrainer, M.; Rominger, A.; Albert, N.L.; **Brendel, M.** IgLON5 – a case with predominant cerebellar tau-deposits and leptomeningeal inflammation. Neurology. 2018, 91(4):180-182. doi: 10.1212/WNL.0000000000005859. (IF: 8.689)

6. Buchholtz, M.L.; Bücklein, V.; Brendel. M.; Paal, M. Superior vena cava syndrome related to mediastinal lymphoma in late pregnancy: A case report. Case Reports in Womens Health. 2018. doi: 10.1016/j.crwh.2018.e00065. (IF: 0.291)

7. Conrad, J.; Kremmyda, O.; Högen, T.; **Brendel, M.**; Rominger, A.; Danek, A. Posterior Cortical Atrophy: Only the visual variant of Alzheimer's disease? A case series and literature review. Der Nervenarzt. 2019. doi: 10.1007/s00115-019-0697-3. (IF: 0.824)

8. Vöglein, J.; Willem, M.; Trambauer, J.; Schönecker, S.; Dieterich, M.; Biskup, S.; Giudici, C.; Utz, K.; Oberstein, T.; **Brendel, M.**; Rominger, A.; Danek, A.; Steiner, H.; Haass, C. Identification of a rare presenilin 1 single amino acid deletion mutation (F175del) with unusual amyloid beta processing effects. Neurobiology of Aging. 2019, 84:241e5-241e11. doi: 10.1016/j.neurobiolaging.2019.08.034. (IF: 4.347)

9. Unterrainer, M.; Ruf, V.; Cyran, C.C.; **Brendel, M.**; Thon, N.; Herms, J.; Schüller, U.; Tonn, J.C.; Bartenstein, P.; Albert, N.L. Identification of Distant Metastases From Recurrent Gliosarcoma Using Whole-Body 18F-FDG PET/CT. Clinical Nuclear Medicine. 2019, 44(11):923-924. doi: 10.1097/RLU.0000000000002790. (IF: 6.498)

10. **Brendel, M.***; Catak, C.*; Beyer, L.; Linn, J.; Wahl, H.; Janowitz, D.; Rominger, A.; Patt, M.; Barthel, H.; Sabri, O.; Bartenstein, P.; Wollenweber, F.A. Incident cortical superficial siderosis associated with regional tau and contralesional amyloid deposition in probable cerebral amyloid angiopathy. Case Reports in Neurology. 2020, 12(2):232-237. doi: 10.1159/000506765 (IF: 0.830)

11. Völk, S.; Unterrainer, M.; Albert, N.L.; Havla, J.; Gerdes, L.A.; Schumacher, M.; **Brendel, M.**; Kaiser, L.; Adorjan, K.; Rupprecht, R.; Bartenstein, P.; Kümpfel, T.; Danek, A. MD1 TSPO-PET with 18F-GE-180 to differentiate variants of multiple sclerosis: relapsing-remitting multiple sclerosis, tumefactive demyelination and Baló's concentric sclerosis. Clinical Nuclear Medicine. 2020, 45(10):e447-e448. doi: 10.1097/RLU.0000000000003220. (IF: 7.794)

12. Mittlmeier, L.M.; Ledderose, S.T.; Schott, M.; **Brendel, M.**; Beyer, L.; Theurich, S.; Mayr, D.; Walz, C.; Kunz, W.G.; Ricke, J.; Bartenstein, P.; Ilhan, H.; Staehler, M.; Unterrainer, M. Immature Plasma Cell Myeloma Mimics Metastatic Renal Cell Carcinoma on 18F-PSMA-1007 PET/CT Due to Endothelial PSMA-Expression. Diagnostics. 2021, 11(3):423. doi: 10.3390/diagnostics11030423. (IF: 3.992)

13. Nuebling, G.S.; Prix, C.; **Brendel, M.**; Beyer, L.; Wlasich, E.; Loosli, S.V.; Barthel, H.; Sabri, O.; Bartenstein, P.; Vöglein, J.; Danek, A.; Rominger, A.; Edbauer, D.; Haass, C.; Levin, J.M. Low-degree trisomy 21 mosaicism promotes early-onset Alzheimer disease. Neurobiology of Aging. 2021, 103:147e1-147e5. doi: 10.1016/j.neurobiolaging.2021.02.021. (IF: 5.133)

14. Unterrainer, M.; Mahler, C.; Schumacher, A.; Ruf, V.; Blum, B.; Lietke, S.; **Brendel, M.**; Rupprecht, R.; Bartenstein, P.; Kerschensteiner, M.; Kümpfel, T.; Albert, N.L. Amino acid uptake, glucose metabolism and neuro-inflammation in John Cunningham virus associated progressive multifocal leukoencephalopathy. Clinical Nuclear Medicine. 2022, 47(6):543-544. doi: 10.1097/RLU.0000000000004093. (IF: 7.794)

15. Unterrainer, L.; Todica, A.; Beyer, L.; **Brendel, M.**; Holzgreve, A.; Kauffmann-Guerrero, D.; Unterrainer, M.; Bartenstein, P.; Tufman, A. 68Ga-EMP-100 PET/CT - a novel method for non-invasive assessment of c-MET expression in non-small cell lung cancer. EJNMMI. 2023, 50(2):628-629. doi: 10.1007/s00259-022-05995-3. (IF: 10.057)

16. Palleis, C.; Forbrig, R.; Lehner, L.; Quach, S.; Albert, N.L.; **Brendel, M.**; Schöberl, F.; Straube, A. Lyme neuroborreliosis – an unusual case with extensive (peri)vasculitis of the middle cerebral artery. European Journal of Neurology. 2023, 30(3):785-787. doi: 10.1111/ene.15633. (IF: 6.288)

17. Wischmann, J.; Bartos, L.M.; **Brendel, M.**; Albert, N.L.; Forbig, R.; Straube, A.; Masouris, I. Translocator protein (TSPO)-PET as a diagnostic and monitoring tool in COVID-19 related MRI-negative brainstem encephalitis: a case report. Journal of Neurology. 2023, 270(6):2853-2856. doi: 10.1007/s00415-023-11691-5. (IF: 6.682)

18. Rueb, M.; Rauen, K.; Koerte, I.K.; Gersing, G.; Zetterberg, H.; Simrén, J.; **Brendel, M.***; Kristina Adorjan, K.* Traumatic encephalopathy syndrome and tauopathy in a 19-year-old with child abuse. Neurotrauma Reports. 2023. In press (IF: 2.400)

Verzeichnis von Leitlinien, Übersichtsartikeln und Korrespondenzen

1. Albert, N.L.; Unterrainer, M.; **Brendel, M.**; Kaiser, L.; Zweckstetter, M.; Cumming, P.; Bartenstein, P. In response to: The validity of 18F-GE180 as a TSPO imaging agent. EJNMMI. 2019, 46(6):1208-1211. doi: 10.1007/s00259-019-04294-8. (IF: 7.081)

2. Rösler, T.W.; Marvian, A.T.; **Brendel, M.**; Höllerhage, M.; Hopfner, F.; Koeglsperger, T.; Levin, J.; Meissner, W.G.; Nykänen, N.; Villemagne, V.L.; Barthel, H.; Sabri, O.; Respondek, G.; Schwarz, S.C.; Schweyer, K.; Müller, U.; Kovacs, G.G.; Höglinger, G.U. Four-repeat tauopathies. Progress in Neurobiology. 2019, 180:101644. doi: 10.1016/j.pneurobio.2019.101644. (IF: 10.658)

3. Albert, N.L.; Unterrainer, M.; **Brendel, M.**; Kaiser, L.; Zweckstetter, M.; Cumming, P.; Bartenstein, P. In response to: Anatomy of 18F-GE180, a failed radioligand for the TSPO protein. EJNMMI. 2020, 47(10):2237-2241. doi: 10.1007/s00259-020-04885-w. (IF: 9.236)

4. Unterrainer, M.; Ruzicka, M.; Fabritius, M.P.; Mittlmeier, L.M.; Winkelmann, M.; Rübenthaler, J.; **Brendel, M.**; Subklewe, M.; von Bergwelt-Baildon, M.; Ricke, J.; Kunz, W.; Cyran, C. PET/CT imaging for tumor response assessment to immunotherapy - current status & future directions. European Radiology Experimental. 2020, 4(1):63. doi: 10.1186/s41747-020-00190-1.(IF: 0.920)

5. Beyer, L.; **Brendel, M.** Imaging of tau pathology in neurodegenerative diseases: an update. Seminars in Nuclear Medicine. 2021, 51(3):253-263. doi: 10.1053/j.semnuclmed.2020.12.004. (IF: 4.446)

6. Haeckert, J.; **Brendel, M.**; Beyer, L.; Barthel, H.; Sabri, O.; Hasan, A.; Perneczky, R. Effective Valproic Acid Treatment in a Patient With Delusional Parasitosis Due to Corticobasal Syndrome and Alzheimer Disease. Journal of Clinical Psychopharmacology. 2021, 41(3):335-337. doi: 10.1097/JCP.0000000000001378. (IF: 3.188)

7. Garibotto, V.; Albert, N.; Barthel, H.; van Berckel, B.; Boellaard, R.; **Brendel, M.**; Cecchin, D.; Ekmekcioglu, O.; van de Giessen, E.; Guedj, E.; Lammerstma, A.A.; Semah, F.; Traub-Weidinger, T.; Van Weehaeghe, D.; Morbelli, S. for the EANM Neuroimaging Committee. The approval of a disease-modifying treatment for Alzheimer's disease: impact and consequences for the nuclear medicine community. EJNMMI. 2021, 48(10):3033-3036. doi: 10.1007/s00259-021-05485-y. (IF: 10.057)

8. Guedj, E.; Varrone, A.; Boellaard, R.; Albert, N.L.; Barthel, H.; van Berckel, B.; **Brendel, M.**; Cecchin, D.; Ekmekcioglu, O.; Garibotto, V.; Lammertsma, A.A.; Law, I.; Peñuelas, I.; Semah, F.; Traub-Weidinger, T.; van de Giessen, E.; van de Weehaeghe, D.; Morbelli, S. EANM Procedure Guidelines for Brain PET Imaging using [18F]FDG, version 3. EJNMMI. 2022, 49(2):632-651. doi: 10.1007/s00259-021-05603-w. (IF: 10.057)

9. Bartos, L.M.; Kunte, S.T.; Beumers, P.; Xiang, X.; Wind, K.; Ziegler, S.; Bartenstein, P.; Choi, H.; Lee, D.S.; Haass, C.; von Baumgarten, L.; Tahirovic, S.; Albert, N.L.; Lindner, S.; **Brendel,**

M. Single cell radiotracer allocation via immunomagentic sorting (scRadiotracing) to disentangle PET signals at cellular resolution. Journal of Nuclear Medicine. 2022, 63(10):1459-1462. doi: 10.2967/jnumed.122.264171. (IF: 11.082)

10. Xiang, X.; Tahirovic, S.; Ziegler, S.; Haass, C.; **Brendel, M.** Response to Comment on "Microglial activation states drive glucose uptake and FDG-PET alterations in neurodegenerative diseases. Science Translational Medicine. 2022, 14(659):eabn5104. doi: 10.1126/scitranslmed.abn5104. (IF: 19.319)

11. Verger, A.; Barthel , H.; Tolboom, N.; Fraioli, F.; Cecchin, D.; Albert, N.L.; van Berckel, B.; Boellaard, R.; **Brendel, M.;** Ekmekcioglu, O.; Semah, F.; Traub-Weidinger, T.; van de Weehaeghe, D.; Morbelli, S.; Guedj, E. 2-[18F]-FDG PET for imaging brain involvement in patients with long COVID: perspective of the EANM Neuroimaging Committee. EJNMMI. 2022, 49(11):3599-3606. doi: 10.1007/s00259-022-05913-7. (IF: 10.057)

12. Verger, A.; Yakushev, I.; Albert, N.L.; van Berckel, B.; **Brendel, M.;** Cecchin, D.; Aguiar Fernandez, P.; Fraioli, F.; Guedj, E.; Morbelli, S.; Tolboom, N.; Traub-Weidinger, T.; van de Weehaeghe, D.; Barthel , H.; FDA approval of lecanemab: the real start of widespread amyloid PET use? — the EANM Neuroimaging Committee perspective. EJNMMI. 2023, 50(6):1553-1555. doi: 10.1007/s00259-023-06177-5. (IF: 10.057)

13. Koeglsperger, T.; Rumpf, S.; Schließer, P.; Struebing, F.L.; **Brendel, M.**; Levin, J.; Trenkwalder, C.; Höglinger, G.U.; Herms, J. Neuropathology of incidental Lewy body & prodromal Parkinson's disease. Molecular Neurodegeneration. 2023, 18(1):32. doi: 10.1186/s13024-023-00622-7. (IF: 18.879)

14. Tolboom, N.; Verger, A.; Albert, N.L.; **Brendel, M.**; Cecchin, D.; Aguiar Fernandez, P.; Fraioli, F.; Guedj, E.; Herrmann, K.; Traub-Weidinger, T.; Morbelli, S.; Yakushev, I.; Zucchetta, P.; Barthel, H.; Van Weehaeghe, D.; EANM position paper: theranostics in brain tumours—the present and the future. EJNMMI. 2023, 51(1):202-205. doi: 10.1007/s00259-023-06425-8. (IF: 9.100)

Ihr Beitrag zu den Veröffentlichungen

Dieser kumulativen Dissertationen liegen die folgenden beiden Originalarbeiten zu Grunde:

I) **Brendel, M.***; Barthel, H.*; van Eimeren, T.*; Marek, K.; Beyer, L.; Song, M.; Palleis, C.; Gehmeyr, M.; Fietzek, U.; Respondek, G.; Sauerbeck, J.; Nitschmann, A.; Zach, C.; Hammes, J.; Barbe, M.T.; Onur, O.; Jessen, F.; Saur, D.; Schroeter, M.L.; Rumpf, J.; Rullmann, M.; Schildan, A.; Patt, M.; Neumaier, B.; Barret, O.; Madonia, J.; Russell, D.S.; Stephens, A.; Roeber, S.; Herms, J.; Bötzel, K.; Classen, J.; Bartenstein, P.; Villemagne, V.L.; Levin, J.; Höglinger, G.U.; Drzezga, A.; Seibyl, J.; Sabri, O. Assessment of 18F-PI-2620 as a Biomarker in Progressive Supranuclear Palsy. JAMA Neurology. 2020, 77(11). doi: 10.1001/jamaneurol.2020.2526.

II) Franzmeier, N.*; **Brendel, M.***; Beyer, L.; Sleman, L.; Kovacs, G.; Arzberger, T.; Kurz, C.; Respondek, G.; Lukic, M.J.; Biel, D.; Rubinski, A.; Frontzkowski, L.; Hummel, S.; Finze, A.; Palleis, C.; Joseph, E.; Weidinger, E.; Katzdobler, S.; Song, M.; Biechele, G.; Kern, M.; Scheifele, M.; Rauchmann, B-S.; Perneczky, R.; Rullman, M.; Patt, M.; Schildan, A.; Barthel, H.; Sabri, O.; Rumpf, J.J.; Schroeter, M.L.; Classen, J.; Villemagne, V.; Seybl, J.; Stephens, A.W.; Lee, E.B.; Coughlin, D.G.; Giese, A.; Grossman, M.; McMillan, C.T.; Gelpi, E.; Molina-Porcel, L.; Compta, Y.; van Swieten, J.C.; Laat, L.D.; Troakes, C.; Al-Sarraj, S.; Robinson, J.L.; Xie, S.X.; Irwin, D.J.; Roeber, S.; Herms, J.; Simons, M.; Bartenstein, P.; Lee, V.M.; Trojanowski, J.Q.; Levin, J.; Höglinger, G.U.; Ewers, M. Tau deposition patterns are associated with functional connectivity in primary tauopathies – evidence from tau-PET and histopathology. Nature Communications. 2022, 13(1):1362. doi: 10.1038/s41467-022-28896-3.

1.1 Beitrag zu Paper I

Der Eigenanteil der ersten in JAMA Neurology veröffentlichten Arbeit war die federführende Koordination, Datenanalyse und Publikation einer Multicenter Studie zur Tau-PET Bildgebung als neue Untersuchungsmethode bei Patienten mit PSP. Zunächst bestand der Eigenanteil darin, gemeinsam mit den Kollegen aus Leipzig und Köln die mittels [^{18}F]PI-2620 klinisch gemessenen Tau-PET Daten zu harmonisieren und nach München zu transferieren. Dazu wurden zunächst Phantomdaten in den verschiedenen PET Scannern gemessen und die Rekonstruktion der Tau-PET Daten so adjustiert, dass eine vergleichbare Auflösung während der Analyse vorlag. Zudem wurden Daten von gesunden Kontrollen aus zwei klinischen Studien integriert, welche in New Haven, USA und Melbourne, Australien gemessen wurden. Der Eigenanteil bestand weiterhin darin, den

gesamten Datensatz (60 Patienten mit PSP, 10 Patienten mit Alzheimer Krankheit, 10 Patienten mit alpha-Synukleinopathie, 10 gesunde Kontrollen) via kinetischer Modellierung zu prozessieren und atlasbasiert eine Quantifizierung in vordefinierten Zielregionen vorzunehmen. 53 der insgesamt 90 eingeschlossenen Fälle wurden dabei in München erhoben. Die quantitativen PET Daten wurden dann im Gruppenvergleich analysiert und mit klinischen Parametern (Krankheitsdauer, Schweregrad, Alter) korreliert. Parallel erfolgte die Durchführung einer autoradiographischen Analyse von post-mortem Gewebe (Basalganglien, frontaler Cortex) mittels Inkubation von [^{18}F]PI-2620. Abschließend erfolgte eine visuelle Beurteilung des gesamten Kollektivs durch die drei geteilten Erstautoren des Manuskripts. Die Datenanalyse der visuellen Beurteilung ist ebenfalls dem Eigenanteil der Arbeit zuzuordnen.

1.2 Beitrag zu Paper II

Der Eigenanteil der zweiten in Nature Communications veröffentlichten Arbeit war die Akquisition, Datensammlung und Präprozessierung des verwendeten Multicenter Datensatzes, aufbauend auf der initialen Arbeit in Beitrag I. Das Manuskript wurde gemeinsam mit dem geteilten Erstautor Dr. Franzmeier erstellt. Zusätzlich zu Patienten mit PSP wurden auch Patienten mit einem cortikobasalen Syndrom eingeschlossen und die Kohorte der Patienten mit PSP auf das klassische Richardson Syndrom beschränkt. Außerdem bestand der Eigenanteil darin, eine groß angelegte Autoradiographie Studie durchzuführen, um die in vitro Bindung des Tau-PET Tracers [^{18}F]PI-2620 semiquantitativ gegen den immunhistochemischen Goldstandard zu validieren. Abschließend erfolgte gemeinsam mit dem geteilten Erstautor die Interpretation der Kovarianz Analyse für die in vivo Tau-PET Daten und die post-mortem Tau Verteilung.

2. Einleitung

2.1 Progressive Supranukleäre Blickparese (PSP)

2.1.1 Prävalenz und Klinik der PSP

Die progressive supranukleäre Blickparese (PSP) stellt in Bezug auf ihre Häufigkeit eine seltene neurodegenerative Erkrankung dar, die im höheren Lebensalter weitgehend sporadisch auftritt und mit einer geschätzten Prävalenz von 6,4/100.000 gekennzeichnet ist (Schrag, Ben-Shlomo, & Quinn, 1999). Selten wird sie durch eine autosomal-dominant vererbte Mutationen im Gen des Tau Proteins verursacht (Pastor et al., 2001). Die sporadische PSP wurde genetisch mit einem H1-Haplotyp assoziiert, der bei mindestens 90% der Patienten mit PSP ausgeprägt ist (Höglinger et al., 2011). Der H1-Haplotyp ist jedoch auch durch eine hohe Prävalenz (ca. 60%) in der kaukasischen Bevölkerung, die keine klinische Diagnose einer PSP hat, gekennzeichnet. Daher handelt es sich beim Vorliegen des H1-Haplotyp am ehesten um eine genetische Prädisposition, wobei dann weitere genetische oder umweltbedingte Zusatzfaktoren hinzukommen müssen, um einen manifesten PSP Phänotyp hervorzurufen. Neben der Assoziation zum H1-Haplotyp des Tau-Gens konnten inzwischen auch weitere Genvarianten mit einem erhöhten PSP-Risiko in Verbindung gebracht werden (Höglinger et al., 2011). PSP-Patienten sterben im Durchschnitt 7-8 Jahre nach Beginn der Erkrankung (Rosler et al., 2019). In der Vergangenheit wurde die Diagnose in der Regel 3-4 Jahre nach Krankheitsbeginn gestellt, wobei die Patienten zu diesem Zeitpunkt überwiegend bereits schwere funktionelle Behinderungen hatten. Als typische klinische Manifestation der PSP gilt das frühe Auftreten einer posturalen Instabilität mit Stürzen, einer vertikalen Blickparese und Sprech- und Schluckstörungen. Zudem ist die Erkrankung durch frontale und subkortikale Demenz, sowie Bradykinese und axiale Rigidität gekennzeichnet. Diese klassische Manifestationsform der PSP wird nach dem Erstbeschreiber der Erkrankung als Richardson-Syndrom (PSP-RS) bezeichnet. In multiplen retrospektiven klinisch-pathologischen Studien wurden jedoch in den letzten Jahren mehrere atypische Manifestationsformen beschrieben und als atypische PSP-Phänotypen nach ihrem vorherrschenden klinischen Erscheinungsbild benannt. Darunter zählen die PSP mit Parkinsonismus (PSP-P (Williams et al., 2005)), die PSP mit Akinesie und Gang-Freezing (PSP-PAGF (Williams, Holton, Strand, Revesz, & Lees, 2007)), die PSP mit cortikobasalem Syndrom (PSP-CBS (Josephs et al., 2006)), die PSP mit Frontotemporaler Demenz (PSP-FTD (Han et al., 2010)), die PSP mit nicht-flüssiger Aphasie (PSP-PNFA (Josephs & Duffy, 2008)) und die PSP mit zerebellärer Ataxie (PSP-C (Iwasaki et al., 2013)). Diese PSP-Subtypen zeichnen sich durch eine geringere Frequenz der oben genannten Kernmerkmale aus.

Zur Detektion der Subtypmerkmale im Verlauf der Erkrankung sollten daher neben klinischen Parametern auch biomechanische Verlaufsuntersuchungen zur Charakterisierung und Zuordnung herangezogen werden, wobei diese bislang nur unzureichend etabliert sind.

2.1.2 Topologie der Neuropathologie bei PSP

Histopathologisch ist die PSP durch die Aggregation des Tau-Proteins mit 4 Mikrotubuli-Bindungswiederholungen (4-Repeat-Tau) charakterisiert (Steele, Richardson, & Olszewski, 1964). Bei Patienten mit PSP reichert sich die 4-Repeat-Tau Pathologie überwiegend im Hirnstamm und im Subkortex an, was zu einer Atrophie des Hirnstamms, des Mittelhirns und des Subkortex führt (Boxer et al., 2006; Dutt et al., 2016; Kovacs et al., 2020; Ling et al., 2020; Ling et al., 2016). Bereits vor 15 Jahren wurde eine stufenweise Ausbreitung der Tau Pathologie im Krankheitsverlauf beschrieben, welche sich zunächst in den Kerngebieten des Mesencephalons und der Basalganglien manifestiert (Substantia nigra, Nucleus subthalamicus, Globus pallidus, Putamen) (Williams, Holton, Strand, Pittman, et al., 2007). Im weiteren Krankheitsverlauf kommt es dann zur Ausbreitung der so genannten coiled bodies in den Nucelus Caudatus, den Pons, den Nucleus dentatus und den präfrontalen Cortex, wobei im Spätstadium auch weitere Anteile des Frontallappens und der Parietallappen involviert sind (Williams, Holton, Strand, Pittman, et al., 2007). Neuere histopathologische Analysen haben diese Ausbreitungsmuster in ein sechs-stufiges Staging System kategorisiert (Kovacs et al., 2020): In der ersten Stufe liegt die Tau Pathologie begrenzt auf den Globus pallidus, den Nucleus subthalamicus oder das Striatum vor. In der zweiten Stufe muss die Tau Pathologie sowohl im Globus pallidus, als auch im Nucleus subthalamicus und im Striatum vorliegen, bei zusätzlicher Beteiligung des frontalen Cortex oder des Nucleus dentatus bzw. der cerebellären weissen Substanz. In der dritten Stufe ist eine obligatorische Beteiligung dieser fünf Regionen gefordert. In den Stufen vier bis sechs sind eine zunehmende Tau Pathologie im frontalen Cortex und im Kleinhirn zu beobachten, wobei zusätzlich der Occipitallappen betroffen ist. Trotz überwiegend subkortikaler Tau-Akkumulation in den frühen Stadien der Erkrankung (Franzmeier et al., 2022; Kovacs et al., 2020) weisen Patienten mit PSP oft schon bei Diagnosestellung eine weit verbreitete kortikale neuronale Dysfunktion auf, wie sich beispielsweise durch FDG- oder Perfusions-PET Studien zeigte (Katzdobler et al., 2023; Volter et al., 2022; Zalewski et al., 2014). Dies steht zudem im Einklang mit dem Auftreten kortikaler Symptome, die häufig bei den klinischen Subtypen der PSP beobachtet werden (Dutt et al., 2016). Es bleibt jedoch unklar, ob die mit einer kortikalen Dysfunktion verbundenen Symptome eine direkte Folge von subkortikalem 4R-Tau oder einer Deafferenzierung sind.

2.1.3 Diagnostik bei PSP

Eine gesicherte Diagnose der PSP ist bislang nur durch die post-mortem histologische Untersuchung mit dem Nachweis von 4-Repeat-Tau-immunoreaktiven Aggregaten in Neuronen, Oligodendrozyten und Astrozyten in typischer Verteilung möglich (Litvan, Agid, Jankovic, et al., 1996). Daher wird die PSP auch als 4-Repeat-Tauopathie bezeichnet. Aus Nervenwasser oder Blut gewonnene biologische Marker für eine beweisende in vivo Detektion der Tau Aggregate stehen bislang nicht zur Verfügung. Der Einsatz von bildgebenden Verfahren wie der Magnetresonanztomographie (MRT) kann im Rahmen der Diagnosestellung helfen, jedoch sind die erhobenen Befunde nicht beweisend für die PSP (Burn & Lees, 2002). So liegt eine Mittelhirnatrophie beispielsweise nicht nur bei Patienten mit PSP und 4-Repeat-Tauopathie vor, sondern auch bei mehreren klinisch verwandten Syndromen (Whitwell et al., 2013). Auch die Single Photon Emission Computed Tomographie (SPECT) zur Detektion einer reduzierten Dopamintransporterverfügbarkeit und die Positron-Emissions-Tomografie (PET) zur Detektion von verändertem regionalem Glukosestoffwechsel können unterstützend für die Diagnosestellung herangezogen werden. Als weitere unterstützende Modalität konnten mittels optischer Kohärenztomographie (OCT) bei der PSP spezifische Veränderungen von einzelnen Netzhautschichten nachgewiesen werden (Albrecht et al., 2012). Ebenso konnten mittels Videookulographie (VOG) subtile PSP-spezifische Augenbewegungsstörungen aufgezeichnet werden (Pinkhardt & Kassubek, 2011). Sowohl die OCT als auch die VOG könnten daher als unterstützender Biomarker für Diagnose und Progression der PSP geeignet sein, es bedarf deren Prüfung in größeren Fallserien. Bei einem Großteil der zu Lebzeiten diagnostizierten Patienten mit PSP wird die Diagnose erst gestellt, wenn sich die Patienten in einem weit fortgeschrittenen Krankheitsstadium befinden (Respondek et al., 2013). Eine mögliche Ursache hierfür sind atypische PSP-Verlaufsformen bzw. unterschiedliche Phänotypen der Erkrankung. Da die relative Häufigkeit der PSP vor allem in kleinen oder retrospektiven Fallserien analysiert wurde, sind die Häufigkeiten für atypische Manifestationsformen nicht ausreichend bekannt, so dass die Größenordnung dieser diagnostischen Lücke unklar ist (Respondek et al., 2014). Vor diesem Hintergrund wurden 2017 die evidenzbasierten Movement Disorder Society - Clinical Diagnostic Criteria for PSP (MDS-PSP Kriterien) veröffentlicht (Hoglinger et al., 2017). Das Ziel der neuen Diagnose-Kriterien bestand darin eine frühere und sensitivere Diagnose der PSP zu ermöglichen, indem neben dem klassischen Richardson-Syndrom (PSP-RS) auch atypische PSP-Verlaufsformen bzw. -Varianten (vPSP) miterfasst werden. Darüber hinaus unterscheiden sich die MDS-PSP Kriterien von den NINDS-SPSP Kriterien durch die Einbeziehung von zusätzlichen Symptomen und Merkmalkombinati-

onen für die Stellung einer „possible PSP“ Diagnose und einer zusätzlichen, sehr sensitiven jedoch weniger spezifischen diagnostischen Kategorie namens „suggestive of PSP“ (soPSP). Die prospektive Validierung dieser Kriterien ist jedoch noch ausstehend.

2.1.4 Therapieoptionen und Therapiestudien bei PSP

Derzeit gibt es keine zugelassene kausale Therapie für die PSP und die präventiven und symptomatischen Behandlungsmöglichkeiten sind sehr begrenzt. Da auf das Tau-Protein zielende Therapien zunehmend in die klinische Entwicklung eintreten, ist es nun wichtig, Patienten in einem frühen Stadium der PSP zu diagnostizieren. Darüber hinaus ist es wichtig, ein hohes Maß an Spezifität für die Aufnahme in Anti-Tau Behandlungsstudien zu gewährleisten, um eine ausreichende statistische Aussagekraft zu gewährleisten und unnötige Nebenwirkungen bei klinisch überlappenden Syndromen ohne 4-Repeat-Tau Aggregation zu vermeiden. Durch Autopsie kontrollierte Daten zeigten, dass die klinische Diagnose von PSP nach den neuesten MDS-PSP-Kriterien in frühen Stadien bei moderater Spezifität nur eine begrenzte Sensitivität aufweist (1. Jahr: Sensitivität: 53%, Spezifität: 71%; 2. Jahr: Sensitivität: 59%, Spezifität: 82%; 3. Jahr: Sensitivität: 64%, Spezifität: 76%) (Respondek et al., 2020).

In diesem Zusammenhang besteht unter Neurowissenschaftlern inzwischen Konsens, dass neuroprotektive Therapien so früh wie möglich im Verlauf neurodegenerativer Erkrankungen eingeleitet werden müssen, um eine krankheitsverändernde Wirkung zu erzielen (Boxer et al., 2017). Zielgerichtete Therapien müssen verabreicht werden bevor es zu einer massiven Neurodegeneration gekommen ist, die nicht mehr umkehrbar ist (Boxer et al., 2017). Daher werden bestimmte erfassbare Pathologien inzwischen mit einem erhöhten Risiko für die klinische Manifestation neurodegenerativer Erkrankungen ermittelt. In sehr erfolgreichen Krankheitsbereichen bieten solche Risikobedingungen bereits eine Indikation für krankheitsmodifizierende Therapien. Das National Institute on Aging und die Alzheimer's Association (NIA-AA) haben vor kurzem aktualisierte diagnostische Leitlinien für die Alzheimer-Krankheit veröffentlicht, die als Richtschnur für den Umgang mit diesem Problem bei Tauopathien dienen sollen (Jack et al., 2018). Dabei wurden sechs Krankheitsstadien definiert: Stadium 1 ist eine präsymptomatische Krankheit mit Biomarker-Anomalien, aber wirklich asymptomatischen Patienten, die Stadien 2 und 3 stellen eine leichte kognitive Beeinträchtigung (MCI) ohne alltagsrelevante Beeinträchtigung dar. Die Stadien 4, 5 und 6 entsprechen Patienten mit leichter, mittelschwerer und schwerer Demenz. Parallel dazu hat die U.S. Food and Drug Administration einen überarbeiteten Leitfaden für die Industrie zur Entwicklung von Medikamenten für die Behandlung der frühen Alzheimer-Krankheit erarbeitet. Sie schlagen vor, dass sich therapeutische Versuche im Stadium 3 auf klinisch aussagekräftige Skalen zur Bewertung

subtiler (prädementieller) Defizite und früher kognitiver Beeinträchtigungen stützen sollen, im Stadium 2 auf sensible Messungen der neuropsychologischen Leistung oder der Umwandlung in Stadium 3 und im Stadium 1 auf Biomarker, die charakteristische pathophysiologische Veränderungen aufzeigen.

Die PSP wird sich dieser Entwicklung anschließen müssen. Hier werden die NINDS-SPSP-Diagnosekriterien (National Institute of Neurological Disorders and Stroke and Society for Progressive Supranuclear Palsy) als ante mortem-Diagnosestandard bereits akzeptiert. Aktuelle Therapiestudien (z.B. NCT02460094, NCT03068468, NCT02494024, NCT02880956, NCT04185415) bei der PSP umfassen Patienten in sehr fortgeschrittenen Stadien (bis zu 5 Jahre nach Beginn) mit schweren funktionellen Einschränkungen (z.B. fünf Schritte mit Hilfe gehen). In Anlehnung an die NIA-AA-Kriterien würde dies dem Stadium 4 oder 5 entsprechen. Bei der Alzheimer-Krankheit würden zumindest Studien im Spätstadium nicht mehr initiiert werden. Ein validiertes PSP-Biomarker-Instrument würde Studien der Stufe 2 oder 3 bei PSP erleichtern und könnte die Grundlage für Studien der Stufe 1 bei PSP bilden. Bislang gibt es jedoch kein solches Instrument zur Bewertung von PSP-Patienten im Frühstadium. Daher ist die Entwicklung von Biomarkern für eine Früherkennung der PSP essentiell.

2.2 PET Bildgebung bei PSP

2.2.1 Molekulare Bildgebung bei 4-Repeat Tauopathien

Dank des Einsatzes moderner bildgebender Verfahren und neuer Forschungsarbeiten konnten in den letzten Jahren wichtige neue Erkenntnisse zum besseren Verständnis der Komplexität bei der Entstehung und Progredienz verschiedener neurodegenerativer Erkrankungen und Prozesse gewonnen werden. Mittels spezifischer PET Tracer kann zum Beispiel das zeitliche und räumliche Ineinandergreifen verschiedener molekularpathologischer Mechanismen im Patienten genauer untersucht und sichtbar gemacht werden.

Ab den 90er Jahren wurden umfangreiche Untersuchungen des Glukosestoffwechsels im Gehirn mittels [^{18}F]Fluordesoxyglukose Positronen-Emissions-Tomographie (FDG-PET) bei Patienten mit PSP und CBS als überwiegende Manifestationsformen der 4-Repeat Tauopathien durchgeführt (Amtage et al., 2014; Eckert et al., 2008; Hellwig et al., 2015; Mille et al., 2017; Niethammer et al., 2014; Zhao, Zhang, & Gao, 2012). Die Bildgebung hatte das Ziel krankheitsspezifische Muster eines veränderten Glukoseverbrauchs zu erkennen. Bei PSP-Patienten wurde vor allem eine signifikante Verringerung

der FDG-Aufnahme im bilateralen anterioren cingulären Gyrus und im Mittelhirn festgestellt (Zhao et al., 2012). Der charakteristische FDG-PET Befund bei Patienten mit PSP ist insgesamt durch eine verminderte FDG-Aufnahme im bilateralen frontalen Kortex, einschließlich der vorderen und mittleren cingulären Gyri, des supplementärmotorischen Areals, der ventro- und dorsolateralen prämotorischen Areale, der präfrontalen Areale, des vorderen insulären Kortex sowie des Striatums des Thalamus und des Mittelhirns gekennzeichnet (Blin et al., 1990; D'Antona et al., 1985; Foster et al., 1988; Goffinet et al., 1989; Karbe et al., 1992; Leenders, Frackowiak, & Lees, 1988; Otsuka et al., 1989). Diese Stoffwechselveränderungen wurden bei durch Autopsie nachgewiesenen Fällen mit PSP bestätigt (Pardini et al., 2019; Smith et al., 2017; Zalewski et al., 2014). Bei Patienten mit CBS wurde ein Glukosehypometabolismus in der zentralen Region, den frontalen und parietalen Assoziationsgebieten, dem Putamen kontralateral zur klinisch betroffenen Seite und dem bilateralen Thalamus beobachtet (Mille et al., 2017).

Bis vor kurzem wurde die molekulare Bildgebung des Glukosestoffwechsels in der Differentialdiagnostik der 4-Repeat Tauopathien nicht berücksichtigt (Armstrong et al., 2013; Litvan, Agid, Calne, et al., 1996), obwohl die FDG-PET zumindest and tertiären Zentren häufig zur Feststellung des Vorliegens einer Neurodegeneration bei Verdacht auf PSP und kortikobasale Degeneration (CBD) als Hauptuntergruppe des CBS angefordert wird. Die oben genannten Diagnosekriterien (s. Kapitel 2.1.3) umfassen jedoch nun auch bildgebende Befunde mittels FDG-PET und MRT als unterstützende Kriterien (Hoglinger et al., 2017). Die meisten der erwähnten Studien zur molekularen Bildgebung wurden in akademischen Einrichtungen mit hochgradig charakterisierten Patientenpopulationen durchgeführt und inkludierten teilweise Algorithmen der künstlichen Intelligenz (z.B. maschinelles Lernen). Sensitivität, Spezifität, positive und negative Vorhersagewerte für die Differentialdiagnose verschiedener Parkinson-Syndrome lagen in einer groß angelegten Studie bei Verwendung eines automatisierten bildbasierten Klassifizierungsverfahrens durchweg bei > 80 % (Tang et al., 2010). Demgegenüber ergab eine kürzlich durchgeführte verblindete visuelle Bewertung der FDG-PET Bilder von Patienten mit PSP nur eine Sensitivität von 74% und eine Spezifität von 72% (Buchert et al., 2023). Insbesondere bei Patienten mit atypischer klinischer Verlaufsform einer PSP zeigte sich eine hohe Rate an falsch negativen Befundbewertungen (43%) und die Notwendigkeit zur Etablierung neuer krankheitsspezifischer Radiotracer. Einschränkend ist festzuhalten, dass diese FDG-PET Studien mit der klinischen Diagnose als „Standard of truth“ durchgeführt wurden und kein histologischer Goldstandard vorlag. In Anbetracht der insgesamt nicht optimalen Sensitivität und Spezifität der klinischen Diagnose, insbesondere nach den älteren Diagnosekriterien, kann die Wertigkeit der FDG-PET Bildgebung daher sowohl unter- als auch überschätzt werden. Da die PET Untersuchung mit

einem spezifischen Radiotracer ein sehr teures Verfahren darstellt, befasste sich die Forschung auch mit den Arbeitsabläufen in der klinischen Routine und fand heraus, dass die FDG-PET zumindest als Gatekeeper für die spezifischen PET Untersuchungen bei der PSP fungieren könnte (Beyer et al., 2018).

2.2.2 Tau-PET Bildgebung mit Radiotracern der ersten Generation bei PSP

Mitte der 2000er Jahre gelang es neue Tracer zur Detektion des Tau Proteins zu entwickeln, die zunächst präklinisch erforscht wurden (Yoshiyama et al., 2007). In humanen Studien mit [^{18}F]Flortaucipir- und [^{18}F]THK-5351, die knapp 10 Jahre später durchgeführt wurden, ergaben sich die stärksten quantitativen Bindungsunterschiede für den Globus pallidus, den Nucleus subthalamicus und das Mittelhirn, wenn Patienten mit PSP mit gesunden Kontrollen verglichen wurden (Brendel et al., 2017; Cho et al., 2017; Schonhaut et al., 2017; Whitwell et al., 2017). Die PET Signale entsprachen somit den erwarteten Verteilungsmustern der Tau Pathologie bei PSP (s. Kapitel 2.1.2). Eine PET Querschnittsstudie mit Patienten mit PSP und Kontrollpersonen mit dem Radiotracer [^{18}F]THK-5351, von dem inzwischen bekannt ist, dass er hauptsächlich an Monoaminoxidase-B bindet, zeigte zudem eine Korrelation des PET Signals mit dem Schweregrad der PSP (Brendel et al., 2017). Darüber konnte bestätigt werden, dass die [^{18}F]THK-5351 PET Patienten mit PSP von anderen Parkinson-Syndromen abgrenzen kann (Schonecker et al., 2019), was auf das Potenzial neuartiger Monoaminoxidase-B-Liganden für die Differentialdiagnose hinweist. Ein großer Teil des [^{18}F]THK-5351-Signals in den Basalganglien von PSP-Patienten und gesunden Probanden war jedoch nicht spezifisch für das Tau Protein (Lemoine et al., 2017). In einer früheren Arbeit mit dem alternativen PET-Tracer [^{18}F]FDDNP konnten ebenfalls Bindungsunterschiede zwischen Patienten mit PSP und Kontrollen gefunden werden (Kepe et al., 2013), jedoch war auch dieser Ligand nicht spezifisch für das Tau Protein. Die fehlende Spezifität von Tau Radiotracern der ersten Generation für das Tau Protein bei PSP konnte schließlich auch in Autopsie-Studien gezeigt werden (Soleimani-Meigooni et al., 2020).

2.3 Zielsetzung der Promotionsarbeit

Ziel dieser Arbeit war es daher, die Tau-PET Bildgebung mit einem Radiotracer der zweiten Generation als Biomarker bei Patienten mit PSP zu untersuchen. Eingeschlossen wurden Patienten und Kontrollprobanden, bei denen die [^{18}F]PI-2620 Tau-PET-Bildgebung im Rahmen der diagnostischen Abklärung an tertiären Zentren durchgeführt wurde. Darüber hinaus wurde die Fähigkeit der [^{18}F]PI-2620 Tau-PET Bildgebung untersucht, die Ausbreitung der Tau Pathologie bei 4-Repeat Tauopathien in Korrelation mit post-

mortem Daten zu beurteilen. Methodisch wurden dafür pharmakokinetische Modelle der Tracerbindung, sowie autoradiographische Analysen und Kovarianzanalysen herangezogen.

3. Zusammenfassung:

Biomarker für die Tau Pathologie bei Patienten mit Progressiver Supranukleärer Blickparese (PSP) werden als diagnostisches Einschlusskriterium für Therapiestudien und zum Monitoring von krankheitsverändernden Effekten dringend benötigt. Aktuell existieren jedoch keine zugelassenen Methoden um die 4-Repeat Tau Ablagerungen im Gehirn von Patienten mit PSP zuverlässig detektieren zu können. Im Rahmen dieser Promotionsarbeit wurde der Tau-PET Tracer [^{18}F]PI-2620 bei Patienten mit PSP im Vergleich zu Patienten mit anderen neurodegenerativen Erkrankungen und gesunden Kontrollen als neuer Biomarker für die Tau Pathologie evaluiert. Dafür wurde ein multizentrisch erhobener Datensatz harmonisiert und quantitativ analysiert. In einem zweiten Schritt wurde untersucht, ob sich die Tau Pathologie bei PSP anhand funktionell verbundener Hirnareale ausbreitet.

In einem retrospektiven Design wurden die [^{18}F]PI-2620 Tau-PET Scans von 60 Patienten mit klinischer PSP (40 Patienten mit der typischen Variante eines Richardson Syndroms, 20 mit atypischen Varianten der PSP), 10 Patienten mit Alpha-Synuclein assoziierten Erkrankungen (idiopathische Parkinson Erkrankung und Multisystematrophie), 10 Patienten mit Alzheimer Krankheit und 10 gesunden Kontrollen analysiert. Als Zielregionen wurden das Putamen, der innere und äußere Anteil des Globus pallidus, der Nucleus subthalamicus, die Substantia nigra, das dorsale Mittelhirn, der Nucleus dentatus sowie der dorsolaterale präfrontale Cortex und der mediale präfrontale Cortex definiert. Alle Patienten und Probanden erhielten eine dynamische PET Messung über 60 Minuten, so dass die Bilddaten quantitativ mit einem pharmakokinetischen Modell, relativ zur cerebellären grauen Substanz, berechnet werden konnten. Die [^{18}F]PI-2620 Bindung in den PSP Zielregionen wurde zwischen den Studiengruppen verglichen und mit Krankheitsschwere, Krankheitsdauer, sowie den klinischen Subtypen der PSP korreliert. Abschließend erfolgte in der ersten Studie eine visuelle Beurteilung der [^{18}F]PI-2620 Tau-PET Bilder durch drei nuklearmedizinische Experten. In der zweiten Studie wurde die regionale Kovarianz der [^{18}F]PI-2620 Tau-PET und die regionale Kovarianz der post-mortem Tau Pathologie mit interregionaler funktioneller Konnektivität verglichen. Als Patientenkollektiv dienten dabei 22 Patienten mit typischer PSP und 24 Patienten mit Cortikobasalem Syndrom (CBS) als weitere klinische Manifestationsform der 4-Repeat Tau Neuropathologie. 15 gesunde Kontrollen wurden als Normalkollektiv herangezogen. Für die korrespondierende post-mortem Analyse lagen zwei unabhängige PSP Kollektive aus der LMU München und der University of Pennsylvania vor. Die mittels Tau-PET erhobene quantitative Tau Pathologie im regionalen Epizentrum (Region mit der höchsten Pathologie) wurde zudem mit der regionalen Konnektivität auf Gruppen- und Einzellevel verglichen. Abschließend wurde die Kovarianz der Tau Pathologie im Autopsie-Arm der

Studie hinsichtlich dem betroffenen Zelltyp der Tau Pathologie (Neuronen, Astrozyten, Oligodendrozyten) aufgelöst. In beiden Studien wurden autoradiographische Daten an post-mortem Gewebe von verstorbenen Patienten mit PSP und gesunden Kontrollen erhoben und als hochauflösende Validierung der in vivo Tau-PET Ergebnisse herangezogen.

Patienten mit PSP zeigten im Vergleich zu gesunden Kontrollen ein erhöhtes [^{18}F]PI-2620 Tau-PET Signal im inneren und äußeren Anteil des Globus pallidus, im Putamen, im Nucleus subthalamicus, in der Substantia nigra und im Nucleus dentatus. Die deutlichsten Unterschiede waren im inneren Anteil des Globus pallidus zu beobachten (Cohen's d = 2,28), wobei sich in dieser Region auch signifikant erhöhte Tau-PET Signale zwischen Patienten mit atypischer PSP und gesunden Kontrollen nachwiesen lassen. In den cortikalen Zielregionen konnten bei Patienten mit PSP keine Änderungen des Tau-PET Signals beobachtet werden. Es zeigte sich aber eine erwartete erhöhte [^{18}F]PI-2620 Bindung bei Patienten mit Alzheimer Krankheit gegenüber allen Vergleichsgruppen. Innerhalb der Gruppe von Patienten mit typischer PSP ergaben sich keine Korrelationen zwischen dem Tau-PET Signal in PSP Zielregionen und der Krankheitsschwere oder der Krankheitsdauer. Es zeigten sich jedoch unterschiedlich starke Signalerhöhungen zwischen den verschiedenen klinischen Subtypen der PSP, wobei die höchsten Tau-PET Signale bei typischer PSP beobachtet wurden. Erwähnenswert waren ähnliche Effektgrößen für das erhöhte Tau-PET Signal bei Patienten mit PSP und einem niedrigen Schweregrad (PSP Skala ≤ 30) im Vergleich zu Patienten mit PSP und einem hohen Schweregrad (PSP Skala > 30). Die visuelle Beurteilung als Konsens von drei nuklearmedizinischen Experten ergab eine Sensitivität von 85% und eine Spezifität von 77% für die Detektion der Patienten mit PSP gegenüber gemischten Kontrollen. Mittels Autoradiographie konnte sowohl in den Basalganglien als auch im frontalen Cortex eine erhöhte [^{18}F]PI-2620 Bindung bei post-mortem Gewebe bei Patienten mit PSP festgestellt werden. Gesunde Kontrollen und mit kaltem Tracer prä-inkubierte Schnitte von Patienten mit PSP und gesunden Kontrollen zeigten keine Retention des Radiotracers. Die Analyse der Kovarianz in der Tau-PET zeigte eine hohe Übereinstimmung mit der durch funktionelle Kernspintomographie gemessenen Konnektivität. Dieses Ergebnis konnte sowohl für Patienten mit PSP und CBS, als auch für subcortikale und globale Analysen reproduziert werden (alle $\beta > 0,4$, alle p-Werte $< 0,001$). Durch die Tau-PET konnte außerdem herausgefunden werden, dass Tau-Muster auf Patientenebene mit der Konnektivität subkortikaler Tau-Epizentren verbunden sind. Zwischen der Kovarianz der regionalen Tau Pathologie in post-mortem Gewebe und funktioneller Konnektivität konnte in zwei unabhängigen Datensätzen ein deutlicher Zusammenhang festgestellt werden (LMU München: $\beta = 0,503$, $p < 0,001$; University of Pennsylvania: $\beta = 0,790$, $p < 0,001$).

Bei Zelltyp spezifischer Betrachtung der post-mortem Tau Pathologie zeigte sich, dass diese Assoziation für neuronales Tau stärker als für astrogliales oder oligodendrogliales Tau war. Dies deutet darauf hin, dass Konnektivität in erster Linie mit neuronaler Tau-Akkumulation verbunden ist. Mittels Autoradiographie an post-mortem Gewebe von 16 Patienten mit typischer PSP zeigte sich schließlich eine gute Übereinstimmung der regionalen [^{18}F]PI-2620 Bindung und der durch Immunfärbung erfassten Tau Pathologie, wodurch die in vivo Tau-PET Daten validiert werden konnten.

Die [^{18}F]PI-2620 Tau-PET-Bildgebung bei Patienten mit PSP und bei Kontrollpersonen stellt einen Durchbruch bei dem Versuch dar, die zugrunde liegende Tau Neuropathologie der PSP in vivo darzustellen. Durch die internationale multizentrische Evaluierung dieses Tau-PET Radiotracers der nächsten Generation mit verbesserter Off-Target-Bindung konnte ein großer Fortschritt in der Bildgebung auf dem Gebiet der 4-Repeat-Tauopathien erzielt werden. Die beiden verknüpften Studien zeigen, dass die [^{18}F]PI-2620 Tau-PET Bildgebung zur Diagnose und Differenzierung von Patienten mit Verdacht auf PSP eingesetzt werden kann. Zudem kann auch das Ausbreitungsmuster der Tau Pathologie entlang funktionell verknüpfter Hirnregionen berechnet werden. Die Tau-PET bietet daher bei der PSP möglicherweise eine frühzeitige und zuverlässigere Diagnose, sowie ein verbessertes Erfassen der Krankheitsprogression. Es ist wahrscheinlich, dass dieser Radiotracer für die Stratifizierung klinischer Studien bei PSP verwendet werden kann.

4. Abstract (English):

Biomarkers for tau pathology in patients with progressive supranuclear palsy (PSP) are urgently needed as diagnostic inclusion criteria for therapy studies and for monitoring disease-modifying effects. However, there are currently no approved methods to reliably detect 4-repeat tau deposits in the brain of patients with PSP. In this thesis, the tau-PET tracer [^{18}F]PI-2620 was evaluated as a new biomarker for tau pathology in patients with PSP compared to patients with other neurodegenerative diseases and healthy controls. For this purpose, a multicenter data set was harmonized and quantitatively analyzed. In a second step, it was investigated whether tau pathology spreads in PSP on the basis of functionally connected brain areas.

In a retrospective design, the [^{18}F]PI-2620 tau-PET scans of 60 patients with PSP (40 patients with the typical variant of Richardson syndrome, 20 with atypical variants of PSP), 10 patients with alpha-synuclein associated diseases (idiopathic Parkinson's disease and multisystem atrophy), 10 patients with Alzheimer's disease and 10 healthy controls were analyzed. The putamen, the inner and outer part of the globus pallidus, the subthalamic nucleus, the substantia nigra, the dorsal midbrain, the dentate nucleus as well as the dorsolateral prefrontal cortex and the medial prefrontal cortex were defined as target regions. All patients and subjects received a dynamic PET emission recording over 60 minutes so that the image data could be quantitatively calculated with a pharmacokinetic model relative to the cerebellar gray matter. The [^{18}F]PI-2620 binding in the PSP target regions was compared between the study groups and correlated with disease severity, disease duration and the clinical subtypes of PSP. Finally, in the first study, a visual assessment of the [^{18}F]PI-2620 tau PET images was performed by three nuclear medicine experts. In the second study, the regional covariance of [^{18}F]PI-2620 tau-PET and the regional covariance of post-mortem tau pathology with interregional functional connectivity were compared. The patient cohort consisted of 22 patients with typical PSP and 24 patients with corticobasal syndrome (CBS) as a further clinical manifestation of 4-repeat tau neuropathology. 15 healthy controls were used as a normal collective. Two independent PSP autopsy samples from the LMU Munich and the University of Pennsylvania were available for the corresponding post-mortem analysis. The quantitative tau pathology in the regional epicenter (region with the highest pathology) assessed by tau-PET was also compared with the regional connectivity at group and individual level. Finally, the covariance of tau pathology in the autopsy arm of the study was resolved with respect to the affected cell type of tau pathology (neurons, astrocytes, oligodendrocytes). In both studies, autoradiographic data on post-mortem tissue from deceased patients with PSP and healthy controls were collected and used as high-resolution validation of the in vivo tau-PET results.

Patients with PSP showed increased [^{18}F]PI-2620 tau-PET signal in the inner and outer portions of the globus pallidus, the putamen, the subthalamic nucleus, the substantia nigra and the dentate nucleus compared to healthy controls. The clearest differences were observed in the inner part of the globus pallidus (Cohen's d = 2.28), whereby significantly increased tau-PET signals were also detected in this region between patients with atypical PSP and healthy controls. In the cortical target regions, no changes in the tau PET signal were observed in patients with PSP. However, there was an expected increased [^{18}F]PI-2620 binding in patients with Alzheimer's disease compared to all control groups. Within the group of patients with typical PSP, there were no correlations between tau-PET signal in PSP target regions and disease severity or duration. However, there were varying degrees of signal elevation between the different clinical subtypes of PSP, with the highest tau-PET signals observed in typical PSP. Of note were similar effect sizes for increased tau PET signal in patients with PSP and low severity (PSP scale ≤ 30) compared to patients with PSP and high severity (PSP scale > 30). The visual assessment as a consensus of three nuclear medicine experts showed a sensitivity of 85% and a specificity of 77% for the detection of patients with PSP versus mixed controls. Using autoradiography, increased [^{18}F]PI-2620 binding was detected in post-mortem tissue in both the basal ganglia and frontal cortex in patients with PSP. Healthy controls and slices pre-incubated with cold tracer from patients with PSP and healthy controls showed no retention of the radiotracer. Analysis of covariance in tau-PET showed high agreement with connectivity measured by functional magnetic resonance imaging. This result could be reproduced for patients with PSP and CBS, as well as for subcortical and global analyses (all $\beta > 0.4$, all p-values < 0.001). Tau-PET also revealed that the tau pathology patterns of individual patients are linked to the functional connectivity archetype of tau epicenters in the subcortex. A clear association between the covariance of regional tau pathology in post-mortem tissue and functional connectivity was found in two independent data sets (LMU Munich: $\beta = 0.503$, $p < 0.001$; University of Pennsylvania: $\beta = 0.790$, $p < 0.001$). A specific analysis of cell-type related tau pathology in tissue of deceased patients with PSP showed that the association between functional connectivity and tau spread was strongest for neuronal tau, whereas astroglial or oligodendroglial tau did only show weaker correlation. This suggests that the tau spreading pattern is primarily driven by interconnected neurons with axons tau accumulation. Finally, autoradiography of post-mortem tissue from 16 patients with typical PSP showed good agreement between regional [^{18}F]PI-2620 binding and tau pathology detected by immunostaining, validating the in vivo tau-PET data.

[^{18}F]PI-2620 tau-PET imaging in patients with PSP and control subjects represents a breakthrough in the attempt to visualize the underlying tau neuropathology of PSP in

vivo. The international multicenter evaluation of this next-generation tau-PET radiotracer with improved off-target binding has enabled a major advance in imaging in the field of 4-repeat tauopathies. The two linked studies show that [^{18}F]PI-2620 tau PET imaging can be used to diagnose and differentiate patients with suspected PSP. In addition, the pattern of spread of tau pathology along functionally linked brain regions can also be calculated. Tau-PET may therefore offer an early and more reliable diagnosis of PSP, as well as improved detection of disease progression. It is likely that this radiotracer can be used for the stratification of clinical trials in PSP.

5. Paper I

Research

JAMA Neurology | Original Investigation

Assessment of ^{18}F-PI-2620 as a Biomarker in Progressive Supranuclear Palsy

Matthias Brendel, MD, MHBA; Henryk Barthel, MD, PhD; Thilo van Eimeren, MD; Ken Marek, MD; Leonie Beyer, MD; Mengmeng Song; Carla Palleis, MD; Mona Gehmeyr; Urban Fietzek, MD; Gesine Respondek, MD; Julia Sauerbeck; Alexander Nitschmann; Christian Zach, PhD; Jochen Hammes, MD; Michael T. Barbe, MD; Oezguer Onur, MD; Frank Jessen, MD; Dorothee Saur, MD; Matthias L. Schroeter, MD, PhD, MA; Jost-Julian Rumpf, MD; Michael Rullmann, PhD; Andreas Schildan, PhD; Marianne Patt, PhD; Bernd Neumaier, PhD; Olivier Barret, MD; Jennifer Madonia, MS; David S. Russell, MD, PhD; Andrew Stephens, MD, PhD; Sigrun Roeber, MD; Jochen Herms, MD; Kai Bötzel, MD; Joseph Classen, MD; Peter Bartenstein, MD; Victor Villemagne, MD, PhD; Johannes Levin, MD; Günter U. Höglinger, MD; Alexander Drzezga, MD; John Seibyl, MD; Osama Sabri, MD, PhD

IMPORTANCE Progressive supranuclear palsy (PSP) is a 4-repeat tauopathy. Region-specific tau aggregates establish the neuropathologic diagnosis of definite PSP post mortem. Future interventional trials against tau in PSP would strongly benefit from biomarkers that support diagnosis.

OBJECTIVE To investigate the potential of the novel tau radiotracer ^{18}F-PI-2620 as a biomarker in patients with clinically diagnosed PSP.

DESIGN, SETTING, AND PARTICIPANTS In this cross-sectional study, participants underwent dynamic ^{18}F-PI-2620 positron emission tomography (PET) from 0 to 60 minutes after injection at 5 different centers (3 in Germany, 1 in the US, and 1 in Australia). Patients with PSP (including those with Richardson syndrome [RS]) according to Movement Disorder Society PSP criteria were examined together with healthy controls and controls with disease. Four additionally referred individuals with PSP-RS and 2 with PSP–non-RS were excluded from final data analysis owing to incomplete dynamic PET scans. Data were collected from December 2016 to October 2019 and were analyzed from December 2018 to December 2019.

MAIN OUTCOMES AND MEASURES Postmortem autoradiography was performed in independent PSP-RS and healthy control samples. By in vivo PET imaging, ^{18}F-PI-2620 distribution volume ratios were obtained in globus pallidus internus and externus, putamen, subthalamic nucleus, substantia nigra, dorsal midbrain, dentate nucleus, dorsolateral, and medial prefrontal cortex. PET data were compared between patients with PSP and control groups and were corrected for center, age, and sex.

RESULTS Of 60 patients with PSP, 40 (66.7%) had RS (22 men [55.0%]; mean [SD] age, 71 [6] years; mean [SD] PSP rating scale score, 38 [15]; score range, 13-71) and 20 (33.3%) had PSP-non-RS (11 men [55.0%]; mean [SD] age, 71 [9] years; mean [SD] PSP rating scale score, 24 [11]; score range, 11-41). Ten healthy controls (2 men; mean [SD] age, 67 [7] years) and 20 controls with disease (of 10 [50.0%] with Parkinson disease and multiple system atrophy, 7 were men; mean [SD] age, 61 [8] years; of 10 [50.0%] with Alzheimer disease, 5 were men; mean [SD] age, 69 [10] years). Postmortem autoradiography showed blockable ^{18}F-PI-2620 binding in patients with PSP and no binding in healthy controls. The in vivo findings from the first large-scale observational study in PSP with ^{18}F-PI-2620 indicated significant elevation of tracer binding in PSP target regions with strongest differences in PSP vs control groups in the globus pallidus internus (mean [SD] distribution volume ratios: PSP-RS, 1.21 [0.10]; PSP-non-RS, 1.12 [0.11]; healthy controls, 1.00 [0.08]; Parkinson disease/multiple system atrophy, 1.03 [0.05]; Alzheimer disease, 1.08 [0.06]). Sensitivity and specificity for detection of PSP-RS vs any control group were 85% and 77%, respectively, when using classification by at least 1 positive target region.

CONCLUSIONS AND RELEVANCE This multicenter evaluation indicates a value of ^{18}F-PI-2620 to differentiate suspected patients with PSP, potentially facilitating more reliable diagnosis of PSP.

JAMA Neurol. doi:10.1001/jamaneurol.2020.2526
Published online July 7, 2020.

Supplemental content

Author Affiliations: Author affiliations are listed at the end of this article.

Corresponding author: Matthias Brendel, MD, MHBA, Department of Nuclear Medicine, University of Munich, Marchioninistraße 15, 81377 Munich, Germany (matthias.brendel@med.uni-muenchen.de).

Progressive supranuclear palsy (PSP), initially described by Steele et al,[1] is a primary 4-repeat tauopathy[2] clinically characterized by postural instability with falls and impaired volitional eye movements and leading to death with a median of 8 years after symptom onset.[2] However, clinical symptoms and subtypes of PSP also have strong overlaps with other neurodegenerative disorders such as TDP-43–positive frontotemporal dementia or corticobasal degeneration.[3,4] Thus, clinical assessments in PSP are lacking sensitivity early in the disease course and have a limited specificity for the pathologic entity.[5] Therefore, biomarkers for PSP have a great range of potential utility, for which formal criteria are now available.[6] Current PSP diagnosis criteria already take imaging of atrophy or hypometabolism by magnetic resonance imaging or positron emission tomography (PET) into account.[5] However, no available biomarker currently fulfills the criteria for an ideal biomarker, which would be positive in a presymptomatic stage, specific for any variant of pathology, and anticipate disease progression.[6] As more established readouts (hypometabolism, atrophy) represent late events in the disease course, tau-PET imaging may be able to provide more favorable biomarker information for early detection of PSP. Other tau-PET tracers were reported to be able to differentiate patients with PSP from controls,[7-9] but the observed binding was not confirmed to specifically relate to tau.[10-12] The novel tau-PET tracer ^{18}F-PI-2620 proved absent off-target binding to monoamine oxidases,[13] high affinity to 3/4R tau in Alzheimer disease (AD),[14] but also high affinity to recombinant 4R tau fibrils and PSP brain homogenate,[13] and colocalized binding to proven 4R tau by a combination of micro-autoradiography and immunohistochemistry in PSP tissue.[13]

The main aim of this multicenter evaluation was to investigate the diagnostic capability of ^{18}F-PI-2620 PET imaging in a cohort of patients with clinically diagnosed PSP in vivo. We endeavored to test if patients with PSP can be differentiated from healthy controls and controls with disease by quantitative and visual PET image analyses. Furthermore, we performed postmortem autoradiography from independent brain bank samples to test if the ^{18}F-PI-2620 signal in the basal ganglia and the frontal cortex of PSP can be distinguished and blocked by nonlabeled compound.

Key Points

Question Can tau-positron emission tomography imaging with the novel tau radiotracer ^{18}F-PI-2620 differentiate patients with progressive supranuclear palsy (PSP) from healthy controls and controls with disease?

Findings In this cross-sectional study of 60 patients with PSP, 10 healthy controls, and 20 controls with disease, there was significantly higher ^{18}F-PI-2620 binding in target regions of patients with PSP compared with controls regardless of disease severity. Individual patients with PSP with Richardson syndrome were separated with high sensitivity and specificity.

Meaning ^{18}F-PI-2620 tau-positron emission tomography differentiates patients with PSP from controls at the single-patient level, potentially facilitating a more reliable diagnosis.

Methods

Postmortem Brain Tissue Analyses

Samples from 4 deceased patients with PSP with Richardson syndrome (RS) and those from 4 deceased healthy controls, which were independent from the in vivo cohort, were analyzed by immunohistochemistry and ^{18}F-PI-2620 in vitro autoradiography (2 individuals with PSP-RS and healthy controls each for basal ganglia and frontal cortex evaluation). Autoradiography procedures and more detailed information on cases are provided in the eMethods in the Supplement. Positron emission tomography data analyses and in vitro analyses on human brain samples were approved by the institutional ethics committee at the University Hospital of Munich, LMU Munich, in Munich, Germany. All participants provided written informed consent prior to the PET scan. The observational study was registered at the German Clinical Trials Register (DRKS00016920). Clinical data were collected according to a standardized protocol via the German multicenter prospective ProPSP cohort study.

Investigated Population and Clinical Assessments

Patients with probable or possible PSP according to current diagnosis criteria[5] were examined together with controls with disease and healthy controls at a total of 5 different specialized centers between December 2016 and October 2019. The PSP cohort consisted of patients with PSP-RS and non-RS-variant PSP. The PSP-non-RS group consisted of individuals with predominant corticobasal syndrome, predominant frontal presentation, predominant parkinsonism, predominant speech/language disorder, and progressive gait freezing. Controls with disease were categorized either into suspected α-synucleinopathies or the AD continuum. α-Synucleinopathy controls with disease all had a probable clinical diagnosis[15,16] and consisted of individuals with Parkinson disease and multiple system atrophy. Controls with AD continuum all had a positive β-amyloid PET (^{18}F-florbetaben or ^{18}F-flutemetamol), fulfilled criteria for typical AD,[17] and were composed of individuals with mild cognitive impairment and with dementia. Some individuals of this group had early onset (age <65 years), and others had late-onset disease. Disease duration was defined as the time between symptom onset and PET imaging. The PSP rating scale served as disease severity parameter for the included patients with PSP, and the Montreal Cognitive Assessment (MoCA) or converted Mini-Mental State Examination scores[18] served as a cognition deficit severity parameter. Schwab and England Activities of Daily Living scores were recorded as a global score of function ability.

PET Imaging

^{18}F-PI-2620 PET imaging was performed in a full dynamic setting (0-60 minutes postinjection) at 5 different neuroimaging sites using PET/computed tomography or PET/magnetic resonance imaging systems. Details of radiosynthesis, PET acquisition, reconstruction, framing, image harmonization across scanners, and spatial normalization are provided in the eMethods in the Supplement. The multilinear reference tissue

model 2[19] in PMOD version 3.9 (PMOD Inc) was used to calculate distribution volume ratio images (DVR; DVR = nondisplaceable binding potential + 1) of each full dynamic data set. The cerebellum excluding the dentate nucleus and the central cerebellar white matter as well as the superior and the posterior cerebellar layers (thickness in *z* direction = 1.5 cm each) served as a reference region (eFigure 1 in the Supplement). The clearance rate of the tracer from the reference tissue (k2′) was estimated by parallel running of multilinear reference tissue model.

PET Data Analysis

^{18}F-PI-2620 DVR values were obtained in 9 PSP target regions in the Montreal Neurology Institute space, predefined by the atlas of the basal ganglia,[20] the Brainnetome atlas,[21] and the Hammers atlas,[22] based on earlier autopsy data[23]: globus pallidus (internus and externus), putamen, subthalamic nucleus, substantia nigra, dorsal midbrain, dentate nucleus, dorsolateral prefrontal cortex, and medial prefrontal cortex (eFigure 1 in the Supplement). Additionally, target and reference region values were extracted in single frames to allow calculation of standardized uptake value ratios (SUVr) during the scan time. Thirty- to 60-minute SUVr values were calculated as static ^{18}F-PI-2620 uptake. A dichotomous visual read of DVR maps was performed by 3 expert readers (M.B., H.B., and T.v.E.), as described in the eMethods and in eFigure 2 in the Supplement.

Statistics

SPSS version 25 (IBM) was used for statistical testing. Autoradiography quantification (minimum of 4 slices per sample) of patients with PSP and controls was compared one by one using an unpaired *t* test. Demographics were compared between groups by a 1-way analysis of variance. ^{18}F-PI-2620 DVR values of the target regions were compared between the 5 study groups by a multivariate analysis of variance including age, sex, and center as covariates as well as post hoc Bonferroni correction for multiple group comparisons. Effect sizes (Cohen *d*) were calculated between PSP and control groups. Exploratory comparison of regional DVR *z* scores (*z* Score = [Single DVR of Patient - Mean Value of DVR of Healthy Controls] / SD of DVR of Healthy Controls) between different PSP phenotypes was performed by multivariate analysis of variance (controlled for age, sex, and center) without adjustment for multiple group comparisons. Spearman coefficients of correlation (*r*) were calculated for DVR vs age, PSP rating scale, and disease duration. Pearson coefficient of correlation (*R*) was calculated for DVR and 30- to 60-minute SUVr. *P* values less than .05 were considered significant. For semiquantitative analyses, a regional DVR greater than or equal to the mean value plus 2 SDs of the healthy controls was defined as positive. Here, 1 positive target region defined the participant as positive (dichotomous) for a PSP-like ^{18}F-PI-2620 PET scan.

Results

Postmortem Autoradiography

The unblocked basal ganglia and the frontal cortex of individuals with PSP-RS revealed a visually distinguishable ^{18}F-PI-2620 binding, whereas no binding was observed in healthy controls and after blocking with excessive nonlabeled ^{19}F-PI-2620 in PSP-RS (**Figure 1**A). The ^{18}F-PI-2620 signal was colocalized with AT8-positive aggregated tau (Figure 1A), morphologically attributed to neuronal tau, tufted astrocytes, and coiled bodies.

Quantification revealed increased binding in pairs of individuals with PSP and healthy controls (mean [SD]: globus pallidus internus, 1.60 [0.14] vs 1.07 [0.08]; globus pallidus externus, 1.46 [0.08] vs 0.99 [0.03]; putamen, 1.34 [0.07] vs 1.01 [0.05]; frontal cortex, 1.81 [0.09] vs 1.12 [0.15]; Figure 1B), confirmed by repetition in the second pair (mean [SD]: globus pallidus internus, 1.33 [0.07] vs 0.92 [0.15]; globus pallidus externus, 1.33 [0.11] vs 0.95 [0.13]; putamen, 1.20 [0.04] vs 1.01 [0.07]; frontal cortex, 1.28 [0.12] vs 1.07 [0.14]; eFigure 3 in the Supplement).

Demographics of the In Vivo PET Imaging Population

Of 60 patients with PSP, 40 (66.7%) had RS (22 men [55.0%]; mean [SD] age, 71 [6] years; mean [SD] PSP rating scale score, 38 [15]; score range, 13-71) and 20 had PSP-non-RS (11 men [55.0%]; mean [SD] age, 71 [9] years; mean [SD] PSP rating scale score, 24 [11]; score range, 11-41). Ten healthy controls (2 men; mean [SD] age, 67 [7] years) and 20 controls with disease (of 10 [50.0%] with Parkinson disease and multiple system atrophy, 7 were men; mean [SD] age, 61 [8] years; of 10 [50.0%] with AD, 5 were men; mean [SD] age, 69 [10] years). Demographics and clinical scores of the study cohort are reported in the **Table** and specific information on all subgroups is provided in an extended version (eTable in the Supplement). There was a significant difference in age, indicating that the probable patients with α-synucleinopathy had a lower age (mean [SD], 61 [8] years) compared with both PSP groups (mean [SD] age for individuals with RS: 71 [6] years; mean [SD] age for individuals with non-RS: 71 [9] years). Cognition was significantly different, with the AD-continuum patients yielding a worse cognitive performance (mean [SD] MoCA score, 15.6 [7.8]) compared with individuals with PSP-non-RS (mean [SD] MoCA score, 23.1 [3.9]), α-synucleinopathies (mean [SD] MoCA score, 25.6 [4.1]), and healthy controls (mean [SD] MoCA score, 28.8 [1.6]) but without indicating a significant different cognition compared with PSP-RS (mean [SD] MoCA score, 20.7 [7.5]).

^{18}F-PI-2620 Binding In Vivo

Significant ^{18}F-PI-2620 binding differences among groups were observed for all subcortical PSP target regions except the dorsal midbrain, with strongest differences in the globus pallidus internus. Pairwise group comparisons with post hoc Bonferroni-correction revealed elevated ^{18}F-PI-2620 binding in patients with PSP-RS and PSP-non-RS compared with healthy controls and controls with disease in the globus pallidus internus and externus as well as in the subthalamic nucleus (**Figure 2** and Table). Patients with PSP-RS also indicated higher binding in the putamen, the substantia nigra, and the dentate nucleus compared with healthy controls, whereas patients with PSP-non-RS did not. The dorsolateral prefrontal cortex and the medial prefrontal cortex indicated lower binding in patients with PSP-RS and PSP-non-RS against

Figure 1. In Vitro Evaluation of ^{18}F-PI-2620 Binding in Postmortem Tissue

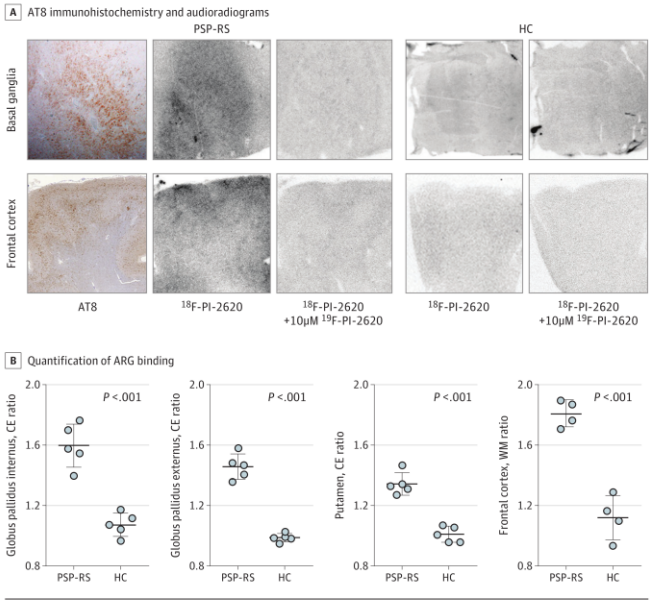

A, The top row depicts AT8 immunohistochemistry together with autoradiograms of basal ganglia slices of a man in his late 60s with a postmortem diagnosis of progressive supranuclear palsy with Richardson syndrome (PSP-RS) after incubation with ^{18}F-PI-2620 alone or with ^{18}F-PI-2620 and excessive cold compound (^{19}F-PI-2620) as well as autoradiograms of basal ganglia slices of a healthy female control in her early 60s. The lower row depicts AT8 immunohistochemistry together with autoradiograms of frontal cortex slices of a woman in her late 60s with a postmortem diagnosis of PSP-RS after incubation with ^{18}F-PI-2620 or ^{18}F-PI-2620 and excessive cold compound (^{19}F-PI-2620) as well as autoradiograms of frontal cortex slices of a healthy male control in his late 30s. B, Quantification of ARG binding by region of interest analysis (basal ganglia: target-to-capsula-externa [CE] ratios; frontal cortex: target-to-white matter [WM] ratios). Four or 5 brain slices of each PSP-RS and healthy control (HC) sample were analyzed and the resulting data were compared by a *t* test. Confirmatory samples are shown in eFigure 3 in the Supplement. Patient details are provided in the eMethods in the Supplement.

patients with AD but no significant binding differences against α-synucleinopathy patients and healthy controls. Exemplary PSP cases with elevated cortical binding are shown in eFigure 4 in the Supplement. For time-activity ratio curves, see eFigure 5 in the Supplement. There was a good to excellent correlation between DVR and 30- to 60-minute SUVr in PSP target regions for the full cohort of 90 individuals (R^2 range, 0.45-0.88; eFigure 6 in the Supplement).

There was no significant correlation of the ^{18}F-PI-2620 DVRs with age for healthy controls or in patients with PSP-RS in PSP target regions with significant elevation in PSP groups, but a significant negative correlation of ^{18}F-PI-2620 DVRs with age for healthy controls in the dorsal midbrain and dorsolateral and medial prefrontal cortices (**Figure 3**A and eFigure 9A in the Supplement). The PSP rating scale values and disease duration were not significantly correlated with ^{18}F-PI-2620 binding in patients with PSP-RS (Figure 3B and C and eFigure 9B and C in the Supplement). A subanalysis of the 16 individuals with PSP-RS with low disease severity (PSP rating scale score, ≤30) indicated similar ^{18}F-PI-2620 DVR effect sizes vs control groups in comparison with the full PSP-RS cohort, as exemplarily reported for the globus pallidus internus (Cohen *d* for individuals with PSP-RS with low disease severity vs full PSP-RS cohort: healthy controls, 2.3 vs 2.3; Parkinson disease/multiple system atrophy, 2.3 vs 2.2; AD, 1.5 vs 1.5).

Among different phenotypes of PSP, the highest ^{18}F-PI-2620 binding was observed in PSP-RS followed by PSP with predominant parkinsonism, PSP with predominant frontal presentation, and PSP with predominant corticobasal syndrome (Figure 3D and E). *z* Scores of ^{18}F-PI-2620 binding in the globus pallidus internus indicated significant differences among PSP phenotypes. Subgroup comparisons revealed higher ^{18}F-PI-2620 DVR *z* scores in PSP-RS compared with PSP with predominant corticobasal syndrome (mean [SD], 2.68 [1.26] vs 1.45 [1.33]).

PSP Diagnosis at the Single-Patient Level

At the single-patient level, 34 of 40 individuals (85%) with PSP-RS and 12 of 20 individuals (60%) with PSP-non-RS were classified as PET-positive by the semiquantitative approach, yielding a sensitivity of 85% for PSP-RS and 65% for PSP-non-RS (**Figure 4**). On the other side, only 1 of 10 individuals with Parkinson disease/multiple system atrophy and 6 of 10 controls with AD were classified as PET-positive in PSP target brain regions, while there was no outlier in the healthy control group. This led to an overall specificity of 77% in the combined 30 controls by the semiquantitative approach. The visual read indicated a sensitivity of 80% for PSP-RS and 55% for PSP-non-RS at a specificity of 83% in the combined 30 controls (Figure 4 and eFigures 7 and 8 in the Supplement). Two individuals with Parkinson disease/multiple system atrophy, 1 with AD, and 2 healthy controls were judged positive for a PSP-like pattern. Interreader and test-retest agreements are reported in the eResults in the Supplement.

Table. Demographics and Quantitative PET Results at the Group Level[a]

Demographic	PSP-RS	PSP-non-RS	α-Synucleinopathies	Individuals with AD	Healthy controls
No.	40	20	10	10	10
Subgroups	NA	PSP-CBS (n = 9), PSP-F (n = 5), PSP-P (n = 4), PSP-SL (n = 1), PSP-PGF (n = 1)	PD (n = 6), MSA (n = 4)	MCI (n = 2), dementia (n = 8)	NA
Age, mean (SD), y	71 (6)	71 (9)	61 (8)	69 (10)	67 (7)
Sex, No. (%)					
Female	18 (45)	9 (45)	3 (30)	5 (50)	8 (80)
Male	22 (55)	11 (55)	7 (70)	5 (50)	2 (20)
Scan site center	MUC (n = 21); LPZ (n = 11); COL (n = 3); MNI (n = 4)	MUC (n = 16); LPZ (n = 4)	MUC (n = 10)	MUC (n = 6); MNI (n = 4)	MNI (n = 5); AUS (n = 5)
PSP rating scale score, mean (SD)	37.2 (15.1)	26.2 (9.6)	NA	NA	NA
PSP, No. (%)					
Possible	6 (15)	12 (60)	NA	NA	NA
Probable	34 (85)	8 (40)	NA	NA	NA
Hoehn and Yahr Scale score, mean (SD)	NA	NA	2.4 (0.8)	NA	NA
UPDRS score, mean (SD)	NA	NA	23.9 (6.2)	NA	NA
Disease duration, mean (SD), mo	49 (38)	42 (37)	20 (17)	28 (29)	NA
MoCA score, mean (SD)	20.7 (7.5)	23.1 (3.9)	25.6 (4.1)	15.6 (7.8)	28.8 (1.6)
SEADL score, mean (SD)	55 (21)	65 (17)	NA	NA	NA
Regional PET results					
Globus pallidus externus					
Mean (SD)	1.16 (0.10)	1.10 (0.11)	1.01 (0.06)	1.05 (0.06)	0.99 (0.05)
Cohen *d*					
Probable α-synucleinopathies	1.83	0.94	NA	NA	NA
AD	1.28	0.47	NA	NA	NA
Healthy controls	2.13	1.20	NA	NA	NA
P value					
Probable α-synucleinopathies	.03	>.99	NA	NA	NA
AD	.01	>.99	NA	NA	NA
Healthy controls	<.001	.02	NA	NA	NA
Globus pallidus internus					
Mean (SD)	1.21 (0.10)	1.12 (0.11)	1.03 (0.05)	1.08 (0.06)	1.00 (0.08)
Cohen *d*					
Probable α-synucleinopathies	2.23	1.08	NA	NA	NA
AD	1.49	0.45	NA	NA	NA
Healthy controls	2.28	1.27	NA	NA	NA
P value					
Probable α-synucleinopathies	.005	>.99	NA	NA	NA
AD	.002	>.99	NA	NA	NA
Healthy controls	<.001	.009	NA	NA	NA
Putamen					
Mean (SD)	1.19 (0.10)	1.14 (0.12)	1.05 (0.06)	1.10 (0.05)	1.02 (0.06)
Cohen *d*					
Probable α-synucleinopathies	1.65	0.93	NA	NA	NA
AD	1.12	0.43	NA	NA	NA
Healthy controls	2.04	1.26	NA	NA	NA
P value					
Probable α-synucleinopathies	.13	>.99	NA	NA	NA
AD	.13	>.99	NA	NA	NA
Healthy controls	.002	.10	NA	NA	NA

(continued)

Table. Demographics and Quantitative PET Results at the Group Level[a] (continued)

Demographic	PSP-RS	PSP-non-RS	α-Synucleinopathies	Individuals with AD	Healthy controls
Subthalamic nucleus					
Mean (SD)	1.21 (0.08)	1.15 (0.09)	1.09 (0.06)	1.10 (0.08)	1.04 (0.09)
Cohen *d*	1.67	0.80	NA	NA	NA
Probable α-synucleinopathies	1.37	0.59	NA	NA	NA
AD	2.02	1.26	NA	NA	NA
Healthy controls					
P value	.06	>.99	NA	NA	NA
Probable α-synucleinopathies	.003	.64	NA	NA	NA
AD	<.001	.005	NA	NA	NA
Substantia nigra					
Mean (SD)	1.17 (0.09)	1.13 (0.09)	1.09 (0.06)	1.12 (0.08)	1.10 (0.07)
Cohen *d*					
Probable α-synucleinopathies	1.08	0.50	NA	NA	NA
AD	0.64	0.14	NA	NA	NA
Healthy controls	0.89	0.35	NA	NA	NA
P value					
Probable α-synucleinopathies	>.99	>.99	NA	NA	NA
AD	.70	>.99	NA	NA	NA
Healthy controls	.04	.53	NA	NA	NA
Dorsal midbrain					
Mean (SD)	0.87 (0.11)	0.89 (0.09)	0.92 (0.07)	0.93 (0.09)	0.92 (0.10)
Cohen *d*					
Probable α-synucleinopathies	−0.50	−0.32	NA	NA	NA
AD	−0.58	−0.43	NA	NA	NA
Healthy controls	−0.54	−0.28	NA	NA	NA
P value					
Probable α-synucleinopathies	>.99	>.99	NA	NA	NA
AD	>.99	>.99	NA	NA	NA
Healthy controls	>.99	>.99	NA	NA	NA
Dentate nucleus					
Mean (SD)	1.13 (0.05)	1.11 (0.05)	1.07 (0.05)	1.08 (0.03)	1.06 (0.04)
Cohen *d*					
Probable α-synucleinopathies	1.26	0.84	NA	NA	NA
AD	1.17	0.67	NA	NA	NA
Healthy controls	1.68	1.18	NA	NA	NA
P value					
Probable α-synucleinopathies	.13	>.99	NA	NA	NA
AD	.08	>.99	NA	NA	NA
Healthy controls	.03	.41	NA	NA	NA
Dorsolateral prefrontal cortex					
Mean (SD)	0.89 (0.09)	0.91 (0.06)	0.91 (0.05)	1.11 (0.24)	0.86 (0.08)
Cohen *d*					
Probable α-synucleinopathies	−0.28	0.09	NA	NA	NA
AD	−1.24	−1.13	NA	NA	NA
Healthy controls	0.28	0.70	NA	NA	NA
P value					
Probable α-synucleinopathies	>.99	>.99	NA	NA	NA
AD	<.001	<.001	NA	NA	NA
Healthy controls	>.99	>.99	NA	NA	NA
Medial prefrontal cortex					
Mean (SD)	0.83 (0.09)	0.86 (0.09)	0.89 (0.06)	0.98 (0.12)	0.89 (0.08)

(continued)

Table. Demographics and Quantitative PET Results at the Group Level[a] (continued)

Demographic	PSP-RS	PSP-non-RS	α-Synucleinopathies	Individuals with AD	Healthy controls
Cohen *d*					
Probable α-synucleinopathies	−0.77	−0.41	NA	NA	NA
AD	−1.39	−1.14	NA	NA	NA
Healthy controls	−0.74	−0.42	NA	NA	NA
P value					
Probable α-synucleinopathies	.91	>.99	NA	NA	NA
AD	<.001	.008	NA	NA	NA
Healthy controls	>.99	>.99	NA	NA	NA

Abbreviations: AD, Alzheimer disease; AUS, Melbourne, Australia; COL, Cologne, Germany; LPZ, Leipzig, Germany; MCI, mild cognitive impairment; MNI, New Haven, Connecticut; MoCA, Montreal Cognitive Assessment; MSA, multiple system atrophy; MUC, Munich, Germany; MV, mean value; NA, not applicable; PD, Parkinson disease; PET, positron emission tomography; PSP, progressive supranuclear palsy; PSP-CBS, PSP with predominant corticobasal syndrome; PSP-F, PSP with predominant frontal presentation; PSP-P, PSP with predominant parkinsonism; PSP-PGF, PSP with predominant gait freezing; PSP-SL, PSP with predominant speech/language disorder; RS, Richardson syndrome; SEADL, Schwab and England Activities of Daily Living; UPDRS, Unified Parkinson Disease Rating Scale.

[a] *P* values were derived from multivariate analysis of variance including center, age, and sex as covariates and Bonferroni adjustment for multiple comparisons of study groups. Effect sizes were calculated as Cohen *d* for both PSP study groups against different control groups.

Discussion

To our knowledge, we present the first comprehensive in vivo evaluation of a tau-PET tracer with improved off-target binding in patients with clinically diagnosed PSP. In vitro autoradiography experiments on postmortem tissue of 4 individuals with PSP obtained independently from PET imaging showed ^{18}F-PI-2620 binding in PSP target regions in colocalization to 4R tau. Our multicenter in vivo data indicate great potential to diagnose patients with suspected PSP using ^{18}F-PI-2620 PET. Dichotomous evaluation at the single-patient level yielded high sensitivity and specificity in strong congruence between semiquantitative and visual approaches for the discrimination between patients with clinically diagnosed PSP and controls. Finally, we gained preliminary evidence that the magnitude of ^{18}F-PI-2620 binding in PSP target regions differs between different PSP phenotypes, thus pointing to the potential of assessing regional phenotype variability in PSP by in vivo PET imaging (eDiscussion in the Supplement).

The regions with elevated ^{18}F-PI-2620 binding in PSP are in line with those found by earlier tau tracers. ^{18}F-flortaucipir and ^{18}F-THK5351 studies found the strongest binding differences for the globus pallidus, the subthalamic nucleus, and the midbrain when comparing individuals with PSP with healthy controls.[7,8,24,25] However, large proportions of the basal ganglia signal of ^{18}F-THK5351 in individuals with PSP and healthy controls were not specific for tau.[26] We observed only minor elevation above a DVR of 1.0 in healthy controls for ^{18}F-PI-2620 in all brain regions apart from the substantia nigra, suggesting low off-target binding for ^{18}F-PI-2620 in PSP target regions. This lower off-target background together with lower variance of tracer binding in PSP target regions of healthy controls for ^{18}F-PI-2620 compared with that of earlier tau PET tracers[8,23] might lead to higher effect sizes in PSP diagnosis. However, proof of this hypothesis would require head-to-head tracer comparison studies. Importantly, we also observed no significant elevations of ^{18}F-PI-2620 binding in basal ganglia regions in suspected tau-negative controls with disease (Parkinson disease/multiple system atrophy) compared with healthy controls. Therefore, a relevant ^{18}F-PI-2620 off-target binding to α-synuclein or coexisting neuroinflammatory processes seems unlikely. However, we still note that regions with elevated in vivo ^{18}F-PI-2620 binding in PSP in our study are known off-target regions of earlier tau ligands. Thus, although the binding in these regions was only low in controls, there could be potential off-target source of a parallel PSP-related pathologic process contributing to the net difference between individuals with PSP and controls. In this regard, it is of interest that no group differences were found in the frontal cortex and the dorsal midbrain in vivo, while in vitro autoradiography revealed a signal in the frontal cortex (eDiscussion in the Supplement). The detailed contributions of possible specific and off-target ^{18}F-PI-2620 signal sources in PSP remain to be elucidated by correlative studies between PET and autopsy. Differing topology of neuropathology among individuals, regional differences in target abundance, and an unfavorable regional target-to-atrophy relationship also need to be considered as a potential reason for lacking regional PET differences in vivo.

In contrast to other PSP target regions, there was an elevated DVR (mean, 1.10) for the substantia nigra, which likely is attributable to neuromelanin off-target binding as shown in vitro for tau PET tracers.[13,27] With regard to disease specificity, we observed a slightly elevated signal in the basal ganglia of some investigated individuals with AD, which has been reported previously.[14] This finding could be explained by a 2019 Japanese autopsy study, which reported on the presence of tau in the basal ganglia of individuals with AD.[28] Potential effects of differing ^{18}F-PI-2620 binding affinity to 3/4R and 4R tau on the observed basal ganglia signal in AD and on the reported time-activity curves are discussed in the eDiscussion in the Supplement. Identification of an AD-like pattern appeared to be the main advantage of a visual PSP classification, as it facilitated negation of a PSP-like pattern by the reader despite semiquantitative positivity of basal ganglia or frontal cortex target regions. Thus, a combination of both the semiquantitative and visual PET data analysis approaches could increase the specificity for PSP identification when AD is a potential differential diagnosis.

Figure 2. ^{18}F-PI-2620 Binding in Predefined PSP Target Regions

A Average ^{18}F-PI-2620 distribution volume ratio

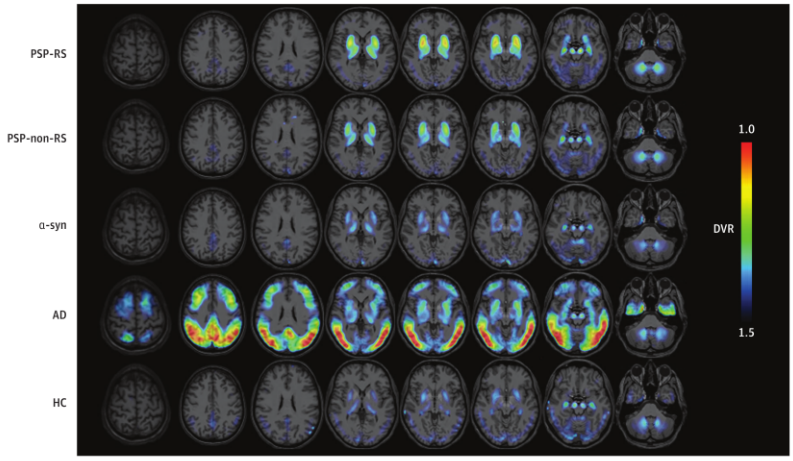

B Average ^{18}F-PI-2620 distribution volume ratio comparisons

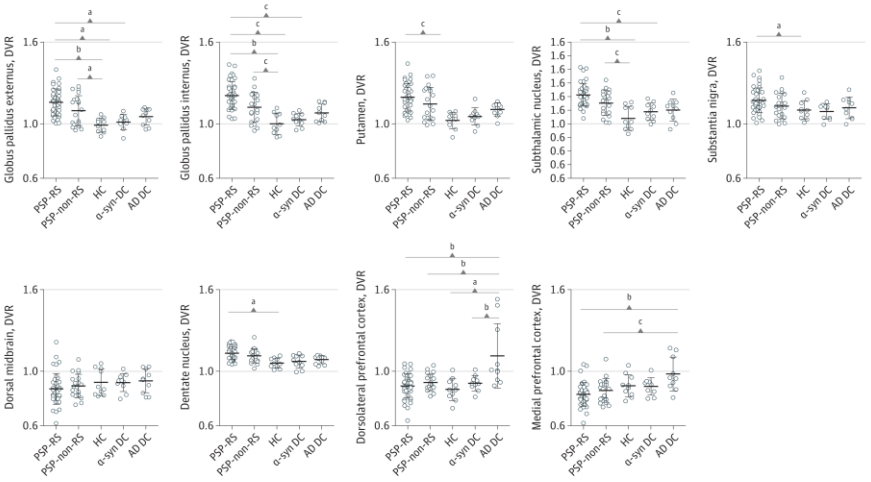

A, Average ^{18}F-PI-2620 distribution volume ratio (DVR) binding maps presented as axial overlays on a standard magnetic resonance imaging template for all study groups. Extracerebral voxels were masked. B, ^{18}F-PI-2620 DVR comparison between different study groups for the 9 evaluated progressive supranuclear palsy (PSP) target regions. Statistics derive from multivariate analysis of variance including center, age, and sex as covariates and Bonferroni adjustment for multiple comparisons. Error bars indicate mean (SD).

α-syn indicates probable α-synucleinopathies; AD, Alzheimer disease; DC, controls with disease; HC, healthy controls; RS, Richardson syndrome.

[a] $P < .050$.

[b] $P < .001$.

[c] $P < .010$.

Figure 3. Association of ^{18}F-PI-2620 Binding With Age, Disease Severity, Disease Duration, and Phenotype

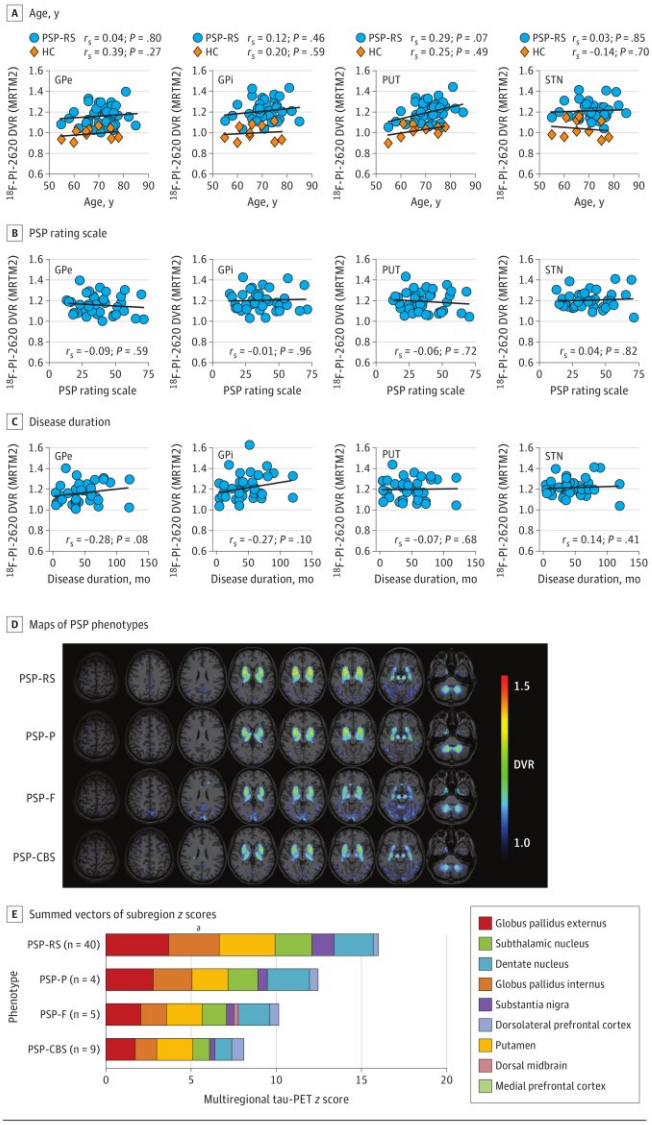

^{18}F-PI-2620 binding as a function of age (A), disease severity (B), and disease duration (C), expressed as correlation plots. Additional plots are in eFigure 9 in the Supplement. r_S indicates Spearman coefficients of correlations. Average ^{18}F-PI-2620 distribution volume ratio (DVR) maps of different progressive supranuclear palsy (PSP) phenotypes illustrated by axial slice overlays on a standard magnetic resonance imaging template (D) and quantified by summed vectors of subregion *z* scores (E). GPe indicates globus pallidus externus; GPi, globus pallidus internus; HC, healthy controls; MRTM2, multilinear reference tissue modeling 2; PSP-CBS, PSP with predominant corticobasal syndrome; PSP-F, PSP with predominant frontal presentation; PSP-P, PSP with predominant parkinsonism; PSP-RS, PSP with Richardson syndrome; PUT, putamen; STN, subthalamic nucleus.

[a] Significantly differing regional ^{18}F-PI-2620 binding among PSP subtypes.

Figure 4. Evaluation of ^{18}F-PI-2620 for Detection of Progressive Supranuclear Palsy (PSP) at the Single-Patient Level

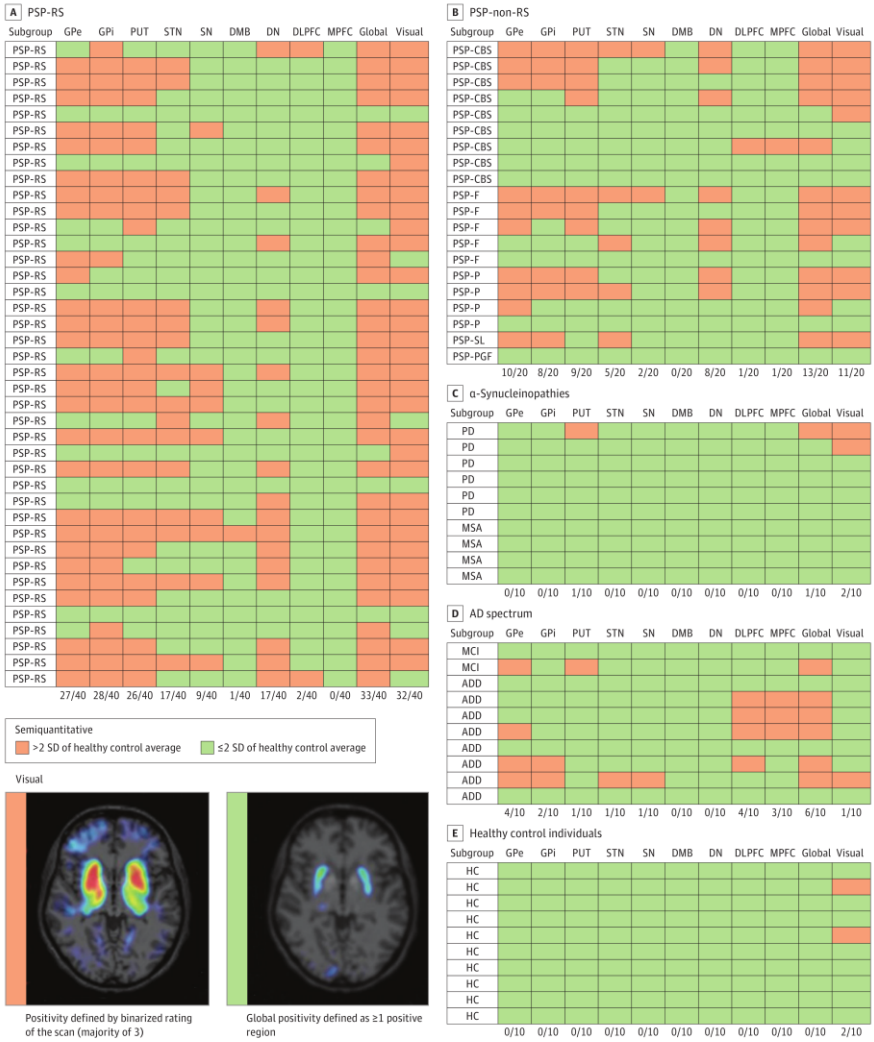

Semiquantitative classification of PSP target regions. A single region defined the scan as global positive. Visual classification was performed by dichotomous rating of the ^{18}F-PI-2620 scan by 3 raters, who defined positivity/negativity for a PSP-like pattern. The bottom of each panel indicates the number of positive regions and total regions. AD indicates Alzheimer disease; ADD, dementia due to AD; DLPFC, dorsolateral prefrontal cortex; DMB, dorsal midbrain; DN, dentate nucleus; GPe, globus pallidus externus; GPi, globus pallidus internus; HC, healthy controls; MCI, mild cognitive impairment due to AD; MPFC, medial prefrontal cortex; MSA, multiple system atrophy; PD, Parkinson disease; PUT, putamen; PSP-CBS, PSP with predominant corticobasal syndrome; PSP-F, PSP with predominant frontal presentation; PSP-P, PSP with predominant parkinsonism; PSP-PGF, PSP with progressive gait freezing; PSP-RS, PSP with Richardson Syndrome; PSP-SL, PSP with predominant speech/language impairment; SN, substantia nigra; STN, subthalamic nucleus.

Interestingly, we did not observe a correlation between ^{18}F-PI-2620 binding and clinical severity or disease duration in any of the target regions for patients with PSP-RS. Previous correlative results between tau-PET tracer binding and PSP disease severity have been inconsistent, showing no[7] or positive association.[8,25] Especially for ^{18}F-THK5351, this could be explained by increased monoaminoxidase-B expression in this disorder as a neuroinflammation event. Loss of tracer signal due to partial volume effects caused by increasing atrophy could potentially mask effects in individuals with PSP with long disease duration. Thus, the use of partial volume effect correction on ^{18}F-PI-2620 PET data to diagnose PSP will be an interesting task of future studies. Furthermore, there is limited autopsy data investigating tau deposition in PSP as a function of disease duration.[23] However, longitudinal in vivo imaging data on PSP clearly indicated changes over time in magnetic resonance imaging measures of atrophy but only minor changes of ^{18}F-flortaucipir binding.[29] In summary, large-scale longitudinal studies are needed to investigate the value of ^{18}F-PI-2620 as a progression biomarker in PSP.

Limitations

Among the limitations of our study, the small number of participants needs to be considered. This might mask effects such as age dependency of tracer binding at the current stage. Further, given the nature of an observational multicenter evaluation, we cannot fully rule out effects of disproportional distribution of study groups and phenotype subgroups among centers. Center bias was mitigated by harmonization of the PET data across all sites and inclusion of the center as a covariate in the statistical analyses.

Unpublished analyses by the authors reveal a higher off-rate for ^{18}F-PI-2620 from 4R tau when compared with 3/4R tau, which deserves more detailed investigation of binding characteristics. We are aware of the missing autopsy data. Nearly all patients are still alive, and no brains have been donated so far. Thus, we have no pathologic validation of tau positivity for our in vivo results and potential clinical misdiagnoses, especially in the non-RS-PSP cohort, need to be taken into consideration. The current study provides the opportunity of follow-up ^{18}F-PI-2620 imaging to study disease progression.

Conclusions

This multicenter evaluation indicates that ^{18}F-PI-2620 PET imaging can aid in diagnosing and differentiating patients with suspected PSP, potentially facilitating a more reliable diagnosis of PSP. Additional studies need to focus on autopsy validation and longitudinal imaging to test if this radiotracer also has potential as a PSP progression biomarker.

ARTICLE INFORMATION

Accepted for Publication: May 1, 2020.

Published Online: July 7, 2020. doi:10.1001/jamaneurol.2020.2526

Author Affiliations: Department of Nuclear Medicine, University Hospital of Munich, LMU Munich, Munich, Germany (Brendel, Beyer, Song, Sauerbeck, Nitschmann, Zach, Bartenstein); Department of Nuclear Medicine, University of Leipzig, Leipzig, Germany (Barthel, Rullmann, Schildan, Patt, Sabri); Department of Nuclear Medicine, University Hospital Cologne, Cologne, Germany (van Eimeren, Hammes, Neumaier, Drzezga); Department of Neurology, University Hospital Cologne, Cologne, Germany (van Eimeren, Barbe, Onur); German Center for Neurodegenerative Diseases (DZNE), Bonn-Cologne, Germany (van Eimeren, Jessen, Drzezga); InviCRO LLC, Boston, Massachusetts (Marek, Barret, Madonia, Russell, Seibyl); Molecular Neuroimaging, A Division of InviCRO, New Haven, Connecticut (Marek, Barret, Madonia, Russell, Seibyl); Department of Neurology, University Hospital of Munich, LMU Munich, Munich, Germany (Palleis, Gehmeyr, Fietzek, Bötzel, Levin); Department of Neurology, Hannover Medical School, Hannover, Germany (Respondek, Höglinger); Department of Psychiatry, University Hospital Cologne, Cologne, Germany (Jessen); Center for Memory Disorders, University Hospital Cologne, Cologne, Germany (Jessen); Department of Neurology, University of Leipzig, Leipzig, Germany (Saur, Rumpf, Classen); Clinic for Cognitive Neurology, University of Leipzig, Leipzig, Germany (Schroeter); LIFE-Leipzig Research Center for Civilization Diseases, University of Leipzig, Leipzig, Germany (Schroeter); Max Planck Institute for Human Cognitive and Brain Sciences, Leipzig, Germany (Schroeter); Forschungszentrum Jülich GmbH, Institute of Neuroscience and Medicine, Nuclear Chemistry (INM-5), Jülich, Germany (Neumaier, Drzezga); Life Molecular Imaging GmbH, Berlin, Germany (Stephens); Center for Neuropathology and Prion Research, University Hospital of Munich, LMU Munich, Munich, Germany (Roeber, Herms); German Center for Neurodegenerative Diseases (DZNE), Munich, Germany (Herms, Levin, Höglinger); Munich Cluster for Systems Neurology (SyNergy), Munich, Germany (Bartenstein, Höglinger); Department of Molecular Imaging & Therapy, Austin Health, Heidelberg, Victoria, Australia (Villemagne); Department of Medicine, Austin Health, The University of Melbourne, Melbourne, Victoria, Australia (Villemagne); Department of Neurology, Technical University Munich, Munich, Germany (Höglinger).

Author Contributions: Dr Brendel had full access to all of the data in the study and takes responsibility for the integrity of the data and the accuracy of the data analysis. Drs Brendel, Barthel, and van Eimeren contributed equally.
Concept and design: Brendel, Barthel, van Eimeren, Marek, Barret, Russell, Stephens, Herms, Bartenstein, Levin, Höglinger, Drzezga, Sabri.
Acquisition, analysis, or interpretation of data: Brendel, Barthel, van Eimeren, Marek, Beyer, Song, Palleis, Gehmeyr, Fietzek, Respondek, Sauerbeck, Nitschmann, Zach, Hammes, Barbe, Onur, Jessen, Saur, Schroeter, Rumpf, Rullmann, Schildan, Patt, Neumaier, Barret, Madonia, Russell, Roeber, Boetzel, Classen, Bartenstein, Villemagne, Höglinger, Drzezga, Seibyl, Sabri.
Drafting of the manuscript: Brendel, Barthel, van Eimeren, Nitschmann, Zach, Schildan, Madonia, Drzezga, Sabri.
Critical revision of the manuscript for important intellectual content: Brendel, Barthel, van Eimeren, Marek, Beyer, Song, Palleis, Gehmeyr, Fietzek, Respondek, Sauerbeck, Hammes, Barbe, Onur, Jessen, Saur, Schroeter, Rumpf, Rullmann, Patt, Neumaier, Barret, Madonia, Russell, Stephens, Roeber, Herms, Boetzel, Classen, Bartenstein, Villemagne, Levin, Höglinger, Drzezga, Seibyl, Sabri.
Statistical analysis: Brendel, Barthel, Song, Fietzek, Nitschmann, Rullmann, Madonia, Sabri.
Obtained funding: Schroeter, Bartenstein, Höglinger.
Administrative, technical, or material support: van Eimeren, Marek, Beyer, Palleis, Gehmeyr, Sauerbeck, Zach, Hammes, Barbe, Onur, Jessen, Schroeter, Patt, Neumaier, Barret, Russell, Stephens, Roeber, Bartenstein, Levin, Drzezga, Seibyl, Sabri.
Supervision: Brendel, Barthel, van Eimeren, Marek, Barret, Russell, Herms, Boetzel, Bartenstein, Villemagne, Levin, Höglinger, Drzezga, Seibyl, Sabri.

Conflict of Interest Disclosures: Dr Brendel reported personal fees from Life Molecular Imaging and personal fees from GE Healthcare outside the submitted work. Dr van Eimeren reported personal fees from Lundbeck and Eli Lilly outside the submitted work; Life Molecular Imaging provided the precursor for PI-2620 free of charge as part of a research collaboration agreement. Dr Marek reported other support from GE Healthcare, Life Molecular Imaging, Roche, Takeda, Lundbeck, NeuroDerm, UCB, Denali, and InviCRO outside the submitted work. Dr Fietzek reported personal fees from Ipsen and Allergan outside the submitted work.

Dr Respondek reported serving on the advisory boards for UCB and Biogen. Dr Barbe reported grants from Medtronic and Boston Scientific and personal fees from Medtronic, St Jude, UCB, Bial, GE Healthcare, and Institute for Quality and Efficiency in Health Care outside the submitted work. Dr Jessen reported personal fees from Eisai, Biogen, GE Healthcare, Roche, and AC Immune outside the submitted work. Dr Patt reported grants from Life Molecular Imaging during the conduct of the study. Dr Barret reported other support from Piramal during the conduct of the study. Dr Russell reported other from InviCRO during the conduct of the study. Dr Stephens reported personal fees from Life Molecular Imaging outside the submitted work. Dr Villemagne reported grants from Piramal Imaging during the conduct of the study and personal fees from Shanghai Green Valley outside the submitted work. Dr Levin reported nonfinancial support from AbbVie and personal fees from MODAG GmbH, Axon Neuroscience, Bayer, Thieme Medical Publishers, and Kohlhammer GmbH Medical Publishers outside the submitted work. Dr Höglinger reported personal fees from AbbVie, Asceneuron, Biogen, Biohaven, Lundbeck, Novartis, Roche, Sanofi, and UCB outside the submitted work. Dr Drzezga reported nonfinancial support from Life Molecular Imaging during the conduct of the study; grants and personal fees from Siemens Healthineers, personal fees and nonfinancial support from Avid/Eli Lilly, and personal fees and nonfinancial support from GE Healthcare outside the submitted work. Dr Seibyl reported other support from InviCRO and Life Molecular Imaging during the conduct of the study and other support from Roche and Biogen outside the submitted work. No other disclosures were reported.

Funding/Support: Life Molecular Imaging provided material support for the manufacturing of PI-2620 and financial support to separate studies from which data are included in this analysis. Dr Höglinger was funded by the Deutsche Forschungsgemeinschaft (German Research Foundation) under Germany's Excellence Strategy within the framework of the Munich Cluster for Systems Neurology (EXC 2145 SyNergy; No. 390857198) and the NOMIS Foundation (FTLD project). This project was supported by the German Center for Neurodegenerative Diseases (DZNE; DescribePSP Study) and the German Parkinson's Association (DPG; ProPSP Study).

Role of the Funder/Sponsor: Life Molecular Imaging was involved in the analysis and interpretation of the data. The other funders had no role in the design and conduct of the study; collection, management, analysis, and interpretation of the data; preparation, review, or approval of the manuscript; and decision to submit the manuscript for publication.

Meeting Presentation: This paper was presented at NuklearMedizin 2020-Digital; July 7, 2020; online presentation.

Additional Contributions: We thank all patients, their caregivers, and cyclotron, radiochemistry, and positron emission tomography imaging crews.

REFERENCES

1. Steele JC, Richardson JC, Olszewski J. Progressive supranuclear palsy: a heterogeneous degeneration involving the brain stem, basal ganglia and cerebellum with vertical gaze and pseudobulbar palsy, nuchal dystonia and dementia. *Arch Neurol*. 1964;10:333-359. doi:10.1001/archneur.1964.00460160003001

2. Rösler TW, Tayaranian Marvian A, Brendel M, et al. Four-repeat tauopathies. *Prog Neurobiol*. 2019;180:101644. doi:10.1016/j.pneurobio.2019.101644

3. Williams DR, Lees AJ. Progressive supranuclear palsy: clinicopathological concepts and diagnostic challenges. *Lancet Neurol*. 2009;8(3):270-279. doi:10.1016/S1474-4422(09)70042-0

4. Boxer AL, Yu JT, Golbe LI, Litvan I, Lang AE, Höglinger GU. Advances in progressive supranuclear palsy: new diagnostic criteria, biomarkers, and therapeutic approaches. *Lancet Neurol*. 2017;16(7):552-563. doi:10.1016/S1474-4422(17)30157-6

5. Höglinger GU, Respondek G, Stamelou M, et al; Movement Disorder Society-endorsed PSP Study Group. Clinical diagnosis of progressive supranuclear palsy: the movement disorder society criteria. *Mov Disord*. 2017;32(6):853-864. doi:10.1002/mds.26987

6. van Eimeren T, Antonini A, Berg D, et al. Neuroimaging biomarkers for clinical trials in atypical parkinsonian disorders: proposal for a neuroimaging biomarker utility system. *Alzheimers Dement (Amst)*. 2019;11:301-309. doi:10.1016/j.dadm.2019.01.011

7. Schonhaut DR, McMillan CT, Spina S, et al. ^{18}F-flortaucipir tau positron emission tomography distinguishes established progressive supranuclear palsy from controls and Parkinson disease: A multicenter study. *Ann Neurol*. 2017;82(4):622-634. doi:10.1002/ana.25060

8. Brendel M, Schönecker S, Höglinger G, et al. [^{18}F]-THK5351 PET correlates with topology and symptom severity in progressive supranuclear palsy. *Front Aging Neurosci*. 2018;9:440. doi:10.3389/fnagi.2017.00440

9. Passamonti L, Vázquez Rodríguez P, Hong YT, et al. 18F-AV-1451 positron emission tomography in Alzheimer's disease and progressive supranuclear palsy. *Brain*. 2017;140(3):781-791. doi:10.1093/brain/aww340

10. Ishiki A, Harada R, Kai H, et al. Neuroimaging-pathological correlations of [^{18}F]THK5351 PET in progressive supranuclear palsy. *Acta Neuropathol Commun*. 2018;6(1):53. doi:10.1186/s40478-018-0556-7

11. Marquié M, Normandin MD, Meltzer AC, et al. Pathological correlations of [F-18]-AV-1451 imaging in non-Alzheimer tauopathies. *Ann Neurol*. 2017;81(1):117-128. doi:10.1002/ana.24844

12. Marquié M, Verwer EE, Meltzer AC, et al. Lessons learned about [F-18]-AV-1451 off-target binding from an autopsy-confirmed Parkinson's case. *Acta Neuropathol Commun*. 2017;5(1):75. doi:10.1186/s40478-017-0482-0

13. Kroth H, Oden F, Molette J, et al. Discovery and preclinical characterization of [^{18}F]PI-2620, a next-generation tau PET tracer for the assessment of tau pathology in Alzheimer's disease and other tauopathies. *Eur J Nucl Med Mol Imaging*. 2019;46(10):2178-2189. doi:10.1007/s00259-019-04397-2

14. Mueller A, Bullich S, Barret O, et al. Tau PET Imaging with ^{18} F-PI-2620 in patients with Alzheimer disease and healthy controls: a first-in-humans study. *J Nucl Med*. 2020;61(6):911-919. doi:10.2967/jnumed.119.236224

15. Gilman S, Wenning GK, Low PA, et al. Second consensus statement on the diagnosis of multiple system atrophy. *Neurology*. 2008;71(9):670-676. doi:10.1212/01.wnl.0000324625.00404.15

16. Postuma RB, Berg D, Stern M, et al. MDS clinical diagnostic criteria for Parkinson's disease. *Mov Disord*. 2015;30(12):1591-1601. doi:10.1002/mds.26424

17. Dubois B, Feldman HH, Jacova C, et al. Advancing research diagnostic criteria for Alzheimer's disease: the IWG-2 criteria. *Lancet Neurol*. 2014;13(6):614-629. doi:10.1016/S1474-4422(14)70090-0

18. Lawton M, Kasten M, May MT, et al. Validation of conversion between mini-mental state examination and Montreal cognitive assessment. *Mov Disord*. 2016;31(4):593-596. doi:10.1002/mds.26498

19. Ichise M, Liow JS, Lu JQ, et al. Linearized reference tissue parametric imaging methods: application to [11C]DASB positron emission tomography studies of the serotonin transporter in human brain. *J Cereb Blood Flow Metab*. 2003;23(9):1096-1112. doi:10.1097/01.WCB.0000085441.37552.CA

20. Keuken MC, Bazin PL, Backhouse K, et al. Effects of aging on T_1, T_2*, and QSM MRI values in the subcortex. *Brain Struct Funct*. 2017;222(6):2487-2505. doi:10.1007/s00429-016-1352-4

21. Fan L, Li H, Zhuo J, et al. The Human Brainnetome Atlas: a new brain atlas based on connectional architecture. *Cereb Cortex*. 2016;26(8):3508-3526. doi:10.1093/cercor/bhw157

22. Hammers A, Allom R, Koepp MJ, et al. Three-dimensional maximum probability atlas of the human brain, with particular reference to the temporal lobe. *Hum Brain Mapp*. 2003;19(4):224-247. doi:10.1002/hbm.10123

23. Williams DR, Holton JL, Strand C, et al. Pathological tau burden and distribution distinguishes progressive supranuclear palsy-parkinsonism from Richardson's syndrome. *Brain*. 2007;130(Pt 6):1566-1576. doi:10.1093/brain/awm104

24. Cho H, Choi JY, Hwang MS, et al. Subcortical ^{18} F-AV-1451 binding patterns in progressive supranuclear palsy. *Mov Disord*. 2017;32(1):134-140. doi:10.1002/mds.26844

25. Whitwell JL, Lowe VJ, Tosakulwong N, et al. [^{18} F]AV-1451 tau positron emission tomography in progressive supranuclear palsy. *Mov Disord*. 2017;32(1):124-133. doi:10.1002/mds.26834

26. Lemoine L, Gillberg PG, Svedberg M, et al. Comparative binding properties of the tau PET tracers THK5117, THK5351, PBB3, and T807 in postmortem Alzheimer brains. *Alzheimers Res Ther*. 2017;9(1):96. doi:10.1186/s13195-017-0325-z

27. Aguero C, Dhaynaut M, Normandin MD, et al. Autoradiography validation of novel tau PET tracer [F-18]-MK-6240 on human postmortem brain tissue. *Acta Neuropathol Commun*. 2019;7(1):37. doi:10.1186/s40478-019-0686-6

28. Hamasaki H, Honda H, Suzuki SO, et al. Tauopathy in basal ganglia involvement is exacerbated in a subset of patients with Alzheimer's disease: the Hisayama study. *Alzheimers Dement (Amst)*. 2019;11:415-423. doi:10.1016/j.dadm.2019.04.008

29. Whitwell JL, Tosakulwong N, Schwarz CG, et al. MRI outperforms [18F]AV-1451 PET as a longitudinal biomarker in progressive supranuclear palsy. *Mov Disord*. 2019;34(1):105-113. doi:10.1002/mds.27546

6. Paper II

nature COMMUNICATIONS

ARTICLE

https://doi.org/10.1038/s41467-022-28896-3 OPEN

Tau deposition patterns are associated with functional connectivity in primary tauopathies

Nicolai Franzmeier[1,36✉], Matthias Brendel[2,3,36], Leonie Beyer[2], Luna Slemann[2], Gabor G. Kovacs[4,5,6], Thomas Arzberger[3,7,8,9], Carolin Kurz[7,8], Gesine Respondek[7,10,11], Milica J. Lukic[7,12], Davina Biel[1], Anna Rubinski[1], Lukas Frontzkowski[1], Selina Hummel[2], Andre Müller[13], Anika Finze[2], Carla Palleis[3,7,14], Emanuel Joseph[2], Endy Weidinger[14], Sabrina Katzdobler[14], Mengmeng Song[2], Gloria Biechele[2], Maike Kern[2], Maximilian Scheifele[2], Boris-Stephan Rauchmann[15], Robert Perneczky[3,7,8,16], Michael Rullman[17], Marianne Patt[17], Andreas Schildan[17], Henryk Barthel[17], Osama Sabri[17], Jost J. Rumpf[2,18], Matthias L. Schroeter[2,18], Joseph Classen[19], Victor Villemagne[20,21,22], John Seibyl[23,24], Andrew W. Stephens[13], Edward B. Lee[4], David G. Coughlin[25,26], Armin Giese[9], Murray Grossman[25,27], Corey T. McMillan[25,27], Ellen Gelpi[28,29], Laura Molina-Porcel[28,29], Yaroslau Compta[30], John C. van Swieten[31], Laura Donker Laat[32], Claire Troakes[33], Safa Al-Sarraj[33], John L. Robinson[4], Sharon X. Xie[34], David J. Irwin[10,27], Sigrun Roeber[9], Jochen Herms[7], Mikael Simons[7], Peter Bartenstein[2], Virginia M. Lee[4], John Q. Trojanowski[4], Johannes Levin[3,7,14], Günter Höglinger[7,35,37] & Michael Ewers[1,7,37]

Tau pathology is the main driver of neuronal dysfunction in 4-repeat tauopathies, including cortico-basal degeneration and progressive supranuclear palsy. Tau is assumed to spread prion-like across connected neurons, but the mechanisms of tau propagation are largely elusive in 4-repeat tauopathies, characterized not only by neuronal but also by astroglial and oligodendroglial tau accumulation. Here, we assess whether connectivity is associated with 4R-tau deposition patterns by combining resting-state fMRI connectomics with both 2nd generation ^{18}F-PI-2620 tau-PET in 46 patients with clinically diagnosed 4-repeat tauopathies and post-mortem cell-type-specific regional tau assessments from two independent progressive supranuclear palsy patient samples ($n = 97$ and $n = 96$). We find that inter-regional connectivity is associated with higher inter-regional correlation of both tau-PET and post-mortem tau levels in 4-repeat tauopathies. In regional cell-type specific post-mortem tau assessments, this association is stronger for neuronal than for astroglial or oligodendroglial tau, suggesting that connectivity is primarily associated with neuronal tau accumulation. Using tau-PET we find further that patient-level tau patterns are associated with the connectivity of subcortical tau epicenters. Together, the current study provides combined in vivo tau-PET and histopathological evidence that brain connectivity is associated with tau deposition patterns in 4-repeat tauopathies.

A full list of author affiliations appears at the end of the paper.

Progressive supranuclear palsy (PSP) and cortico-basal degeneration (CBD) are primary 4-repeat (4 R) tauopathies characterized by glial and neuronal 4R-tau inclusions, manifesting as progressive movement and cognitive disorders[1–4]. In PSP and CBD, 4R-tau pathology accumulates initially in the brainstem and subcortex, with subsequent cortical manifestation at more advanced disease stages[5, 6].

Postmortem studies have reported a strong clinico-pathological correlation between 4R-tau deposition patterns and clinical phenotype: PSP most commonly presents as Richardson's syndrome (PSP-RS, i.e., a combination of postural instability and ocular motor deficits), associated with brainstem and subcortical tau followed by progressive tau accumulation in parietal and motor cortices at later disease stages[7, 8]. Further variant predominance types include, among others, PSP with speech/language disorder with left inferior frontal tau aggregation or PSP with cognitive/behavioral presentation with fronto-temporal tau pathology, suggesting that clinical variability is driven by spatially heterogeneous tau patterns[8–10]. In accord with this concept, CBD patients often present with mixed cortical/movement disorders termed cortico-basal syndrome (CBS), associated with tau accumulation in the motor cortex, brainstem, subthalamic nucleus, and striatum, yet clinical variants present as progressive aphasia, frontal-behavioral syndrome or Richardson's syndrome[11, 12]. Since 4 R tau deposition patterns in PSP and CBD are considered key determinants of disease phenotype and progression, a detailed understanding of the mechanisms that facilitate tau spreading is of pivotal clinical interest.

There is converging preclinical evidence suggesting cell-to-cell tau pathology transmission across functionally interconnected neurons:[13] First, pathological tau strains obtained from patients with primary or secondary tauopathies have been shown to induce template-based misfolding of physiological tau, suggesting prion-like tau propagation[14, 15]. Second, injection of pathological tau seeds in mouse brains triggers tau spread to regions anatomically connected to the injection site rather than tau diffusion to spatially adjacent regions[15–19]. Third, synapses and neuronal activity are considered to be key drivers of tau spreading[20, 21], where opto-genetically enhanced activity of tau harboring neurons is associated with accelerated trans-synaptic tau spreading in vitro and in vivo[22]. Collectively, these preclinical findings provide strong support for neuronal connectivity as a key route for tau spreading in tauopathies. However, it remains unclear whether tau pathology progresses preferentially between connected brain regions in human 4 R tauopathies. This spreading mechanism needs to be specifically questioned in 4 R tauopathies since tau is exclusively present not only in neurons but also in astroglia and oligodendroglia[8].

Here, we combined in vivo tau-PET and postmortem tau assessments from 4 R tauopathy patients with fMRI-based connectivity assessments obtained in a healthy reference sample. Using ^{18}F-PI-2620 PET for tau imaging in clinically diagnosed CBS ($n = 24$) and PSP-RS patients ($n = 22$), we tested if (i) functionally connected brain regions show correlated ^{18}F-PI-2620 PET levels and whether (ii) brain-wide tau-PET uptake patterns are associated with the functional connectivity pattern of subcortical epicenters with highest tau pathology. In CBS, which is typically associated with more widespread cortical tau[23], we further tested whether subthreshold cortical Aβ levels may enhance the spread of tau-PET from subcortical tau epicenters to the cortex. This analysis was motivated by previous reports showing clinical and pathophysiological overlap between CBS and AD[24], where a substantial number of clinical CBS cases had co-occurring Aβ pathology[23, 25], i.e., a key driver of cortical tau spreading in AD[26]. In a key validation step, we translated the in vivo tau-PET analyses to two independent postmortem samples (Munich-European consortium/collection): $n = 97$, University of Pennsylvania [UPENN]: $n = 96$) with confirmed PSP pathology and gold-standard regional histopathological 4 R tau assessments and further performed in vitro binding assays and autoradiographic analyses that support PI-2620 binding to 4 R tau. Inclusion of this postmortem sample allowed cell-type-specific stratification of tau pathology (i.e., neuronal, astroglial, and oligodendroglial tau) to specifically test the hypothesis that inter-regional connectivity is associated with the deposition of neuronal tau pathology. By combining cell-type-specific postmortem tau assessments with atlas-based functional connectivity data, we tested the hypothesis that higher functional connectivity between postmortem sampled brain regions is associated with more correlated tau levels, and that this association is primarily driven by neuronal tau. Our results confirm that functional connectivity is associated with subcortical and cortical tau-PET patterns in PSP and CBS patients and that the association between functional connectivity and histopathologically assessed tau is strongest for neuronal tau levels.

Results

We obtained tau-PET in 46 patients with clinically suspected 4 R tauopathies, including 24 CBS patients, 22 PSP-RS patients, and 15 cognitively normal controls (CN). All subjects underwent 3 T structural MRI and ^{18}F-PI-2620 PET imaging[27]. Aβ-positive CBS patients (as determined by cerebrospinal fluid Aβ levels or amyloid-PET, which was available for all CBS cases) were considered to have underlying 3 R/4 R tau AD pathology and were therefore excluded from the current study[28]. Sample characteristics are presented in Table 1. Group-average ^{18}F-PI-2620 SUVR maps intensity normalized to the inferior cerebellar gray matter are shown in Fig. 1 for CN (Fig. 1A), PSP-RS (Fig. 1B) and CBS (Fig. 1C). For neuropathological validation of the tau-PET data, we included regional postmortem tau assessments from two independent samples (Munich-European consortium/collection sample, $n = 97$; UPENN sample, $n = 96$) with histopathologically confirmed PSP, defined as the presence of neurofibrillary tau tangles (NFT) in the subthalamic nucleus, substantia nigra, and globus pallidus together with tufted astrocytes in the striatum and frontal cortex[3, 8]. In addition, we included postmortem data from 16 patients with histopathologically confirmed PSP for autoradiographic assessment of PI-2620 binding to tau pathology. For functional connectivity, we included resting-state fMRI data of 69 cognitively normal subjects from the Alzheimer's disease neuroimaging initiative (ADNI, age = 67.89 ± 5.88, sex[f/m] = 39/30) cohort without evidence of amyloid or tau pathology as indicated by ^{18}F-florbetapir amyloid-PET and ^{18}F-flortaucipir tau-PET[29, 30]. Age and sex in the ADNI resting-state fMRI sample were not statistically different from age and sex distributions in the PSP-RS or CBS groups ($p > 0.05$).

Elevated tau-PET binding in PSP-RS/CBS. First, we assessed ^{18}F-PI-2620 PET binding in CBS and PSP-RS patients vs. CN, using voxel-wise ANCOVAs, controlling for age, sex, and study site (alpha-threshold = 0.005, cluster-extent threshold > 100 voxels). Compared to CN, PSP-RS patients showed higher subcortical and inferior frontal tau-PET binding (Fig. 1D), congruent with previous work in a partly overlapping sample[27]. In CBS[31], we not only found significantly elevated subcortical, brainstem, and inferior frontal^{18}F-PI-2620 PET binding but also more widespread occipital, frontal, and parietal elevations of ^{18}F-PI-2620 PET binding (Fig. 1E). When comparing ^{18}F-PI-2620 PET between CBS and PSP (Fig. 1F), we found higher cortical ^{18}F-PI-2620 PET binding in CBS in the midbrain, entorhinal and lateral temporal cortex, motor cortex, anterior cingulate, frontal eye

Table 1 Subject demographics.

Tau-PET sample ($N = 61$)

	Controls ($n = 15$)	PSP-RS ($n = 22$)	CBS ($n = 24$)	P
Age	62.67 ± 8.97[b]	72.07 ± 6.40[a]	67.71 ± 8.46	0.001
Sex (f/m)	9/6	10/18	14/10	0.175
Disease duration (months)	NA	39.48 ± 25.01	28.86 ± 21.48	0.143
PSP Rating Scale	NA	36.21 ± 15.12[d]	24.95 ± 11.85[e]	0.011
SEADL	NA	55.5 ± 20.89[f]	64.36 ± 20.89[e]	0.162
MoCA	NA	22.73 ± 4.10[g]	23.18 ± 5.39[e]	0.807

MoCA Montreal Cognitive Assessment Battery, *SEADL* Schwab and England Activities of Daily Living.
[a]Significantly different from controls ($p < 0.05$).
[b]Significantly different from PSP-RS ($p < 0.05$).
[c]Available for 19/22 PSP-RS subjects.
[d]Available vor 22/24 CBS subjects.
[e]Available for 20/22 PSP-RS subjects.
[f]Available for 11/22 PSP-RS subjects.

fields, and parietal cortex. In line with histopathological studies[3], these analyses suggest elevated tau in patients with suspected 4 R tauopathies vs. CN, particularly in the subcortex, with more widespread cortical tau in CBS vs. PSP-RS[23].

PI2620 signal reflects 4 R tau pathology. To validate whether PI-2620 has the ability to detect 4 R tau, we performed an in vitro competition assay to compare the affinity of PI-2620 to 4 R tau fibrils vs. the 1st-generation tau-PET tracer Flortaucipir. As shown in Fig. 2A, we found higher IC50 values of PI-2620 to 4 R tau fibrils (IC50 = 2.7 nM) compared to Flortaucipir (IC50 = 18.4 nM), suggesting that PI-2620 shows higher in vitro affinity to 4 R tau. In addition, we performed combined PI-2620 autoradiography and AT8 immunohistochemistry in 233 postmortem probes derived from 16 histopathologically confirmed PSP cases across three brain regions (i.e., frontal cortex: $n = 105$, pallidum: $n = 56$; putamen: $n = 72$). AT8 staining was assessed semiquantitatively by expert neuropathologists (i.e., low = +, medium = ++, high = +++) and autoradiography was quantified as the ratio of PI-2620 signal in the target tissue (i.e., frontal cortex, pallidum, and putamen) divided by PI-2620 signal in AT8-negative white matter. Using spearman correlation, we found a positive association between semiquantitative AT8 assessments and PI-2620 autoradiographic signal (Frontal cortex: $r = 0.44$, $p < 0.001$; Pallidum: $r = 0.47$, $p < 0.001$; Putamen: $r = 0.4$, $p < 0.001$), as well as significant differences in PI-2620 autoradiography signals between semiquantitatively assessed AT8 staining groups using ANOVAs (Frontal cortex: $F = 10.42$, $p < 0.001$; Putamen: $F = 12.08$, $p < 0.001$; Pallidum: $F = 8.36$, $p < 0.001$, Fig. 2B). Together, these results suggest that PI-2620 can detect 4 R tau pathology. Example images for the autoradiographic PI-2620 signal vs. AT8 staining are shown in Fig. 2C for the Frontal cortex and Fig. 2D for the basal ganglia.

Functional connectivity is associated with correlated tau-PET binding in CBS/PSP-RS. Next, we tested the major hypothesis whether inter-regional connectivity is associated with inter-regionally correlated tau accumulation in CBS or PSP-RS. To this end, we parcellated patient-specific ^{18}F-PI-2620 PET images into 232 regions-of-interests (ROIs) by combining non-overlapping functional MRI-based parcellations of the cortex (200 ROIs, Fig. 1G)[32] and subcortex (32 ROIs, Fig. 1H)[33]. Primary analyses focused on the subcortex (32 ROIs, Fig. 1G), which showed consistently elevated ^{18}F-PI-2620 PET binding in CBS and PSP-RS (see Fig. 1E, F). For secondary analyses we also included the neocortex (i.e., 32 subcortical plus 200 cortical ROIs, Fig. 1G), which was less consistently affected by elevated ^{18}F-PI-2620 PET binding in PSP-RS/CBS (see Fig. 1E, F).

We determined the covariance in inter-regional ^{18}F-PI-2620 PET binding within CBS and PSP-RS groups, defined as partial correlation of ROI-based ^{18}F-PI-2620 PET SUVRs, accounting for age, sex, and imaging site as confounds (methods illustrated in Fig. 3A, for subcortical tau covariance matrices see Fig. 3B for PSP-RS and Fig. 3C for CBS). For functional connectivity, we applied the same 232 ROI-based parcellation to preprocessed resting-state fMRI data of 69 cognitively normal ADNI subjects. Based on this healthy control sample, we determined a group-average functional connectivity template (see Fig. 3D). Using linear regression, we next assessed whether higher inter-regional functional connectivity was associated with higher inter-regional covariance of ^{18}F-PI-2620 PET binding, controlling for between-ROI Euclidean distance to ensure that associations were not driven by spatial proximity. For our primary analyses on the subcortex (i.e., where tau-PET was significantly elevated in PSP-RS and CBS compared to controls), we found the expected associations between higher functional connectivity and higher ^{18}F-PI-2620 PET covariance in PSP-RS ($\beta = 0.616$, $p < 0.001$, Fig. 4A) and CBS ($\beta = 0.561$, $p < 0.001$, Fig. 4B). To test the robustness of these findings, we recomputed these models 1000 times generating for each trial a new connectivity null-model (i.e., shuffled connectivity matrix with preserved weight- and degree distribution), yielding a distribution of null-model derived β-values (Fig. 4A, B, beeswarm panels). Comparing the actual β-values estimated using the observed true connectivity matrix with the null-distributions using an exact test (i.e., determine the probability of null-distribution derived β-values surpassing the true β-value), yielded p-values <0.001 for CBS and PSP-RS. Together, these analyses support the view that functionally connected subcortical regions show covarying tau-PET levels in CBS/PSP-RS. We obtained consistent results when extending these analyses to the whole brain (Fig. 1G, H), where higher connectivity was again associated with higher ^{18}F-PI-2620 PET covariance in PSP-RS (Fig. 4, $\beta = 0.450$, $p < 0.001$) and CBS (Fig. 4D, $\beta = 0.402$, $p < 0.001$), controlling for inter-regional Euclidean distance. Exact tests using shuffled connectivity data yielded consistent results ($p < 0.001$, Fig. 4C, D, beeswarm panels). Repeating the above-described analyses using partial-volume corrected tau-PET data or omitting Euclidean Distance as a covariate yielded consistent results (Supplementary Fig. 1, Supplementary Tables 1, 3). We next tested whether the association between connectivity and covariance in tau-PET was consistent across subcortico-cortical and cortico-cortical connections. Again, associations between connectivity and ^{18}F-PI-2620 PET covariance were found for cortico-cortical (PSP-RS: $\beta = 0.397$, $p < 0.001$; CBS: $\beta = 0.397$, $p < 0.001$) and subcortico-cortical

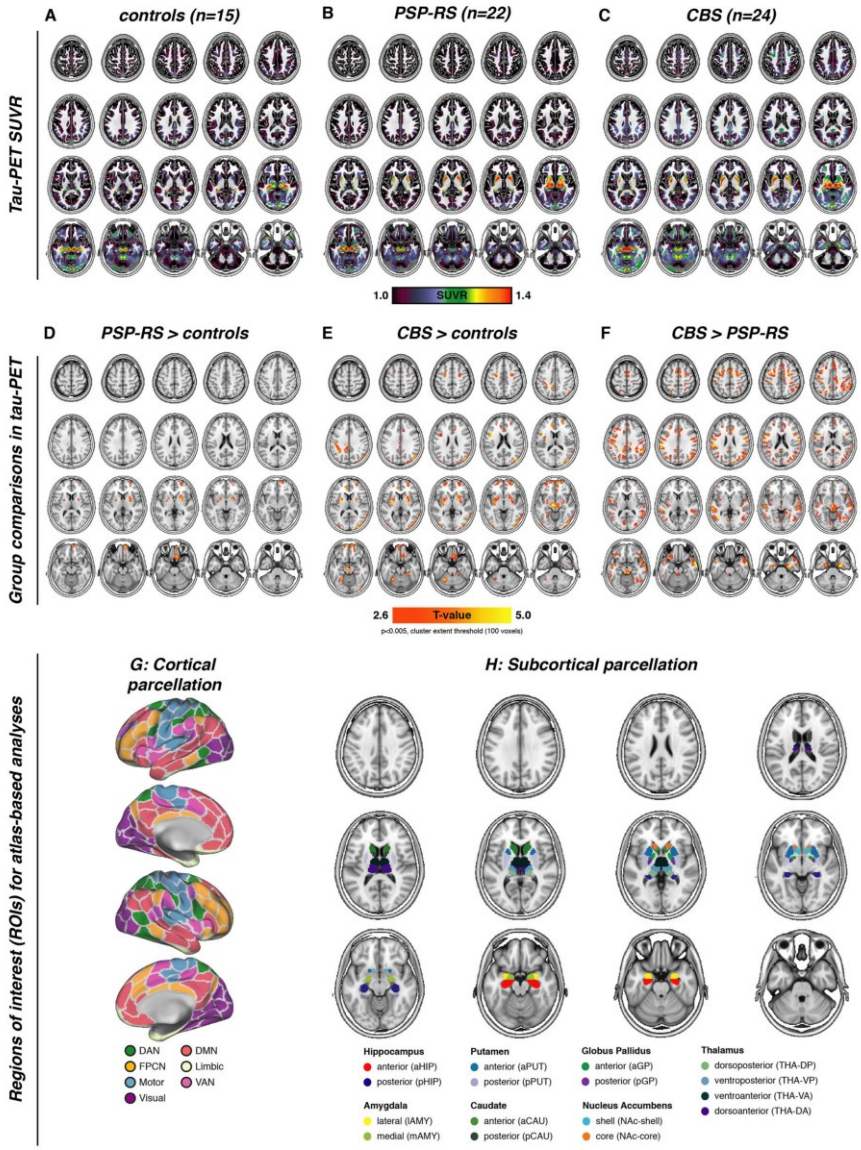

Fig. 1 PI-2620 tau-PET uptake patterns in controls/patients and brain parcellation scheme. Group-average maps of tau-PET SUVRs (i.e., intensity normalized to the inferior cerebellar gray) for controls (**A**), PSP-RS (**B**), and CBS patients (**C**). Voxel-wise group comparisons were conducted to compare tau-PET SUVRs between PSP-RS vs. controls (**D**), CBS vs. controls (**E**), and CBS vs. PSP-RS (**F**), at a voxel threshold of $p < 0.005$ with a cluster size of at least 100 spatially contiguous voxels. Illustration of the 200 ROI cortical (**G**) and 32 ROI subcortical (**H**) brain atlases that were used for all tau-PET vs. connectivity analyses.

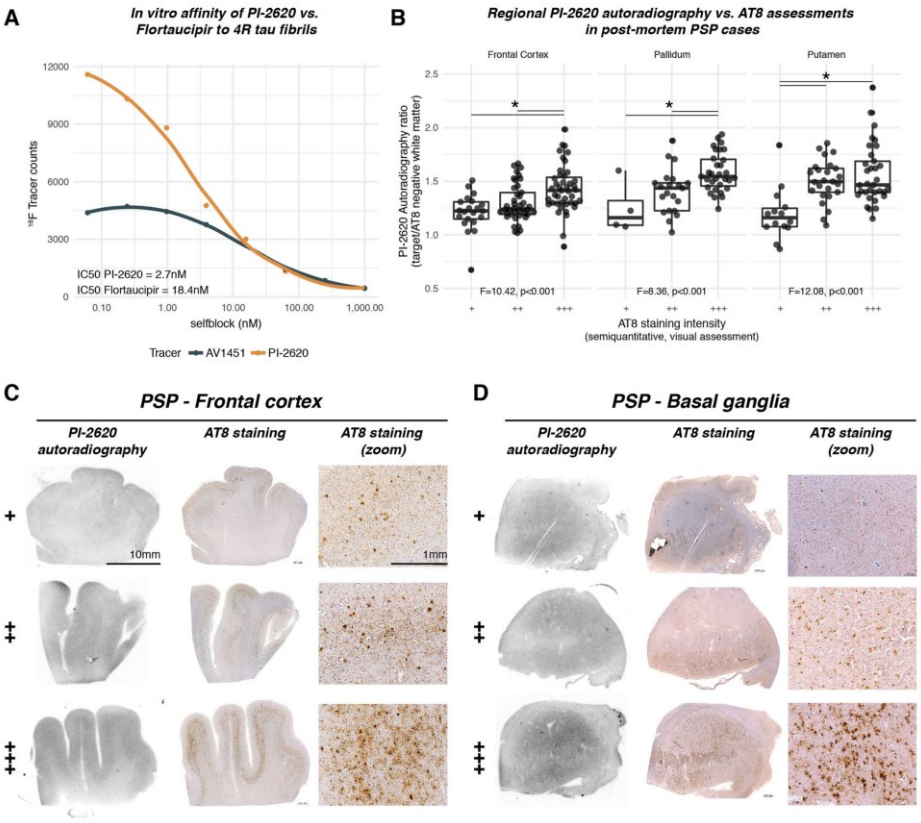

Fig. 2 Autoradiographic assessment of PI-2620 binding in PSP patients. In vitro competition assay, showing stronger affinity of PI-2620 to 4R tau fibrils than the first generation tau-PET tracer Flortaucipir (**A**). In addition, we performed autoradiographic assessments in 233 brain samples derived from 16 patients with histopathologically confirmed PSP pathology. Samples were obtained from the frontal cortex ($n = 105$), pallidum ($n = 56$), and putamen ($n = 72$). AT8 staining intensity was judged by visual expert read (low = +, medium = ++, high = +++), autoradiography was quantified as the intensity of the autoradiographic signal in the target tissue divided by signal in AT8-negative white matter. Boxplot illustrating the comparisons between autoradiography signal and AT8 staining intensity are shown in **B**, examples of autoradiography samples and AT8 staining are shown for the frontal cortex in **C**, and the basal ganglia in **D**. Two-sided *p*-values have been determined via ANOVAs. Boxplots are displayed as median (center line) ± interquartile range (box boundaries) with whiskers including observations falling within the 1.5 interquartile range. Source data are provided as a Source Data file.

connections (PSP-RS: $\beta = 0.329$, $p < 0.001$; CBS: $\beta = 0.379$, $p < 0.001$). Together, these findings of correlated tau-PET among functionally connected regions support the idea that connectivity shapes tau deposition patterns in 4 R tauopathies.

Functional connectivity predicts tau-PET binding in PSP-RS/CBS. We next determined whether group-average ^{18}F-PI-2620 PET patterns follow the connectivity pattern of subcortical tau epicenters (i.e., 20% of brain regions with highest tau-PET). We found that for epicenter regions with highest ^{18}F-PI-2620 PET binding, higher seed-based functional connectivity was associated with higher tau-PET binding in strongly connected subcortical regions in both PSP-RS (Fig. 5A, $\beta = 0.880$, $p < 0.001$) and CBS (Fig. 5B, $\beta = 0.933$, $p < 0.001$), controlling for between-ROI Euclidean Distance. In turn, for coldspot regions with lowest ^{18}F-PI-2620 PET binding, higher seed-based functional connectivity was associated with lower subcortical ^{18}F-PI-2620 PET binding in strongly connected regions in PSP-RS (Fig. 5, $\beta = -0.613$, $p < 0.001$) and CBS (Fig. 5D, $\beta = -0.617$, $p < 0.001$), controlling for between-ROI Euclidean distance. This result pattern was reflected in a strong positive correlation between the seed ROIs ^{18}F-PI-2620 PET binding and their functional connectivities' predictive weight (i.e., regression-derived β-value) on ^{18}F-PI-2620 PET binding in remaining ROIs (PSP-RS: $\beta = 0.929$, $p < 0.001$, Fig. 5E; CBS: $\beta = 0.937$, $p < 0.001$, Fig. 5F). A fully congruent result pattern was detected when extending this approach to the whole brain (see Fig. 5G–L). Consistent results were detected when repeating the analyses using partial-volume corrected data or when omitting Euclidean distance as a covariate (Supplementary Fig. 2; supplementary Tables 1, 3). Together, these findings suggest that regions with high tau-PET levels are primarily

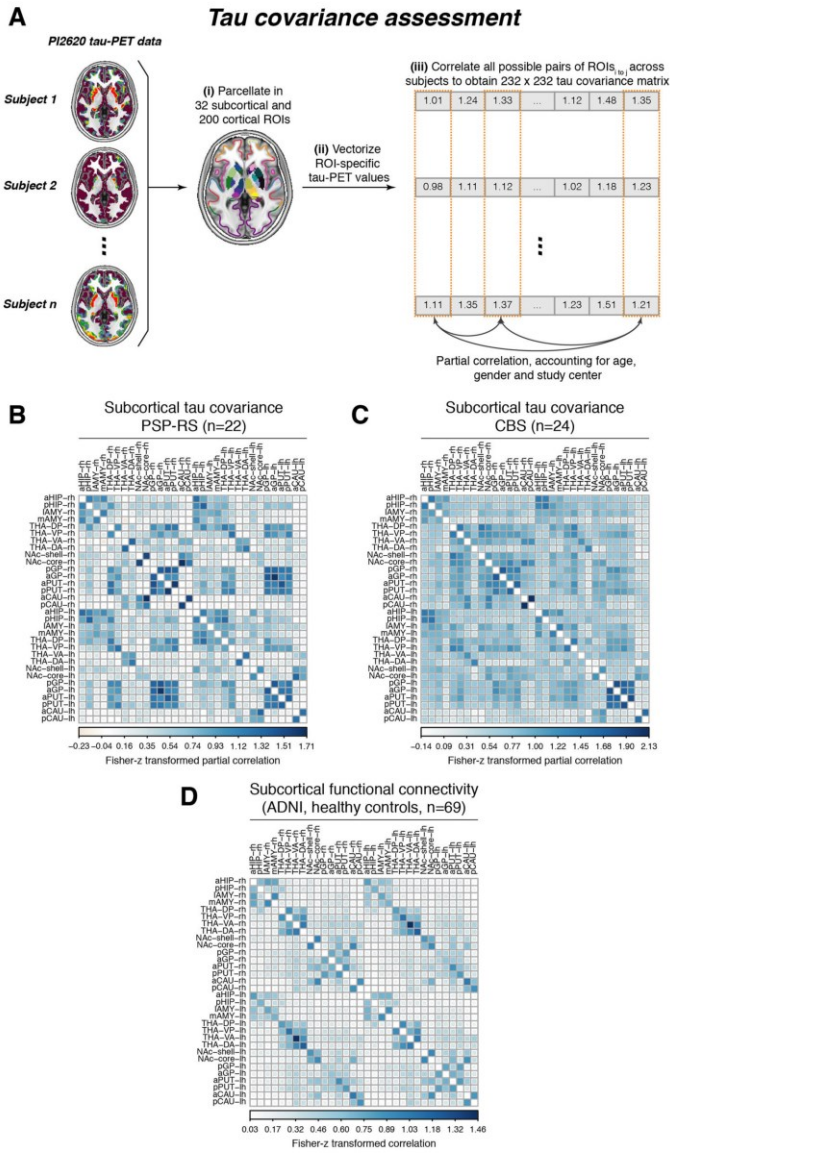

Fig. 3 Assessment of tau covariance. Flow-chart illustrating the assessment of tau covariance (**A**). Subject-level tau-PET data were parcellated into 200 cortical and 32 subcortical ROIs (i), mean tau-PET was extracted for each region of interest (ROI), vectorized to 232-element vectors and concatenated across subjects (ii). Fisher-z transformed partial correlations between inter-regional tau-PET SUVRs were determined for each group (i.e., progressive supranuclear palsy—Richardson syndrome [PSP-RS] and cortico-basal syndrome [CBS]), accounting for age, sex, and study site (iii). The resulting tau covariance matrices for the subcortical brain parcellation which was used for primary analyses is shown for PSP-RS (**B**) and CBS (**C**) patients. For the same ROIs, group-average functional connectivity was computed based on resting-state fMRI of 69 cognitively normal, amyloid and tau negative ADNI participants (**D**). Source data are provided as a Source Data file.

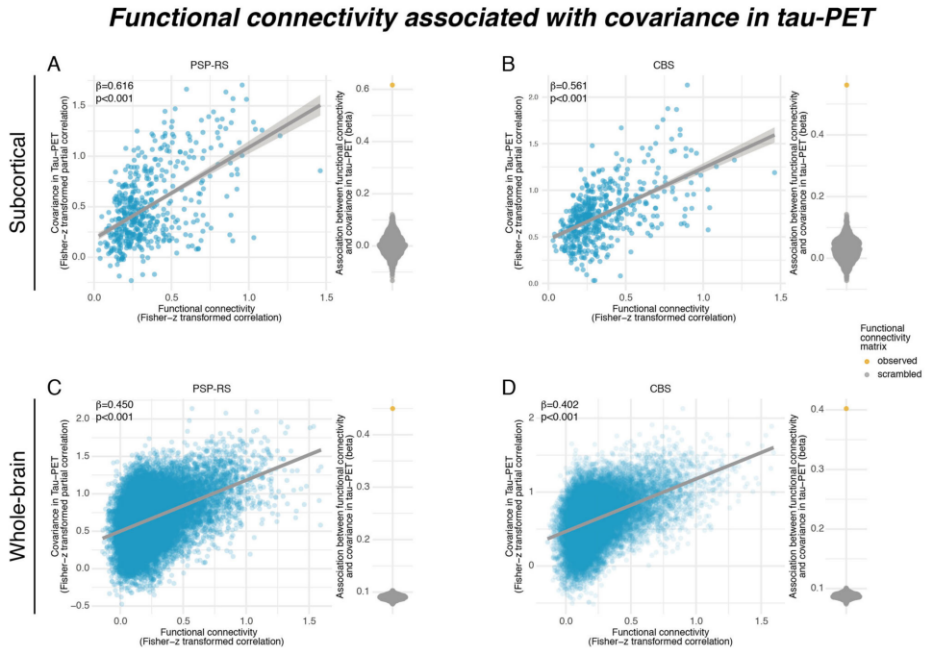

Fig. 4 Association between connectivity and covariance in tau-PET. Scatterplots illustrating the association between functional connectivity and covariance in 18-F-PI2620-PET among subcortical regions in progressive supranuclear palsy—Richardson syndrome (PSP-RS, **A**) and cortico-basal syndrome (CBS) groups (**B**), as well as among subcortical and cortical regions for PSP-RS (**C**) and CBS groups (**D**). Standardized beta- and *p*-values were derived from linear regression controlling for Euclidean distance between regions of interest (ROIs). Beeswarm plots illustrate the distribution of standardized beta-values derived from repeating the analysis 1000 times using scrambled connectomes with preserved weight- and degree distribution (gray points) vs. the beta-value derived from the association with the actual observed connectivity matrix that is illustrated in the scatterplot (yellow point). Two-sided *p*-values have been determined via linear regression. Linear model fits are indicated together with 95% confidence intervals. Source data are provided as a Source Data file.

interconnected with regions also harboring high tau, whereas regions with low tau are primarily connected to other low tau regions.

Connectivity of patient-specific tau epicenters predicts individual tau-PET binding in 4 R tauopathy patients. As shown by the group-level analyses, epicenter regions with highest tau-PET binding were most strongly connected to other regions with high ^{18}F-PI-2620 PET in PSP-RS (Fig. 5A, G) and CBS (Fig. 5B, H). Next, we extended this analysis to the subject level, i.e., we defined each PSP-RS and CBS patients' tau epicenter as those ~20% of subcortical ROIs with the highest ^{18}F-PI-2620 PET SUVR[34]. Adopting our previously established approach[34], the remaining non-epicenter subcortical ROIs were grouped for each subject into 4 quartiles depending on the mean connectivity strength to a given subjects' tau epicenter (Q1 = strongest connectivity to the tau epicenter vs. Q4 = weakest connectivity to the tau epicenter) as illustrated in Fig. 6A. We expected a gradient of ^{18}F-PI-2620 PET decrease from tau epicenters across functionally connected regions (i.e., highest tau in Q1, vs. lowest tau in Q4). Using linear mixed models, we could confirm that connectivity strength to the epicenter was predictive of ^{18}F-PI-2620 PET binding in connected Q1–Q4 regions for PSP-RS (b-value/standard error [b/SE] = 0.097/0.015, $p < 0.001$, Fig. 6B) and CBS (Fig. 6D, b/SE = 0.086/0.013, $p < 0.001$). As hypothesized, highest ^{18}F-PI-2620 PET binding was found in Q1, which is most strongly connected to the tau epicenter, whereas tau-PET levels gradually decreased to Q4, which is only weakly connected to the tau epicenter. Linear mixed models were controlled for age, sex, study site, mean Euclidean distance to the tau epicenter as well as random intercept. When extending this analysis to the cortex, we found a similar result pattern, with highest ^{18}F-PI-2620 PET binding in those cortical regions that were most closely connected to subcortical tau epicenters (i.e., Q1) vs. lowest ^{18}F-PI-2620 PET binding in those cortical regions that were most weakly connected to subcortical tau epicenters (i.e., Q4) in PSP-RS (Fig. 6C, b/SE = 0.036/0.008, $p < 0.001$) and CBS (Fig. 6E, b/SE = 0.032/0.005, $p < 0.001$). A topological frequency mapping of tau epicenters is shown in Fig. 6H for PSP-RS and Fig. 6I for CBS. Consistent results were obtained when using partial-volume corrected tau-PET data or when omitting Euclidean distance as a covariate (supplementary Fig. 3; supplementary Tables 2, 4). Together, these findings support the view that tau deposition patterns follow the connectivity pattern of subcortical tau epicenters in PSP-RS and CBS.

Subthreshold amyloid levels are associated with neocortical tau deposition in CBS. In a subset of 22 CBS patients with available

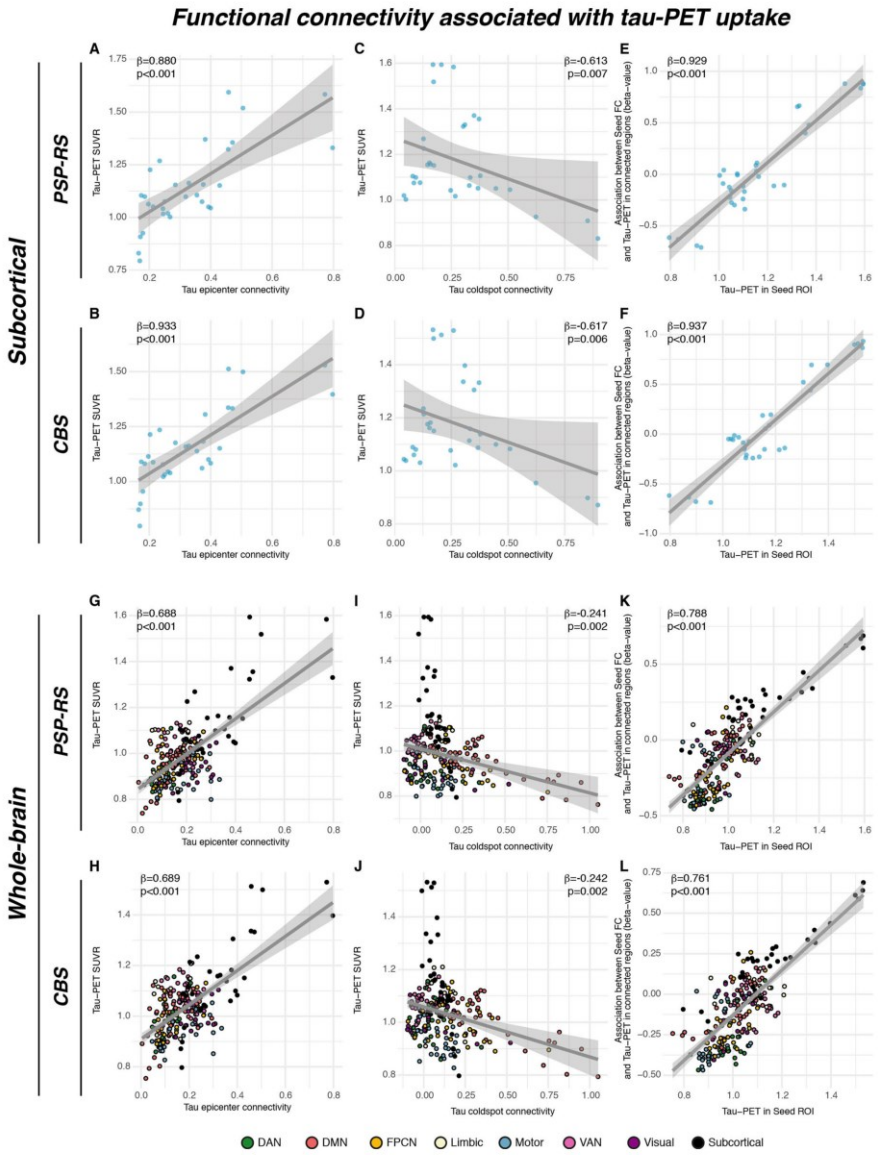

^{18}F-flutemetamol amyloid-PET (i.e., all rated Aβ-negative on expert visual read), we tested the hypothesis that subthreshold Aβ levels are associated with enhanced cortical tau at a given level of subcortical tau deposition. Here, we repeated the subject-level analyses illustrated in Fig. 6D, E, this time including a main effect for high vs. low Aβ as defined via median split of global ^{18}F-flutemetamol amyloid-PET SUVRs, intensity normalized to the pons. No difference in ^{18}F-PI-2620 PET binding was found within subcortical tau epicenters between high and low Aβ groups ($p > 0.05$). Further, the association between epicenter connectivity and ^{18}F-PI-2620 PET binding in connected subcortical Q1–Q4 ROIs was the same across high/low Aβ groups (main effect of Aβ: b/SE = −0.02/0.051, $p = 0.653$, Fig. 6F), controlling for age, sex, study site, Euclidean distance to the tau epicenter, and random

Fig. 5 Group-level epicenter connectivity vs. tau-PET patterns. Associations between group-average subcortical 18-F-Pi-2620-PET data and seed-based functional connectivity of tau epicenters (i.e., regions with highest group-average tau) in progressive supranuclear palsy—Richardson syndrome (PSP-RS, **A**) and cortico-basal syndrome (CBS, **B**), illustrating that regions with high connectivity to the tau epicenter show high tau-PET. The same association was plotted for tau coldspots (i.e., regions with lowest tau-PET) for PSP-RS (**C**) and CBS (**D**), illustrating that regions closely connected to the tau coldspots show also low tau-PET. Standardized beta- and *p*-values were derived from linear regression controlling for Euclidean distance between ROIs. The analysis was repeated for all regions of interest (ROIs), and the respective seed ROIs tau-PET uptake was plotted against the regression-derived beta-value, showing that seed regions with higher tau-PET show a positive association between seed-based connectivity and tau-PET in connected regions, whereas regions with lower tau-PET show a negative association between seed-based connectivity and tau-PET in connected regions in PSP (**E**) and CBS (**F**). These findings indicate that seed ROIs are preferentially connected to other regions with similar tau-PET levels. All analyses were repeated including using the combined set of 200 cortical and 32 subcortical ROIs, showing a fully consistent result pattern across the entire brain (**G**–**L**). Two-sided *p*-values have been determined via linear regression. Linear model fits are indicated together with 95% confidence intervals. Source data are provided as a Source Data file.

intercept. However, for cortical regions, we found that the high Aβ group showed overall higher ^{18}F-PI-2620 PET binding across cortical Q1 to Q4 ROIs (main effect of Aβ: b/SE = 0.078/0.006, $p = 0.031$, Fig. 6G), yet with the same gradient of tau deposition from tau epicenters throughout connected regions, controlling for age, sex, study site, Euclidean distance to the tau epicenter, and random intercept. This result pattern supports the view that subcortical to cortical tau propagation may be enhanced in the presence of subtle subthreshold Aβ accumulation in CBS.

Functionally connected brain regions show correlated postmortem tau levels in PSP. Lastly, we aimed to replicate the association between covariance in ^{18}F-PI-2620 PET binding and functional connectivity using gold-standard postmortem tau assessments since the in vivo ^{18}F-PI-2620 signal could still be driven by a parallel phenomenon not directly reflecting tau. The histopathological data of our study were derived from regional and cell-type-specific semiquantitative AT8 (Munich sample) or PHF-1 (UPENN sample) stained tau assessments (i.e., for neuronal, astrocyte, and oligodendrocyte tau) in two independent samples with confirmed PSP 4 R tau pathology:[8] Using the neuropathological probe extraction protocols, we reconstructed spatially matching bilateral ROIs from established cortical and subcortical anatomical atlases[33, 35], as shown in Fig. 7A for the Munich-European consortium/collection sample ($n = 97$, 16 ROIs) and Fig. 7B for the UPENN sample ($n = 96$, 9 ROIs). For these ROIs, we computed covariance in postmortem stained neuronal tau levels, defined as the partial Spearman correlation between inter-regional neuronal tau, accounting for age at death and gender (Fig. 7C, E). Using the same ROIs shown in Fig. 7A, B, we determined inter-regional functional connectivity in the sample of 69 cognitively normal, amyloid-PET, and tau-PET-negative ADNI subjects (Fig. 7D, F). As for the ^{18}F-PI-2620 PET analyses, we tested the association between inter-regional functional connectivity and covariance in postmortem tau, focusing particularly on neuronal tau which we hypothesized to be most strongly driven by connectivity-mediated tau spreading. As for ^{18}F-PI-2620 PET, these analyses were controlled for inter-regional Euclidean distance, to ensure that associations between connectivity and tau covariance were independent of spatial proximity between ROIs. In line with the ^{18}F-PI-2620 PET data, we found the expected association between functional connectivity and covariance in neuronal tau levels in the Munich-European consortium/collection ($\beta = 0.503$, $p < 0.001$, Fig. 7G) and UPENN sample ($\beta = 0.790$, $p < 0.001$, Fig. 7H). Again, these associations were confirmed by exact tests ($p < 0.001$, beeswarm plots in Fig. 6G, H), i.e., by comparing the actual β-value with a null-distribution of β-values obtained via repeating the analysis 1000 times using shuffled connectomes with preserved weight- and degree distribution. For direct comparison of the postmortem and tau-PET analyses, we also determined the covariance in tau-PET in PSP-RS patients for the postmortem atlas regions shown in Fig. 7A, B. In line with the postmortem data, we found a strong association between functional connectivity and covariance in tau-PET in PSP-RS, controlling for Euclidean distance (Munich parcellation [Fig. 7A], $\beta = 0.66$, $p < 0.001$; UPENN parcellation [Fig. 7B], $\beta = 0.52$, $p < 0.001$). In the postmortem data, we further tested whether the association between functional connectivity and covariance in tau was strongest for neurons. To this end, we recomputed the above-described analyses with measures of neuronal, astroglial, and oligodendroglial tau in 1000 bootstrapped samples that were randomly drawn from the overall samples. Plotting the resulting β-value distributions revealed that the associations between functional connectivity was indeed highest for neuronal tau, followed by oligodendrocyte and lastly astrocyte tau consistently across the Munich-European consortium/collection (Fig. 7I) and UPENN sample (Fig. 7J). Together, these postmortem findings in two large independent samples replicate the in vivo ^{18}F-PI-2620 PET findings, showing an association between functional connectivity and covariance in tau pathology, which is strongest for neuronal tau.

Discussion

Our major aim was to investigate whether functional connectivity is associated with the deposition patterns of tau pathology in 4 R tauopathy patients. To this end, we combined template-based resting-state fMRI connectomics with (i) in vivo tau-PET in 46 PSP-RS and CBS patients and (ii) regional postmortem tau assessments in two independent samples with histopathologically confirmed 4 R tau PSP pathology ($n = 97$/$n = 96$). Using the next generation tracer ^{18}F-PI-2620 for imaging tau pathology[27], we found elevated PET binding in clinically diagnosed CBS and PSP-RS patients, particularly in subcortical predilection sites of 4 R tau pathology. Binding of PI-2620 to 4 R tau pathology was further supported by competitive in vitro self-blocking assessments and autoradiography in PSP patient samples. Across CBS and PSP-RS, we show that functionally interconnected subcortical and cortical regions show correlated tau-PET levels. Moreover, we report that patient-level ^{18}F-PI-2620 PET patterns could be predicted by the seed-based connectivity patterns of subcortical tau epicenters, suggesting that gradual tau aggregation expands from subcortical tau starting sites throughout connected regions. In CBS, which is typically characterized by more widespread cortical tau[23], we show further that subthreshold Aβ-levels are associated with elevated cortical ^{18}F-PI-2620 PET in regions that are closely connected to the subcortical tau epicenters. By translating the tau-PET vs. connectivity analysis approach to regionally sampled postmortem data from two independent PSP patient samples, we replicated the association between in-vivo-derived inter-regional connectivity and inter-regional covariance in AT8/PHF-1-stained tau pathology. Here, we could show further that the association between connectivity and covariance in postmortem-assessed tau pathology was strongest for neuronal tau compared to glial tau

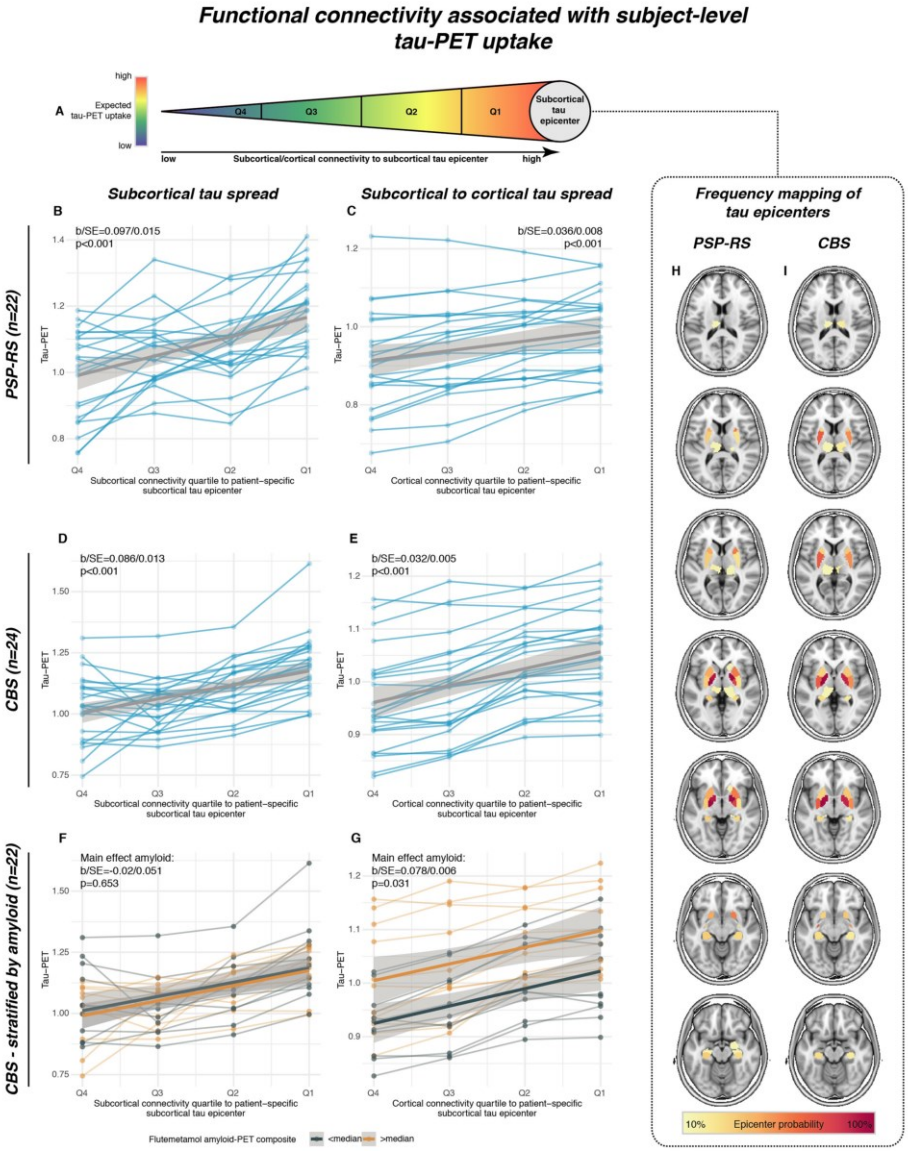

levels, supporting the view that connectivity is particularly associated with trans-neuronal tau propagation. Together, our findings provide comprehensive translational evidence for a key role of connectivity in the propagation of 4 R tau pathology[36, 37].

When assessing disease-associated tau-PET patterns, we found elevated ^{18}F-PI-2620 PET binding in CBS/PSP-RS patients particularly in the basal ganglia, i.e., typical sites of 4 R tau aggregation[7, 8], congruent with a previous ^{18}F-PI-2620 PET study in a partly overlapping sample[27]. Further, the epicenters of ^{18}F-PI-2620 PET spatially matched the earliest signs of tau pathology in the pallido-nigrolusyian axis as detected in postmortem analyses of 4 R tauopathy patients with various clinical phenotypes[8]. CBS patients, which are characterized by a clinically mixed subcortical/cortical phenotype, showed more widespread cortical

Fig. 6 Subject-level epicenter connectivity vs. tau-PET patterns. Using subject-level tau-PET data, we determined for each progressive supranuclear palsy—Richardson syndrome (PSP-RS) and cortico-basal syndrome (CBS) patient the subcortical tau epicenter (**A**), i.e., defined as 20% of ROIs with highest tau-PET SUVRs. The remaining regions of interest (ROIs) were grouped for each subject into quartiles, depending on connectivity strength to the subject-specific tau epicenter. Highest tau-PET was expected for regions most closely connected to the tau epicenter (i.e., quartile 1 = Q1) whereas lowest tau-PET was expected for ROIs only weakly connected to the tau epicenter. Subject-specific tau-PET data for subcortical Q1–Q4 ROIs (**B**, **D**) as well cortical Q1–Q4 ROIs (**C**, **E**) is shown, illustrating that tau-PET was highest in subcortical and cortical regions that are most closely connected to the subcortical tau epicenter (i.e., Q1), with gradual decreases across less strongly connected regions. For a subset of CBS patients ($n = 22$), we further stratified these analyses by above vs. below median global amyloid-PET SUVRs (i.e., subthreshold amyloid, as all subjects were amyloid negative on visual read). Amyloid-stratified analyses illustrate that above median amyloid levels were not associated with elevated tau spread from subcortical epicenters to subcortical Q1–Q4 ROIs (**F**), but with increased tau spread from subcortical epicenters to cortical Q1–Q4 ROIs (**G**). All statistical indices (i.e., b-values, standard errors and *p*-values) were derived from linear mixed models, controlling for age, sex, study center, mean Euclidean distance of Q1–Q4 ROIs to the tau epicenter and random intercept. A probability mapping of subcortical epicenter locations is illustrated in panels **H** for PSP-RS and **I** for CBS patients. Two-sided *p*-values have been determined via linear mixed effects models. Linear model fits are indicated together with 95% confidence intervals. Source data are provided as a Source Data file.

^{18}F-PI-2620 PET elevations than PSP-RS, in line with post-mortem observations[23]. Together, the ^{18}F-PI-2620 PET patterns observed in PSP-RS and CBS are congruent with histopathologically observed 4 R tau patterns in CBD/PSP[7, 8].

Nevertheless, we note as a limitation that in vivo and post-mortem data were not assessed in the same patients in the current study. Thus, although we and others provide autoradiographic evidence for ^{18}F-PI-2620 binding to 4 R tau[27, 38], the observed signal could still derive from a source closely paralleling 4 R tau. Regarding our main finding, we observed that functionally connected brain regions exhibit correlated ^{18}F-PI-2620 PET levels in CBS and PSP-RS. This result echoes previous evidence of covarying cross-sectional tau-PET levels and longitudinal tau-PET accumulation rates among functionally interconnected regions in AD, suggesting a consistent association between tau deposition patterns and brain connectivity across different tauopathies[39–41]. This interpretation is also supported by preclinical work, showing that pathological tau species from 4-repeat (i.e., CBD/PSP) and mixed 3/4-repeat tauopathies (i.e., AD) consistently trigger trans-cellular tau spread across connected brain regions while recapitulating disease-specific neuropathological hallmark features (e.g., neuronal tau in AD vs. neuronal and glial tau in CBD/PSP)[15, 17, 42]. Recent studies have emphasized, however, that CBD and PSP tau show distinguishable molecular characteristics[43–45], hence it will be important in future studies to assess whether molecular differences in CBD and PSP tau modulate the spreading potential of tau pathology. Importantly, we found an association between connectivity and covariance in ^{18}F-PI-2620 PET binding not only for subcortical 4 R tau predilection sites but also for cortico-cortical and subcortico-cortical connections. This indicates that associations between connectivity and tau deposition patterns are not spatially restricted to particularly vulnerable brain regions, in line with previous evidence in AD patients[34, 39, 40] and preclinical tauopathy models[15, 17, 42].

In a critical validation step, we were able to translate these in vivo tau-PET vs. connectivity analyses to postmortem tau assessments in two pre-existing datasets of patients with histopathologically confirmed PSP[8]. In these unique samples with gold-standard regional tau assessments, we found a highly consistent result pattern with strong associations between in-vivo-assessed inter-regional functional connectivity and inter-regional correlations of AT8 or PHF-1 stained tau levels. Importantly, these associations were replicated across both independent postmortem samples with regionally different postmortem sampling (see Fig. 7A, B), supporting the robustness of our findings. Even more important, cell-type-specific tau assessments confirmed the hypothesis that the association between connectivity and covariance in tau was strongest for neuronal tau pathology when compared to astroglial and oligodendrocyte-specific tau, thus supporting neuronal connectivity as the main driver of trans-synaptic tau propagation[22]. Consistent across both postmortem samples, the second strongest association between connectivity and tau covariance was observed for oligodendrocytes, i.e., the main constituents of myelin sheaths along axonal tracts. Previous work in mice has shown that 4 R oligodendrocyte tau propagates along white matter tracts, even in the absence of neuronal tau pathology, suggesting oligodendrocyte tau propagation along anatomically interconnected pathways[46]. A recent study evaluating cell-specific sequences showed more overlap of the patterns of neuronal and oligodendrocytic tau deposition, and albeit early steps of astrocytic tau deposition deviates from the neuronal, it converges in later steps[8]. Astrocytic tau accumulation may be seen without local neuronal tau pathology in regions with high connectivity to regions with existing neuronal tau pathology[47], which together with a preclinical study that observed astrocytic tau pathology only in the presence of neuronal tau[46], are in line with the observation that astrocytes phagocytose neuronally released tau[15], either from local neurons or projecting from other regions[48]. Altogether, these may explain why connectivity and astrocytic tau were associated, albeit to a weaker extent compared to neuronal and oligodendrocytic tau. Thus, these preclinical findings converge with our result pattern of strongest associations between connectivity and neuronal tau, followed by oligodendrocyte and astrocyte tau. In summary, our findings provide compelling postmortem replication of an association between connectivity and 4 R tau spreading.

Importantly, all associations between connectivity and covariance in postmortem tau or in vivo ^{18}F-PI-2620 PET were detected while statistically controlling for inter-regional Euclidian distance, highlighting that the association between tau and connectivity is not driven by mere spatial proximity. This result pattern supports the view that tau spread is driven by connectivity and not proximity[21, 49, 50], in line with preclinical studies, showing that cerebral tau injections trigger tau spread to connected rather than spatially adjacent regions[15, 42].

In the ^{18}F-PI-2620 PET sample, we further show that brain regions with highest tau (i.e., tau epicenters) are closely functionally connected to other high tau regions, whereas low tau regions are most closely connected to other low tau regions. These findings are congruent with postmortem tau staging schemes, showing that 4 R tau pathology is initially confined to circumscribed epicenters from where it progresses gradually throughout the brain[8]. Further supporting this, we found that connectivity patterns of subject-level tau-PET epicenters predicted a gradient of tau deposition, with highest tau in subcortical/cortical regions that were most closely connected to the tau epicenter, while tau levels were gradually lower in farther connectivity-based distance to the tau epicenter. In line with findings in other tauopathies such as AD[34, 39, 41, 51], these results suggest tau spreading patterns in 4 R tauopathies are determined

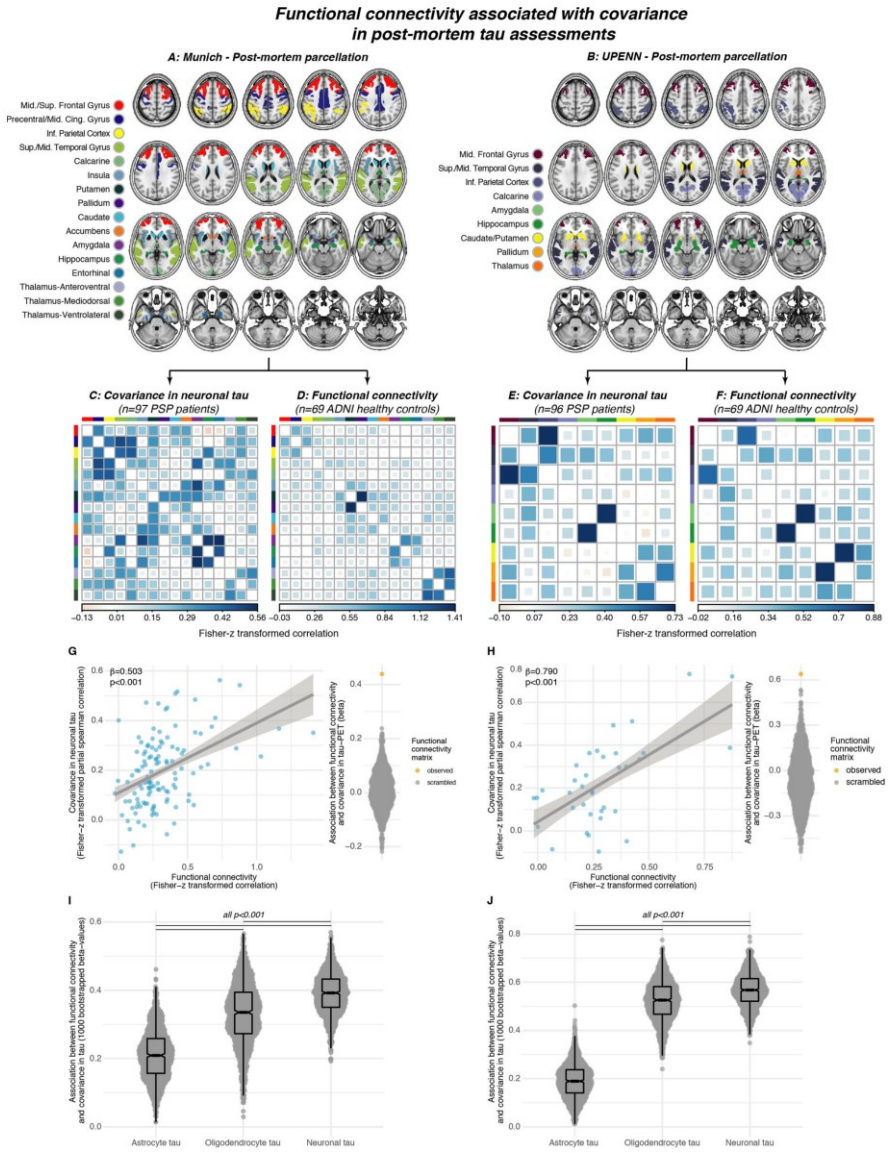

by the connectivity pattern of the tau epicenter, thereby strongly supporting the concept of connectivity-based tau spreading. Importantly tau spreading concepts applied to PET imaging could facilitate patient-tailored precision medicine since they may facilitate prediction of the future accumulation pattern of tau pathology and the progression/development of symptoms on a patient-level[34]. By implication, identifying sites that are vulnerable to tau spreading could also serve as a imaging-guided primary read-out in tau targeting trials of 4 R tauopathies.

In an exploratory subanalysis in CBS patients with available global amyloid-PET data, we found further that subthreshold Aβ-levels were associated with higher cortical tau-PET-levels following the same connectivity gradient of subcortical tau epicenters (Fig. 5G). A potential explanation is that subtly elevated

Fig. 7 Connectivity vs. Post-mortem tau deposition patterns. Association between functional connectivity and regional postmortem tau assessments (i.e., AT8 staining) in two independent samples with histopathologically confirmed progressive supranuclear palsy (PSP = . For each sample, covariance in neuronal tau levels was assessed among cortical and subcortical ROIs (**A**, **B**) using the methods illustrated in Fig. 3A, yielding a covariance in AT8-stained tau matrix of partial correlations accounting for age at death and sex. for the Munich (**C**) and UPENN sample (**E**). Using the same brain atlases (**A**, **B**), functional connectivity was determined based on resting-state fMRI data in the sample of $n = 69$ healthy controls from ADNI (**D**, **F**). Scatterplots illustrate the association between functional connectivity and covariance in postmortem stained neuronal tau pathology for the Munich (**G**, AT8 tau staining) and UPENN (**H**, PHF-1 tau staining) sample. Standardized beta- and *p*-values were derived from linear regression controlling for Euclidean distance between ROIs. Robustness of the association in panels **D**, **E** was again tested by contrasting the beta-value derived from the association between the actual functional connectivity matrix with covariance in tau against beta-values derived from the same analyses repeated a 1000 times using scrambled functional connectivity matrices with preserved degree- and weight distribution (see beeswarm plots in panels **G**, **H**). The same analysis was repeated for cell-specific tau levels (i.e., astrocyte tau, oligodendrocyte tau, neuronal tau) using 1000 bootstrapping iterations, i.e., the association between functional connectivity and covariance in cell-specific tau was repeated on 1000 randomly drawn samples. The resulting beta-value distributions are shown for the Munich (**I**) and UPENN (**J**) sample, illustrating that the association between functional connectivity and covariance in tau is strongest for neuronal tau levels. Two-sided *p*-values have been determined via linear models for scatterplots. Linear model fits in scatterplots are indicated together with 95% confidence intervals. Boxplots are displayed as median (center line) ± interquartile range (box boundaries) with whiskers including observations falling within the 1.5 interquartile range. Two-sided *p*-values in boxplots have been obtained using ANOVAs. Source data are provided as a Source Data file.

Aβ levels (i.e., all CBS patients were by definition Aβ-negative), which have been previously shown to accelerate AD-typical tau spreading[52], also accelerate subcortical to cortical tau spreading in CBS patients. As a limitation, we note that different binding characteristics of ^{18}F-PI-2620 to 3/4 R and 4 R tau isoforms could also explain our observation since the Aβ status impacts the predominant tau isoform and tau isoform shifts[53]. Yet, this finding is preliminary and requires further systematical investigation by larger dedicated studies and longitudinal analyses. In addition, a potential association between cortical Aβ-levels and elevated cortical tau-PET should be explored in PSP cases, especially in those with cortical phenotypes (e.g., language variant PSP) once sufficient data become available.

Several limitations should be considered when interpreting our results. First, the ^{18}F-PI-2620 PET cohort includes PSP-RS and CBS patients with clinically diagnosed 4 R tauopathies, since biomarker-based 4 R tauopathy diagnosis is not yet clinically established[12, 28]. Further, PI-2620 controls were significantly younger than PSP-RS patients, hence age-related increase in tau-PET signal may potentially bias group comparisons between controls and PSP-RS groups, despite age adjustment of voxel-wise analyses. Importantly, however, ^{18}F-PI-2620 PET patterns in PSP-RS and CBS groups matched the tau patterns that are typically observed in histopathological assessments[7, 8], and subcortical ^{18}F-PI-2620 PET was significantly higher relative to controls, thus supporting the view that the ^{18}F-PI-2620 PET signal in these 4 R tau predilection sites reflects no off-target signal but an increase in tau pathology[27]. This is supported by our in vitro binding assay data, showing a stronger affinity of PI-2620 to 4 R tau fibrils than Flortaucipir (Fig. 2A), as well as the post-mortem autoradiography assessments in PSP patients, showing that stronger PI-2620 signal is observed in brain regions with higher AT8-stained tau pathology (Fig. 2C, D). Further, a recent study refined PI-2620 binding sites to tau from cryo-EM metadynamics simulations in order to provide atomic resolution of the binding modes and thermodynamic properties[54]. Here, several binding sites for PI-2620 were observed on 4 R Tau CBD fibrils which support sufficient PI-2620 in vivo binding to 4 R tau. Nevertheless, the affinity of ^{18}F-PI-2620 PET to 4 R tau needs to be characterized further and our findings warrant replication with other candidate tracers for 4 R tau (e.g., ^{18}F-PM-PBB3)[55]. In addition, ^{18}F-PI2620 shows off-target binding to neuromelanin[38], hence tau deposition in neuromelanin harboring brainstem regions, which typically show early tau accumulation in 4 R tauopathies[8], can currently not be assessed with ^{18}F-PI-2620 PET. To further guard against the impact of confounding 3/4 R pathology, all patients with CBS were rated Aβ negative as determined via cerebrospinal fluid or amyloid-PET assessments, suggesting that elevated ^{18}F-PI-2620 PET is not primarily explained by AD-typical 3 R/4 R tau[56, 57]. Second, the current study focused on functional connectivity, i.e., shared inter-regional BOLD activity, which is to a large degree but not entirely matched by structural connectivity as assessed via diffusion MRI[58]. This structural/functional connectivity mismatch is partly determined by technical limitations of MRI-based tractography to detect crossing-fibers or short-range cortico-cortical connections[59]. On the other hand, the slow temporal resolution of fMRI may introduce connectivity between regions without direct but rather indirect multi-synaptic connections[60]. Thus, our results on tau covariance vs. connectivity likely reflect a mixture of direct and indirect connections. In addition, the fMRI BOLD signal stems from multiple cellular sources including astrocytes, neurons, and vasculature[61], and while fMRI-assessed connectivity is associated with electrophysiological brain activity[62], fMRI connectivity does potentially not fully match neuronal connectivity. However, the advantage of functional MRI in the current study is the possibility to map a proxy of brain connectivity between spatially adjacent subcortical nuclei, where connections are not accessible with diffusion-based tractography. In addition, the current study used connectivity templates derived from healthy individuals. Thus, it remains to be determined by future studies whether subject-specific connectivity differences (i.e., connectome fingerprinting) contribute to heterogeneity in tau spreading patterns. Here, it will also be important to assess whether disease-related connectivity changes, such as tau-related disruptions in functional connectivity further modulate downstream tau spread that deviates from tau spreading patterns modeled with a healthy connectome template. Third, the current study is cross-sectional in nature and thus does not assess the association between connectivity and the spatio-temporal progression of tau pathology. In order to test the predictive value of connectivity for regional changes in tau-PET, longitudinal tau-PET studies are necessary, which will be conducted as soon as large enough data are available.

In conclusion, the current study demonstrates a close link between 4 R tau deposition patterns and connectivity, thereby supporting the concept of trans-neuronal tau spreading in 4 R tauopathies[13, 22, 37]. A clear strength of the current study is the translational study design with independent validation of the association between inter-regional functional connectivity and covariance in tau pathology across in vivo ^{18}F-PI-2620 PET and cell-specific postmortem histopathological tau assessments in multiple independent samples. The current results may be used as a starting point for future studies with detailed phenotyping of

cognitive and motor function to map tau spreading patterns and downstream neurodegeneration to cognitive and motor phenotypes in patients with 4 R tauopathies. Since tau pathology is closely assumed to be a key driver of disease progression[5, 7, 8], our results suggest that interventions that target tau spreading are potentially key therapeutic strategies.

Methods

Tau-PET sample. We included 61 subjects recruited at four sites (Munich & Leipzig, Germany; Melbourne, Australia; New Haven, United States), including 15 cognitively normal individuals (i.e., without evidence of cognitive decline, any motor symptoms or cerebral tau pathology), 24 patients with clinical diagnosis of possible or probable cortico-basal syndrome (CBS) and 22 patients with clinical diagnosis of PSP-RS. CBS diagnosis was made according to the revised Armstrong Criteria of probable CBS[12] or the Movement Disorders Society criteria of possible PSP with predominant CBS[28]. PSP-RS was diagnosed following state-of-the-art diagnostic criteria[28]. All patient data derive from a PSP cohort recruited in Munich and Leipzig[27] and a CBS cohort recruited in Munich[31]. Inclusion criteria for the current study were age above 45 years, stable pharmacotherapy for at least 1 week before the tau-PET examination, negative family history for Parkinson's and Alzheimer's disease and availability of 3D T1-weighted structural MRI. Exclusion criteria were severe neurological or psychiatric disorders other than PSP and CBS or positive Aβ status, as determined via expert visual read of 18-F-Flutemetamol or 18-F-florbetaben amyloid-PET or by cerebrospinal fluid analyses of Aβ levels using locally established cut-offs (i.e., $A\beta_{42/40}$-ratio < 5.5% or $A\beta_{1\text{-}42}$ < 375 pg/ml). The 18-F-PI2620 PET imaging protocol was approved by local ethics committee of the LMU Munich. Written informed consent was obtained from all participants in accordance with the Declaration of Helsinki. The full study protocol including all samples and all PET data analyses were approved by the local ethics committee (LMU Munich, application numbers 17-569 and 19-022) and the German radiation protection (BfS-application: Z 5 − 22464/2017-047-K-G) authorities. The study was carried out according to the principles of the Helsinki Declaration, patients received no compensation for study participation. All work complied with ethical regulations for work with human participants.

Neuroimaging acquisition. All structural MRI data were collected on 3 T scanners using 3D MPRAGE and MP2RAGE sequences. Radiosynthesis of 18-F-PI-2620 was achieved by nucleophilic substitution on a butyloxycarbonyl-protected nitro precursor using an automated synthesis module (Synthera, IBA Louvain-la-neuve, Belgium). The protecting group was cleaved under radiolabeling conditions. The product was purified by semipreparative high performance liquid chromatography, resulting in radiochemical purity of >97%. Non-decay corrected yields were about 30% with a molar activity of $3 \cdot 10^6$ GBq/mmol at the end of synthesis. 18-F-PI-2620 PET imaging in combination with computed tomography (CT) or magnetic resonance (MR) was performed in a full dynamic setting (minimum scan duration: 0–60 min post-injection) using pre-established standard PET scanning parameters at each site: In Munich, Germany, dynamic tau-PET was acquired on a Siemens Biograph True point 64 PET/CT (Siemens, Erlangen, Germany) or a Siemens mCT scanner (Siemens, Erlangen, Germany) in 3D list-mode over 60 min and reconstructed into a 336 × 336 × 109 matrix (voxel size: 1.02 × 1.02 × 2.03 mm^3) using the built-in ordered subset expectation maximization (OSEM) algorithm with 4 iterations, 21 subsets, and a 5 mm Gaussian filter. A low dose CT was used for attenuation correction. In Leipzig, Germany, dynamic tau-PET was acquired on a hybrid PET/MR system (Biograph mMR, Siemens Healthineers, Erlangen, Germany) in 3D list-mode over 60 min and reconstructed into a 256 × 256 matrix (voxel size: 1.00 × 1.00 × 2.03 mm^3) using the built-in ordered subset expectation maximization algorithm with 8 iterations, 21 subsets, and a 3 mm Gaussian filter. For attenuation correction, the vendor-provided HiRes method was employed, combining the individual Dixon attenuation correction approach with a bone attenuation template[63]. For tau-PET data of control subjects imaged in New Haven, US, dynamic PET was acquired on a Siemens ECAT EXACT HR + camera from 0 to 90 and 120 to 180 min. Images were reconstructed in a 128 × 128 matrix (zoom = 2, pixel size of 2.574 × 2.574 mm) with an iterative reconstruction algorithm (OSEM 4 iterations, 16 subsets) and a post-hoc 5 mm Gaussian filter. Standard corrections for random, scatter, system dead time and attenuation provided by the camera manufacturer were performed. 18-F-PI-2620 PET assessments of control subjects in Melbourne was performed on a Philips Gemini TF 64 PET/CT (Philips, Eindhoven, The Netherlands). PET images were acquired dynamically from 0 to 60 min and 80 to 120 min post-injection. Images were reconstructed using LOR-RAMLA and CT attenuation correction was performed. Images were binned into a 128 × 128 × 89 matrix (voxel size: 2.00 × 2.00 × 2.00 mm^3).

The injected dose was 168–334 MBq, applied as a bolus injection. Site-specific attenuation correction ensured multi-site harmonization of data acquisition[63]. Further, data from Hofmann brain phantoms were used to obtain scanner-specific filter functions which were consequently used to generate images with a similar spatial resolution for voxel-wise analyses (full-width-at-half-maximum = 9 × 9 × 10 mm; determined by the scanner in New Haven), following the Alzheimer's Disease Neuroimaging Initiative image harmonization procedure[64]. Resulting smoothing factors were 3.5 × 3.5 × 7.0 mm for Munich, 6.0 × 6.0 × 6.0 mm for Leipzig, and 4.0 × 4.0 × 4.0mm for Melbourne. All dynamic datasets were visually checked for artifacts and motion-corrected using rigid-registration. Mean SUV images were obtained for 20–40 min time frames to obtain SUVR images, which show comparable performance in signal sensitivity and were less subject to artifacts when compared to 0–60 min or 0–40 min DVR images[65].

Structural MRI and tau-PET preprocessing. All structural MRI and PET data were processed using the Advanced Normalization Tools (ANTs) toolbox (http://stnava.github.io/ANTs/). In an initial step, 18-F-PI-2620 PET images were rigidly co-registered to native-space T1-weighted MRI images. For T1-weighted structural MRI data we performed bias field correction, brain extraction, and segmentation into gray-matter, white matter and cerebrospinal fluid tissue maps using the ANTs cortical thickness pipeline. Brain extracted T1-weighted images were nonlinearly normalized to MNI space (2 mm isotropic voxels) using ANTs high-dimensional warping algorithm[66]. By combining the rigid 18-F-PI-2620 PET to T1-native space and nonlinear T1 to MNI space spatial normalization parameters, all brain-atlas-derived ROI data was transformed from MNI space back to PET native space, including the Tian 32 ROI subcortical brain atlas[33] (Fig. 1H), the Schaefer 200 ROI cortical brain atlas[32] (Fig. 1G), as well as the inferior cerebellar reference ROI for intensity normalization of tau-PET[67]. All brain-atlas data and the inferior cerebellar reference ROI were further masked with binary subject-specific gray-matter maps in order to restrict later extraction of ROI-mean values to gray-matter regions.

Tau-PET images were intensity normalized to the mean tracer uptake of the inferior cerebellar gray, to determine standardized uptake value ratio (SUVR). Mean tau-PET SUVR values were extracted for each subject for the 32 subcortical and 200 cortical ROIs from unsmoothed native-space PET data. For voxel-wise analyses, subject-specific tau-PET SUVR images were warped to MNI space by combining the linear PET to T1 and nonlinear T1 to MNI transformation parameters, followed by spatial smoothing with site-specific smoothing kernels. Usage of an alternative reference ROI (i.e., eroded white matter) yielded congruent analyses with those presented in the manuscript. To determine whether ROI-based estimation of tau-PET ROIs was biased by gray-matter atrophy, we further obtained partial-volume effect (PVE) corrected tau-PET SUVRs, using the Gaussian transfer method[68].

Postmortem sample. To replicate tau-PET vs. connectivity associations using postmortem assessments of tau pathology, we included histopathological tau data from two independent samples, including $n = 97$ PSP subjects recruited, sampled, and examined at several different sites across Europe with centralized final analysis at the Department of Neuropathology, LMU, in Munich and $n = 96$ PSP subjects from the University of Pennsylvania. An in-depth description of data selection and data acquisition has been published previously[8]. Cases were selected based on presence of neurofibrillary tangles in the subthalamic nucleus, substantia nigra, and pallidum, as well as based on the presence of tufted astrocytes in the striatum and frontal cortex[3, 69]. All donors or their next of a kin had given written informed consent according to the Declaration of Helsinki for the use of brain tissue and medical records for research purposes. Usage of the material was in accordance with the directives of local ethics commissions regarding the use of archive material for research purposes. The postmortem tau histopathological examinations of brain tissue in PSP patients were approved by the ethics committee of the medical faculty of the university of Marburg, Germany.

Extraction of neuropathological samples followed a standardized pre-established procedure[8]. Formalin-fixed and paraffin-embedded tissue blocks from the PSP cases were evaluated using tau immunostaining with the anti-tau AT8 antibody (Ser202/Thr205, 1:200, Invitrogen/Thermofischer, MN1020, Carlsbad, USA) for the Munich sample, and with anti-tau PHF-1 (Ser396/Ser404, 1:2000) for the UPENN sample. For each sample, we included data from postmortem sampled regions of interest, which were judged accessible with functional MRI, resulting in 16 ROIs for the Munich sample and 9 ROIs for the UPENN sample. Neuropathological ROIs were reconstructed in MNI space based on the neuropathological examination protocol using predefined ROIs from established anatomical brain atlases (Fig. 6A, B)[33, 35]. Neuronal tangle pathology was graded for each region in a semiquantitative score (none = 0, mild = 1, moderate = 2, severe = 3).

For direct comparison with the autoradiography signal, tau immunostaining from formalin-fixed and paraffin-embedded tissue blocks from 16 PSP cases and three brain regions (frontal cortex, putamen, and pallidum) was processed and graded as described above. For each patient and brain region, autoradiography with 18-F-PI-2620 was performed on ≥4 sections (Superiority of Formalin-Fixed Paraffin-Embedded Brain Tissue for in vitro Assessment of Progressive Supranuclear Palsy Tau Pathology With [18 F]PI-2620, Willroider et al. 2021). In short, sections were incubated for 45 min (21.6 µCi/ml after dilution to a volume of 50 ml with phosphate buffered saline solution, pH 7.4, specific activity 480 ± 90 GBq/µmol), washed, dried, placed on imaging plates for 12 h and scanned at 25.0 µm resolution. Regions of interest were drawn on each sample with AT8 staining of adjacent section serving for precise anatomical definition with AT8-negative white matter as reference region. Binding ratios were correlated with semiquantitative AT8 assessment using spearman correlation and differences between groups were assessed using ANOVA.

In vitro competition assay. K18 fibrils, depicting 4 R tau deposits (~5 µg protein per well) were incubated with ^{18}F-PI-2620 or ^{18}F-AV1451 (0.7 kBq per well) and the respective cold compound(s) ranging from 0.61 nM to 1000 nM for 45 min at 37 °C in a 96-well plate. The assay was performed in a total volume of 200 µL PBS w/o Ca + +/Mg ++ containing 0.1% BSA and 2% DMSO. Nonspecific signal was determined with samples containing ^{18}F-labeled tau-tracer in the presence of assay buffer w/o brain substrate and competitor. The assay controls without brain homogenate were incubated with the tracer in parallel. After 45 min incubation, the samples were filtered under vacuum on a GF/B filter plate (PerkinElmer 6005177). The GF/B filters were equilibrated with PBS (w/o Ca + +/Mg + +, 0.1% BSA, 2% DMSO) at least 1 h before filtration. Afterwards, the filters were washed two times with 200 µL PBS (w/o Ca + +/ Mg + +, 0.1 % BSA, 2% DMSO). The top and bottom side of the filter plates were sealed and a phospho-imaging plate was placed on top of the filter plate and exposed overnight. The imaging plate was scanned using the BASReader 5000 (Fuji) and quantified with the AIDA software. Specific binding was calculated by subtracting the nonspecific signal from the measured sample signals. The unblocked ^{18}F-labeled tracer signal was defined as total binding. IC_{50} values were calculated using Prism V8.

Assessment of covariance in tau-PET and postmortem tau. We assessed the inter-regional covariance in 18-F-PI-2620 PET SUVRs (see Fig. 2A for an analysis flow-chart) for 22 PSP-RS and 24 CBS patients. The analysis pipeline was adopted from previous studies using this approach to determine FDG-PET covariance (i.e., metabolic covariance), gray-matter covariance (i.e., structural connectivity), or 18-F-AV1451 PET covariance across brain regions[39, 40, 70, 71]. First, we computed the mean tau-PET uptake within each of the 200 cortical (Fig. 1G) and 32 subcortical (Fig. 1H) ROIs for each subject (Fig. 2, A(i)). Next, we vectorized mean ROI SUVR values to subject-specific 232-element vectors (Fig. 2, A(ii)). Using these 232-element 18-F-PI-2620 PET SUVR vectors, we then assessed across subjects the pairwise ROI-to-ROI partial correlation of 18-F-PI-2620 PET uptake (Fig. 2, A(iii)), adjusting for subject-specific age, gender, and PET imaging and MRI protocol as potential confounds. This analysis resulted in a 232 × 232 sized 18-F-PI-2620 PET covariance matrix each for each group (i.e., PSP, CBS). Within this 18-F-PI-2620 PET covariance matrix, autocorrelations were set to zero and all correlations were Fisher-z transformed.

An equivalent approach was used for postmortem tau data. For each sample, we determined the inter-regional partial Spearman correlation of postmortem AT8-stained tau pathology across the 16 ROIs of the Munich-European consortium/collection sample (Fig. 6A) or 9 ROIs of the UPENN sample (Fig. 6B), adjusting for age at death and gender, yielding a covariance in postmortem tau matrix (Fig. 6C, E). Note that we specifically used partial Spearman correlation since postmortem ratings were done on an ordinal scale. Again, autocorrelations within this matrix were set to zero and all remaining correlations were Fisher-z transformed.

Functional connectivity assessment. For assessing functional connectivity, we used resting-state fMRI data from 69 cognitively normal controls of the ADNI cohort. Ethics approval was obtained by ADNI investigators at participating ADNI sites, all study participants provided written informed consent. These subjects were selected based on absence of objective or subjective signs of cognitive impairment and had no evidence of clinically relevant cerebral amyloid or tau pathology, as indicated by negative ^{18}F-florbetapir amyloid-PET (i.e., global SUVR < 1.11)[72] and negative ^{18}F-flortaucipir tau-PET scans (i.e., global SUVR < 1.3)[29].

MRI scans were obtained on Siemens scanners using unified scanning protocols. T1-weighted structural MRI was recorded using a MPRAGE sequence with 1 mm isotropic voxel-space and a TR = 2300 ms. For functional MRI, for each subject a total of 200 resting-state fMRI volumes were recorded using a 3D echo-planar imaging (EPI) sequence in 3.4 mm isotropic voxel resolution with a TR/TE/flip angle = 3000/30/90°.

All images were inspected for artifacts prior to preprocessing. Using ANTs, T1-weighted structural MRI images were bias corrected, brain extracted, segmented and nonlinearly spatially normalized to MNI space[66]. Functional EPI images were slice-time and motion-corrected (i.e., realignment to the first volume) and co-registered to the native T1 images. Using rigid-transformation parameters, T1-derived gray-matter, white matter, and cerebrospinal fluid segments were transformed to EPI space. To denoise the EPI images, we regressed out nuisance covariates (i.e., average white matter and cerebrospinal fluid signal and motion parameters estimated during motion correction), removed the linear trend and applied band-pass filtering with a 0.01–0.08 Hz frequency band in EPI native space. To further minimize the impact of motion which may compromise FC assessment[73], we performed motion scrubbing, where we censored volumes that showed a frame-wise displacement of >1 mm, as well as one prior and two subsequent volumes. In line with our previous work[74], only subjects for whom less than 30% of volumes had to be censored were included in the current study. Note that we did not spatially smooth the functional images during preprocessing to avoid signal spill-over between adjacent brain regions that may artificially enhance functional connectivity between adjacent brain regions during ROI-based connectivity assessment.

To determine functional connectivity, we warped the 232 cortical and subcortical ROIs for tau-PET analyses (Fig. 1G, H) as well as the postmortem ROIs for the Munich-European consortium/collection and UPENN sample (Fig. 6A, B) to the denoised and preprocessed fMRI images in native EPI space, by combining the linear EPI to T1 and nonlinear T1 to MNI transformation parameters. ROI maps in EPI space were masked with subject-specific gray matter. Fisher-z transformed Pearson-Moment correlations between time-series averaged across voxels within an ROI were determined to assess subject-specific functional connectivity matrices. Functional connectivity data were averaged across all 69 ADNI subjects in order to determine group-average functional connectivity matrices for the in vivo tau-PET analyses as well as for the postmortem analyses.

For the group-average functional connectivity matrices, we further determined 1000 null-models of functional connectivity respectively, by shuffling the functional connectivity matrices while preserving the overall degree- and weight-distribution, using the null_model_und_sign.m function of the brain connectivity toolbox (https://sites.google.com/site/bctnet/).

Statistics. Sample demographics were compared between the groups using ANOVAs for continuous measures and Chi-squared tests for categorical measures. Voxel-wise comparisons in 18-F-PI-2620 PET SUVRs were determined on spatially normalized and smoothed tau-PET images using ANCOVAs in SPM12, controlling for age, gender, and study site, applying a voxel-wise alpha-threshold of 0.005 and a cluster-extent threshold of >100 spatially contiguous voxels.

To test the association between functional connectivity and covariance in 18-F-PI-2620 PET, we used linear regression with covariance in 18-F-PI-2620 PET as a dependent variable and ADNI-derived group-average functional connectivity as an independent variable, controlling for inter-regional Euclidean distance (i.e., distance between ROI-specific centers of mass). This analysis was stratified by CBS and PSP-RS and conducted for subcortical ROIs only (i.e., primary analysis) as well as for the whole brain (i.e., secondary analysis). The same analysis was performed for postmortem tau assessments in the Munich-European consortium/collection and UPENN dataset, using regional semiquantitative tau data (i.e., 16 ROIs in the Munich sample vs. 9 ROIs in the UPENN sample) rather than tau-PET. To determine the robustness of the association between connectivity and covariance in 18-F-PI-2620 PET/postmortem tau, the analysis was repeated 1000 times using shuffled connectomes with preserved weight- and degree distribution to obtain a distribution of null-model β-values. We then performed an exact test, i.e., we determined the probability of null-distribution derived β-values surpassing the true β-value. For postmortem data, we further assessed cell-type-specific associations between tau covariance (i.e., neuronal, astroglial and oligodendroglial tau covariance) and functional connectivity. To this end we computed regression-based association between covariance in tau and functional connectivity for each cell type, based on 1000 bootstrapped samples that were randomly drawn from the respective sample (i.e., UPENN or Munich). The resulting β-value distributions reflecting the association between connectivity and cell-type-specific tau covariance were compared between cell-types using paired *t*-tests.

Using 18-F-PI-2620 PET, we further tested, whether functional connectivity patterns of tau epicenters (i.e., ROIs with highest tau) are predictive of 18-F-PI-2620 PET binding in remaining brain regions. Again, this analysis was determined stratified by group (i.e., PSP-RS vs. CBS) and conducted for subcortical ROIs only (i.e., primary analysis) as well as for the whole brain parcellation (i.e., secondary analysis). Specifically, we determined group-level 18-F-PI-2620 PET binding, and tested whether higher seed-based connectivity of the epicenter ROI was associated with higher 18-F-PI-2620 PET binding in the remaining ROIs, using linear regression controlling for between-ROI Euclidean distance. The same analysis was performed for the ROI with lowest 18-F-PI-2620 PET binding (i.e., coldspot), for which we assumed that higher connectivity is associated with lower 18-F-PI-2620 PET binding in the remaining regions. In an iterative next step, we repeated this analysis across all ROIs and determined the association between the 18-F-PI-2620 PET level in the seed ROI against the regression-derived β-value of the association between seed-based connectivity and 18-F-PI-2620 PET binding in remaining ROIs. As in our previous studies[39, 40], we expected that ROIs with higher tau-PET binding should be connected to other ROIs with a high binding level (i.e., as reflected in a positive β-value), whereas regions with low tau-PET binding should be connected to other ROIs with a low binding level (i.e., as reflected in a negative β-value).

For subject-level analyses, we adopted our pre-established approach[34] and determined subject-level epicenters as 20% of ROIs with highest tau-PET binding (see Fig. 5H, I for tau epicenter probability maps in PSP-RS and CBS). The remaining non-epicenter ROIs were grouped for each subject into 4 quartiles, based on the connectivity strength to the epicenter (i.e., ROIs grouped in Q1 show highest connected to the tau epicenter, vs. ROIs grouped in Q4 show weakest connectivity to tau epicenters). Note that Q1–Q4 ROIs were determined separately for subcortical and cortical regions. Mean 18-F-PI-2620 PET binding was assessed for each subjects' subcortical/cortical Q1–Q4 ROIs. Using linear mixed models, we then tested the association between connectivity strength (i.e., Q1–Q4) and subcortical or cortical 18-F-PI-2620 PET binding in Q1–Q4 ROIs, controlling for age, sex, study site, mean Euclidean distance to the epicenter as well as random intercept. In an exploratory analysis in the CBS group, we repeated this subject-level analysis while adding an additional main effect for global ^{18}F-Flutemetamol amyloid-PET levels stratified at the median, to determine whether subthreshold levels of Aβ were associated with increased subcortical to cortical tau spread. Altering the definition of epicenters (i.e., 10, 15, 20%, 25, or 30 of ROIs with highest

18-F-PI-2620 PET binding) did not change the result pattern. All analyses were computed using R statistical software (r-project.org).

Reporting summary. Further information on research design is available in the Nature Research Reporting Summary linked to this article.

Data availability

The fMRI data that are used in this study were obtained from the Alzheimer's disease Neuroimaging Initiative (ADNI) and are available from the ADNI database (adni.loni.usc.edu) upon registration and compliance with the data usage agreement. A list of ADNI RIDs that have been used for the current study can be found in the Supplementary Information file. ADNI neuroimaging data (unprocessed or processed) are available from the corresponding authors upon request and upon proof of approved access to the ADNI database. Neuroimaging data (i.e., unprocessed or processed PET & MRI images), as well as spreadsheets with postmortem and autoradiography data from PSP and CBS patients, have been used in previous publications[8, 27], and are available under restricted access from the corresponding author upon request and approval of a dedicated data usage agreement between institutions exchanging data. Data sharing of all data used in the current study is restricted since ethics approvals for PET and Postmortem studies or ADNI terms of use do not allow unrestricted and open-source sharing of patient-specific data with third-parties. Source data are provided with this paper.

Received: 30 July 2021; Accepted: 14 February 2022;
Published online: 15 March 2022

References

1. Dickson, D. W. et al. Office of Rare Diseases neuropathologic criteria for corticobasal degeneration. *J. Neuropathol. Exp. Neurol.* **61**, 935–946 (2002).
2. Flament, S., Delacourte, A., Verny, M., Hauw, J. J. & Javoy-Agid, F. Abnormal Tau proteins in progressive supranuclear palsy. Similarities and differences with the neurofibrillary degeneration of the Alzheimer type. *Acta Neuropathol.* **81**, 591–596 (1991).
3. Dickson, D. W. Neuropathologic differentiation of progressive supranuclear palsy and corticobasal degeneration. *J. Neurol.* **246**, II6–II15 (1999).
4. Rosler, T. W. et al. Four-repeat tauopathies. *Prog. Neurobiol.* **180**, 101644 (2019).
5. Ling, H. et al. Fulminant corticobasal degeneration: a distinct variant with predominant neuronal tau aggregates. *Acta Neuropathol.* **139**, 717–734 (2020).
6. Ling, H. et al. Astrogliopathy predominates the earliest stage of corticobasal degeneration pathology. *Brain* **139**, 3237–3252 (2016).
7. Ling, H. et al. Characteristics of progressive supranuclear palsy presenting with corticobasal syndrome: a cortical variant. *Neuropathol. Appl. Neurobiol.* **40**, 149–163 (2014).
8. Kovacs, G. G. et al. Distribution patterns of tau pathology in progressive supranuclear palsy. *Acta Neuropathol.* **140**, 99–119 (2020).
9. Josephs, K. A. et al. Clinicopathological and imaging correlates of progressive aphasia and apraxia of speech. *Brain J. Neurol.* **129**, 1385–1398 (2006).
10. Bigio, E. H. et al. Cortical synapse loss in progressive supranuclear palsy. *J. Neuropathol. Exp. Neurol.* **60**, 403–410 (2001).
11. Kouri, N. et al. Neuropathological features of corticobasal degeneration presenting as corticobasal syndrome or Richardson syndrome. *Brain J. Neurol.* **134**, 3264–3275 (2011).
12. Armstrong, M. J. et al. Criteria for the diagnosis of corticobasal degeneration. *Neurology* **80**, 496–503 (2013).
13. Gibbons, G. S., Lee, V. M. Y. & Trojanowski, J. Q. Mechanisms of cell-to-cell transmission of pathological Tau: a review. *JAMA Neurol.* **76**, 101–108 (2019).
14. Guo, J. L. & Lee, V. M. Seeding of normal Tau by pathological Tau conformers drives pathogenesis of Alzheimer-like tangles. *J. Biol. Chem.* **286**, 15317–15331 (2011).
15. Narasimhan, S. et al. Pathological Tau strains from human brains recapitulate the diversity of tauopathies in nontransgenic mouse brain. *J. Neurosci.* **37**, 11406–11423 (2017).
16. de Calignon, A. et al. Propagation of tau pathology in a model of early Alzheimer's disease. *Neuron* **73**, 685–697 (2012).
17. Boluda, S. et al. Differential induction and spread of tau pathology in young PS19 tau transgenic mice following intracerebral injections of pathological tau from Alzheimer's disease or corticobasal degeneration brains. *Acta Neuropathol.* **129**, 221–237 (2015).
18. Ahmed, Z. et al. A novel in vivo model of tau propagation with rapid and progressive neurofibrillary tangle pathology: the pattern of spread is determined by connectivity, not proximity. *Acta Neuropathol.* **127**, 667–683 (2014).
19. Clavaguera, F. et al. Brain homogenates from human tauopathies induce tau inclusions in mouse brain. *Proc. Natl Acad. Sci. USA* **110**, 9535–9540 (2013).
20. Pooler, A. M., Phillips, E. C., Lau, D. H., Noble, W. & Hanger, D. P. Physiological release of endogenous tau is stimulated by neuronal activity. *EMBO Rep.* **14**, 389–394 (2013).
21. Calafate, S. et al. Synaptic contacts enhance cell-to-cell Tau pathology propagation. *Cell Rep.* **11**, 1176–1183 (2015).
22. Wu, J. W. et al. Neuronal activity enhances tau propagation and tau pathology in vivo. *Nat. Neurosci.* **19**, 1085–1092 (2016).
23. Tsuboi, Y. et al. Increased tau burden in the cortices of progressive supranuclear palsy presenting with corticobasal syndrome. *Mov. Disord.* **20**, 982–988 (2005).
24. Sakae, N. et al. Clinicopathologic subtype of Alzheimer's disease presenting as corticobasal syndrome. *Alzheimers Dement.* **15**, 1218–1228 (2019).
25. Robinson, J. L. et al. Neurodegenerative disease concomitant proteinopathies are prevalent, age-related and APOE4-associated. *Brain J. Neurol.* **141**, 2181–2193 (2018).
26. Karran, E. & Mercken, M. & De Strooper, B. The amyloid cascade hypothesis for Alzheimer's disease: an appraisal for the development of therapeutics. *Nat. Rev. Drug Discov.* **10**, 698–712 (2011).
27. Brendel, M. et al. Assessment of 18F-PI-2620 as a biomarker in progressive supranuclear palsy. *JAMA Neurol.* **77**, 1408–1419 (2020).
28. Hoglinger, G. U. et al. Clinical diagnosis of progressive supranuclear palsy: the movement disorder society criteria. *Mov. Disord.* **32**, 853–864 (2017).
29. Maass, A. et al. Comparison of multiple tau-PET measures as biomarkers in aging and Alzheimer's disease. *Neuroimage* **157**, 448–463 (2017).
30. Jagust, W. J. et al. The Alzheimer's Disease Neuroimaging Initiative positron emission tomography core. *Alzheimers Dement.* **6**, 221–229 (2010).
31. Palleis, C. et al. In vivo assessment of neuroinflammation in 4-repeat tauopathies. *Mov. Disord.* https://pubmed.ncbi.nlm.nih.gov/33245166/ (2020).
32. Schaefer, A. et al. Local-global parcellation of the human cerebral cortex from intrinsic functional connectivity MRI. *Cereb. Cortex* 1–20 https://pubmed.ncbi.nlm.nih.gov/28981612/ (2017).
33. Tian, Y., Margulies, D. S., Breakspear, M. & Zalesky, A. Topographic organization of the human subcortex unveiled with functional connectivity gradients. *Nat. Neurosci.* **23**, 1421–1432 https://pubmed.ncbi.nlm.nih.gov/33246962/ (2020).
34. Franzmeier, N. et al. Patient-centered connectivity-based prediction of tau pathology spread in Alzheimer's disease. *Sci. Adv.* **6**, (2020).
35. Rolls, E. T., Huang, C. C., Lin, C. P., Feng, J. & Joliot, M. Automated anatomical labelling atlas 3. *NeuroImage* **206**, 116189 (2020).
36. Brunello, C. A., Merezhko, M., Uronen, R. L. & Huttunen, H. J. Mechanisms of secretion and spreading of pathological tau protein. *Cell Mol. Life Sci.* **77**, 1721–1744 (2020).
37. Mudher, A. et al. What is the evidence that tau pathology spreads through prion-like propagation? *Acta Neuropathol. Commun.* **5**, 99 (2017).
38. Kroth, H. et al. Discovery and preclinical characterization of [(18)F]PI-2620, a next-generation tau PET tracer for the assessment of tau pathology in Alzheimer's disease and other tauopathies. *Eur. J. Nucl. Med. Mol. imaging* **46**, 2178–2189 (2019).
39. Franzmeier, N. et al. Functional brain architecture is associated with the rate of tau accumulation in Alzheimer's disease. *Nat. Commun.* **11**, 347 (2020).
40. Franzmeier, N. et al. Functional connectivity associated with tau levels in ageing, Alzheimer's, and small vessel disease. *Brain J. Neurol.* https://pubmed.ncbi.nlm.nih.gov/30770704/ (2019).
41. Sintini, I. et al. Tau and amyloid relationships with resting-state functional connectivity in atypical Alzheimer's disease. *Cereb. Cortex* **31**, 1693–1706 (2021).
42. He, Z. et al. Transmission of tauopathy strains is independent of their isoform composition. *Nat. Commun.* **11**, 7 (2020).
43. Shi, Y. et al. Structure-based classification of tauopathies. *Nature* **598**, 359–363 (2021).
44. Arai, T. et al. Identification of amino-terminally cleaved tau fragments that distinguish progressive supranuclear palsy from corticobasal degeneration. *Ann. Neurol.* **55**, 72–79 (2004).
45. Taniguchi-Watanabe, S. et al. Biochemical classification of tauopathies by immunoblot, protein sequence and mass spectrometric analyses of sarkosyl-insoluble and trypsin-resistant tau. *Acta Neuropathol.* **131**, 267–280 (2016).
46. Narasimhan, S. et al. Human tau pathology transmits glial tau aggregates in the absence of neuronal tau. *J. Exp. Med.* **217**, https://pubmed.ncbi.nlm.nih.gov/31826239/ (2020).
47. Kovacs, G. G. et al. Sequential stages and distribution patterns of aging-related tau astrogliopathy (ARTAG) in the human brain. *Acta Neuropathol. Commun.* **6**, 50 (2018).
48. Kovacs, G. G. Astroglia and Tau: new perspectives. *Front. Aging Neurosci.* **12**, 96 (2020).
49. Lewis, J. & Dickson, D. W. Propagation of tau pathology: hypotheses, discoveries, and yet unresolved questions from experimental and human brain studies. *Acta Neuropathol.* **131**, 27–48 (2016).
50. Liu, L. et al. Trans-synaptic spread of tau pathology in vivo. *PLoS ONE* **7**, e31302 (2012).

51. Vogel, J. W. et al. Spread of pathological tau proteins through communicating neurons in human Alzheimer's disease. *Nat. Commun.* **11**, 2612 (2020).
52. Leal, S. L., Lockhart, S. N., Maass, A., Bell, R. K. & Jagust, W. J. Subthreshold amyloid predicts Tau deposition in aging. *J. Neurosci.* **38**, 4482–4489 (2018).
53. Uchihara, T. Neurofibrillary changes undergoing morphological and biochemical changes—how does tau with the profile shift of from four repeat to three repeat spread in Alzheimer brain? *Neuropathology* **40**, 450–459 (2020).
54. Zhou, Y., Li, J., Nordberg, A. & Agren, H. Dissecting the binding profile of PET tracers to corticobasal degeneration Tau fibrils. *ACS Chem. Neurosci.* **12**, 3487–3496 (2021).
55. Tagai, K. et al. High-contrast in vivo imaging of Tau pathologies in Alzheimer's and non-Alzheimer's disease tauopathies. *Neuron* **109**, 42–58 e48 (2021).
56. Bloom, G. S. Amyloid-beta and tau: the trigger and bullet in Alzheimer disease pathogenesis. *JAMA Neurol.* **71**, 505–508 (2014).
57. Iqbal, K., Liu, F., Gong, C. X. & Grundke-Iqbal, I. Tau in Alzheimer disease and related tauopathies. *Curr. Alzheimer Res.* **7**, 656–664 (2010).
58. Honey, C. J. et al. Predicting human resting-state functional connectivity from structural connectivity. *Proc. Natl Acad. Sci. USA* **106**, 2035–2040 (2009).
59. Abhinav, K. et al. Advanced diffusion MRI fiber tracking in neurosurgical and neurodegenerative disorders and neuroanatomical studies: a review. *Biochim. Biophys. Acta* **1842**, 2286–2297 (2014).
60. Grandjean, J., Zerbi, V., Balsters, J. H., Wenderoth, N. & Rudin, M. Structural basis of large-scale functional connectivity in the mouse. *J. Neurosci.* **37**, 8092–8101 (2017).
61. Lu, H., Jaime, S. & Yang, Y. Origins of the resting-state functional MRI signal: potential limitations of the "Neurocentric" model. *Front. Neurosci.* **13**, 1136 (2019).
62. Shi, Z. et al. On the relationship between MRI and local field potential measurements of spatial and temporal variations in functional connectivity. *Sci. Rep.* **9**, 8871 (2019).
63. Ladefoged, C. N. et al. A multi-centre evaluation of eleven clinically feasible brain PET/MRI attenuation correction techniques using a large cohort of patients. *NeuroImage* **147**, 346–359 (2017).
64. Jagust, W. J. et al. The Alzheimer's disease neuroimaging initiative 2 PET core: 2015. *Alzheimers Dement.* **11**, 757–771 (2015).
65. Song, M. et al. Feasibility of short imaging protocols for [18F]PI-2620 Tau-PET in progressive supranuclear palsy. *Res. Sq.* https://pubmed.ncbi.nlm.nih.gov/34021393/ (2020).
66. Avants, B. B. et al. A reproducible evaluation of ANTs similarity metric performance in brain image registration. *NeuroImage* **54**, 2033–2044 (2011).
67. Baker, S. L., Maass, A. & Jagust, W. J. Considerations and code for partial volume correcting [(18)F]-AV-1451 tau PET data. *Data Brief.* **15**, 648–657 (2017).
68. Rousset, O. G., Ma, Y. & Evans, A. C. Correction for partial volume effects in PET: principle and validation. *J. Nucl. Med.* **39**, 904–911 (1998).
69. Litvan, I. et al. Natural history of progressive supranuclear palsy (Steele-Richardson-Olszewski syndrome) and clinical predictors of survival: a clinicopathological study. *J. Neurol. Neurosurg. Psychiatry* **60**, 615–620 (1996).
70. Di, X. et al. Do all roads lead to Rome? A comparison of brain networks derived from inter-subject volumetric and metabolic covariance and moment-to-moment hemodynamic correlations in old individuals. *Brain Struct. Funct.* **222**, 3833–3845 (2017).
71. Pagani, M. et al. Functional pattern of brain FDG-PET in amyotrophic lateral sclerosis. *Neurology* **83**, 1067–1074 (2014).
72. Landau, S. M. et al. Amyloid deposition, hypometabolism, and longitudinal cognitive decline. *Ann. Neurol.* **72**, 578–586 (2012).
73. Power, J. D. et al. Methods to detect, characterize, and remove motion artifact in resting state fMRI. *Neuroimage* **84**, 320–341 (2014).
74. Franzmeier, N. et al. Left frontal hub connectivity delays cognitive impairment in autosomal-dominant and sporadic Alzheimer's disease. *Brain J. Neurol.* https://pubmed.ncbi.nlm.nih.gov/29462334/ (2018).

Acknowledgements

We acknowledge all members of the German Imaging Initiative for Tauopathies (GII4T) and the Alzheimer's Disease Neuroimaging Initiative (see supplementary information for a list of consortium members). We wish to thank the patients and their families, without whose support and altruism this research would not have been possible. Further, we would like to acknowledge Prof. Christian Haass (DZNE, Munich) for his consultation on study design, the European Reference Network for Rare Neurological Diseases—Project ID No 739510 and the Neurological Tissue Bank of the Biobanc-Hospital Clinic-IDIBAPS for sample and data procurement. This work was supported by the NIH (P30AG010124, P01AG066597, U19AG062418, and R01-NS109260), the National Center for Advancing Translational Sciences (TL1TR001880), the German Research Foundation (DFG; SCHR 774/5-1, DFG, INST 409/193-1 FUGG) the SyNergy excellence cluster (EXC 2145/ID 390857198). N.F. was supported by the Hertie foundation for clinical neurosciences. G.G.K. is supported by the Rossy Foundation and Safra Foundation. G.H. was funded by the Deutsche Forschungsgemeinschaft (DFG, HO2402/18-1 MSAomics), the German Federal Ministry of Education and Research (BMBF, 01EK1605A HitTau), VolkswagenStiftung and Lower Saxony Ministry for Science (Niedersächsisches Vorab), Petermax-Müller Foundation (Etiology and Therapy of Synucleinopathies and Tauopathies). M.B. was supported by the Hirnliga e.V. (Manfred-Strohscheer-Stiftung) and by the Alzheimer Forschung Initiative e.V. (grant number #19063p).

Author contributions

N.F., M.B.: study concept and design, data analyses, interpretation of the results, drafting the manuscript; L.B., L.S., G.K., T.A., C.K., G.R., M.L., D.B., A.R., L.F., S.H., A.M., A.F., C.P., E.J., E.W., S.K., M.S., G.B., M.K., M.S., B.R., R.P., M.R., M.P., A.S., H.B., O.S., J.R., M.S., J.C., V.V., J.S., A.S., E.L., D.C., A.G., M.G., C.M., E.G., L.M.P., Y.C., J.S., L.D.L., C.T., S.A.S., J.R., S.X., D.I., S.R., J.H., M.S., P.B., V.L., J.T.: data acquisition, critical revision of the manuscript; J.L., G.H., M.E.: study concept and design, interpretation of the results, critical revision of the manuscript.

Funding

Open Access funding enabled and organized by Projekt DEAL.

Competing interests

The authors declare no competing interests.

Additional information

Supplementary information The online version contains supplementary material available at https://doi.org/10.1038/s41467-022-28896-3.

Correspondence and requests for materials should be addressed to Nicolai Franzmeier.

Peer review information *Nature Communications* thanks Masato Hasegawa, Heidi Jacobs and William Jagust for their contribution to the peer review of this work. Peer reviewer reports are available.

Reprints and permission information is available at http://www.nature.com/reprints

Publisher's note Springer Nature remains neutral with regard to jurisdictional claims in published maps and institutional affiliations.

[1]Institute for Stroke and Dementia Research, University Hospital of Munich, LMU Munich, Munich, Germany. [2]Department of Nuclear Medicine, University Hospital of Munich, LMU Munich, Munich, Germany. [3]Munich Cluster for Systems Neurology (SyNergy), Munich, Germany. [4]Center for Neurodegenerative Disease Research (CNDR), Institute On Aging and Department of Pathology & Laboratory Medicine, University of Pennsylvania, Philadelphia, PA, USA. [5]Tanz Centre for Research in Neurodegenerative Disease (CRND) and Department of Laboratory Medicine and Pathobiology, University of Toronto, Toronto, ON, Canada. [6]Laboratory Medicine Program and Krembil Brain Institute, University Health

Network, Toronto, ON, Canada. [7]German Center for Neurodegenerative Diseases (DZNE), Munich, Germany. [8]Department of Psychiatry and Psychotherapy, University Hospital, LMU Munich, Munich, Germany. [9]Center for Neuropathology and Prion Research, LMU Munich, Munich, Germany. [10]Department of Neurology, Klinikum Rechts der Isar, Technical University of Munich, Munich, Germany. [11]Department of Neurology, Hannover Medical School, Carl-Neuberg-Str. 1, 30625 Hannover, Germany. [12]Clinic of Neurology, CCS, University of Belgrade, Belgrade, Republic of Serbia. [13]Life Molecular Imaging GmbH, Berlin, Germany. [14]Department of Neurology, University Hospital of Munich, LMU Munich, Munich, Germany. [15]Department of Radiology, University Hospital of Munich, LMU Munich, Munich, Germany. [16]Ageing Epidemiology Research Unit (AGE), School of Public Health, Imperial College, London, UK. [17]Department of Nuclear Medicine, University Hospital Leipzig, Leipzig, Germany. [18]Department of Nuclear Medicine, University Hospital Cologne, Cologne, Germany. [19]Department of Neurology, University Hospital Leipzig, Leipzig, Germany. [20]Department of Molecular Imaging & Therapy, Austin Health, Heidelberg, VIC, Australia. [21]Department of Psychiatry, University of Pittsburgh, Pittsburgh, PA, USA. [22]Department of Medicine, Austin Health, The University of Melbourne, Melbourne, VIC, Australia. [23]InviCRO, LLC, Boston, MA, USA. [24]Molecular Neuroimaging, A Division of inviCRO, New Haven, CT, USA. [25]Frontotemporal Degeneration Center, University of Pennsylvania, Philadelphia, PA, USA. [26]Department of Neurosciences, University of California, La Jolla, San Diego, CA, USA. [27]Department of Neurology, University of Pennsylvania, Philadelphia, PA, USA. [28]Neurological Tissue Bank and Neurology Department, Hospital Clínic de Barcelona, Universitat de Barcelona, IDIBAPS, CERCA, Barcelona, Catalonia, Spain. [29]Institute of Neurology, Medical University of Vienna, Vienna, Austria. [30]Parkinson's Disease & Movement Disorders Unit, Hospital Clínic / IDIBAPS / CIBERNED (CB06/05/0018-ISCIII), / European Reference Network for Rare Neurological Diseases (ERN-RND) / Institut de Neurociències (Maria de Maeztu Center), Universitat de Barcelona, Barcelona, Catalonia, Spain. [31]Department of Neurology, Erasmus Medical Centre, Rotterdam, The Netherlands. [32]Department Clinical Genetics, Erasmus Medical Center, Rotterdam, The Netherlands. [33]London Neurodegenerative Diseases Brain Bank, Institute of Psychiatry, Psychology and Neuroscience, Kings College London, London, UK. [34]Department of Biostatistics, Epidemiology and Informatics, University of Pennsylvania, Philadelphia, PA, USA. [35]Department of Neurology, Hannover Medical School, Hannover, Germany. [36]These authors contributed equally: Nicolai Franzmeier, Matthias Brendel. [37]These authors jointly supervised this work: Günter Höglinger, Michael Ewers. ✉email: Nicolai.franzmeier@med.uni-muenchen.de

7. Literaturverzeichnis

Albrecht, P., Müller, A. K., Südmeyer, M., Ferrea, S., Ringelstein, M., Cohn, E., . . . Methner, A. (2012). Optical coherence tomography in parkinsonian syndromes. *PLoS One, 7*(4), e34891. doi:10.1371/journal.pone.0034891

Amtage, F., Maurer, C., Hellwig, S., Tuscher, O., Kreft, A., Weiller, C., . . . Meyer, P. T. (2014). Functional correlates of vertical gaze palsy and other ocular motor deficits in PSP: an FDG-PET study. *Parkinsonism Relat Disord, 20*(8), 898-906. doi:10.1016/j.parkreldis.2014.05.013

Armstrong, M. J., Litvan, I., Lang, A. E., Bak, T. H., Bhatia, K. P., Borroni, B., . . . Weiner, W. J. (2013). Criteria for the diagnosis of corticobasal degeneration. *Neurology, 80*(5), 496-503. doi:10.1212/WNL.0b013e31827f0fd1

Beyer, L., Meyer-Wilmes, J., Schonecker, S., Schnabel, J., Brendel, E., Prix, C., . . . Brendel, M. (2018). Clinical Routine FDG-PET Imaging of Suspected Progressive Supranuclear Palsy and Corticobasal Degeneration: A Gatekeeper for Subsequent Tau-PET Imaging? *Front Neurol, 9*, 483. doi:10.3389/fneur.2018.00483

Blin, J., Baron, J. C., Dubois, B., Pillon, B., Cambon, H., Cambier, J., & Agid, Y. (1990). Positron Emission Tomography Study in Progressive Supranuclear Palsy - Brain Hypometabolic Pattern and Clinicometabolic Correlations. *Archives of Neurology, 47*(7), 747-752. doi:DOI 10.1001/archneur.1990.00530070035009

Boxer, A. L., Geschwind, M. D., Belfor, N., Gorno-Tempini, M. L., Schauer, G. F., Miller, B. L., . . . Rosen, H. J. (2006). Patterns of brain atrophy that differentiate corticobasal degeneration syndrome from progressive supranuclear palsy. *Arch Neurol, 63*(1), 81-86. doi:10.1001/archneur.63.1.81

Boxer, A. L., Yu, J. T., Golbe, L. I., Litvan, I., Lang, A. E., & Hoglinger, G. U. (2017). Advances in progressive supranuclear palsy: new diagnostic criteria, biomarkers, and therapeutic approaches. *Lancet Neurol, 16*(7), 552-563. doi:10.1016/S1474-4422(17)30157-6

Brendel, M., Schonecker, S., Hoglinger, G., Lindner, S., Havla, J., Blautzik, J., . . . Rominger, A. (2017). [(18)F]-THK5351 PET Correlates with Topology and Symptom Severity in Progressive Supranuclear Palsy. *Front Aging Neurosci, 9*, 440. doi:10.3389/fnagi.2017.00440

Buchert, R., Wegner, F., Huppertz, H.-J., Berding, G., Brendel, M., Apostolova, I., . . . Initiative, f. t. A. s. D. N. (2023). Automatic covariance pattern analysis outperforms visual reading of 18F-fluorodeoxyglucose-positron emission tomography (FDG-PET) in variant progressive supranuclear palsy. *Movement Disorders, 38*(10), 1901-1913. doi:10.1002/mds.29581

Burn, D. J., & Lees, A. J. (2002). Progressive supranuclear palsy: where are we now? *Lancet Neurol, 1*(6), 359-369. doi:10.1016/s1474-4422(02)00161-8

Cho, H., Choi, J. Y., Hwang, M. S., Lee, S. H., Ryu, Y. H., Lee, M. S., & Lyoo, C. H. (2017). Subcortical (18) F-AV-1451 binding patterns in progressive supranuclear palsy. *Mov Disord, 32*(1), 134-140. doi:10.1002/mds.26844

D'Antona, R., Baron, J. C., Samson, Y., Serdaru, M., Viader, F., Agid, Y., & Cambier, J. (1985). Subcortical dementia. Frontal cortex hypometabolism detected by positron tomography in patients with progressive supranuclear palsy. *Brain, 108 (Pt 3)*, 785-799. doi:10.1093/brain/108.3.785

Dutt, S., Binney, R. J., Heuer, H. W., Luong, P., Attygalle, S., Bhatt, P., . . . investigators, A. L. (2016). Progression of brain atrophy in PSP and CBS over 6 months and 1 year. *Neurology, 87*(19), 2016-2025. doi:10.1212/WNL.0000000000003305

Eckert, T., Tang, C., Ma, Y., Brown, N., Lin, T., Frucht, S., . . . Eidelberg, D. (2008). Abnormal metabolic networks in atypical parkinsonism. *Mov Disord, 23*(5), 727-733. doi:10.1002/mds.21933

Foster, N. L., Gilman, S., Berent, S., Morin, E. M., Brown, M. B., & Koeppe, R. A. (1988). Cerebral Hypometabolism in Progressive Supranuclear Palsy Studied with Positron

Emission Tomography. *Annals of Neurology, 24*(3), 399-406. doi:DOI 10.1002/ana.410240308

Franzmeier, N., Brendel, M., Beyer, L., Slemann, L., Kovacs, G. G., Arzberger, T., . . . Ewers, M. (2022). Tau deposition patterns are associated with functional connectivity in primary tauopathies. *Nat Commun, 13*(1), 1362. doi:10.1038/s41467-022-28896-3

Goffinet, A. M., Devolder, A. G., Gillain, C., Rectem, D., Bol, A., Michel, C., . . . Laterre, C. (1989). Positron Tomography Demonstrates Frontal-Lobe Hypometabolism in Progressive Supranuclear Palsy. *Annals of Neurology, 25*(2), 131-139. doi:DOI 10.1002/ana.410250205

Han, H. J., Kim, H., Park, J. H., Shin, H. W., Kim, G. U., Kim, D. S., . . . Kim, Y. J. (2010). Behavioral changes as the earliest clinical manifestation of progressive supranuclear palsy. *J Clin Neurol, 6*(3), 148-151. doi:10.3988/jcn.2010.6.3.148

Hellwig, S., Frings, L., Amtage, F., Buchert, R., Spehl, T. S., Rijntjes, M., . . . Meyer, P. T. (2015). 18F-FDG PET Is an Early Predictor of Overall Survival in Suspected Atypical Parkinsonism. *J Nucl Med, 56*(10), 1541-1546. doi:10.2967/jnumed.115.159822

Höglinger, G. U., Melhem, N. M., Dickson, D. W., Sleiman, P. M., Wang, L. S., Klei, L., . . . Schellenberg, G. D. (2011). Identification of common variants influencing risk of the tauopathy progressive supranuclear palsy. *Nat Genet, 43*(7), 699-705. doi:10.1038/ng.859

Hoglinger, G. U., Respondek, G., Stamelou, M., Kurz, C., Josephs, K. A., Lang, A. E., . . . Movement Disorder Society-endorsed, P. S. P. S. G. (2017). Clinical diagnosis of progressive supranuclear palsy: The movement disorder society criteria. *Mov Disord, 32*(6), 853-864. doi:10.1002/mds.26987

Iwasaki, Y., Mori, K., Ito, M., Tatsumi, S., Mimuro, M., & Yoshida, M. (2013). An autopsied case of progressive supranuclear palsy presenting with cerebellar ataxia and severe cerebellar involvement. *Neuropathology, 33*(5), 561-567. doi:10.1111/neup.12012

Jack, C. R., Jr., Bennett, D. A., Blennow, K., Carrillo, M. C., Dunn, B., Haeberlein, S. B., . . . Contributors. (2018). NIA-AA Research Framework: Toward a biological definition of Alzheimer's disease. *Alzheimers Dement, 14*(4), 535-562. doi:10.1016/j.jalz.2018.02.018

Josephs, K. A., & Duffy, J. R. (2008). Apraxia of speech and nonfluent aphasia: a new clinical marker for corticobasal degeneration and progressive supranuclear palsy. *Curr Opin Neurol, 21*(6), 688-692. doi:10.1097/WCO.0b013e3283168ddd

Josephs, K. A., Petersen, R. C., Knopman, D. S., Boeve, B. F., Whitwell, J. L., Duffy, J. R., . . . Dickson, D. W. (2006). Clinicopathologic analysis of frontotemporal and corticobasal degenerations and PSP. *Neurology, 66*(1), 41-48. doi:10.1212/01.wnl.0000191307.69661.c3

Karbe, H., Grond, M., Huber, M., Herholz, K., Kessler, J., & Heiss, W. D. (1992). Subcortical Damage and Cortical Dysfunction in Progressive Supranuclear Palsy Demonstrated by Positron Emission Tomography. *Journal of Neurology, 239*(2), 98-102. doi:Doi 10.1007/Bf00862982

Katzdobler, S., Nitschmann, A., Barthel, H., Bischof, G., Beyer, L., Marek, K., . . . German Imaging Initiative for, T. (2023). Additive value of [(18)F]PI-2620 perfusion imaging in progressive supranuclear palsy and corticobasal syndrome. *Eur J Nucl Med Mol Imaging, 50*(2), 423-434. doi:10.1007/s00259-022-05964-w

Kepe, V., Bordelon, Y., Boxer, A., Huang, S. C., Liu, J., Thiede, F. C., . . . Barrio, J. R. (2013). PET imaging of neuropathology in tauopathies: progressive supranuclear palsy. *J Alzheimers Dis, 36*(1), 145-153. doi:10.3233/JAD-130032

Kovacs, G. G., Lukic, M. J., Irwin, D. J., Arzberger, T., Respondek, G., Lee, E. B., . . . Hoglinger, G. U. (2020). Distribution patterns of tau pathology in progressive supranuclear palsy. *Acta Neuropathol, 140*(2), 99-119. doi:10.1007/s00401-020-02158-2

Leenders, K. L., Frackowiak, R. S. J., & Lees, A. J. (1988). Steele-Richardson-Olszewski Syndrome - Brain Energy-Metabolism, Blood-Flow and Fluorodopa Uptake Measured

by Positron Emission Tomography. *Brain, 111*, 615-630. doi:DOI 10.1093/brain/111.3.615

Lemoine, L., Gillberg, P. G., Svedberg, M., Stepanov, V., Jia, Z., Huang, J., . . . Nordberg, A. (2017). Comparative binding properties of the tau PET tracers THK5117, THK5351, PBB3, and T807 in postmortem Alzheimer brains. *Alzheimers Res Ther, 9*(1), 96. doi:10.1186/s13195-017-0325-z

Ling, H., Gelpi, E., Davey, K., Jaunmuktane, Z., Mok, K. Y., Jabbari, E., . . . Revesz, T. (2020). Fulminant corticobasal degeneration: a distinct variant with predominant neuronal tau aggregates. *Acta Neuropathol, 139*(4), 717-734. doi:10.1007/s00401-019-02119-4

Ling, H., Kovacs, G. G., Vonsattel, J. P., Davey, K., Mok, K. Y., Hardy, J., . . . Revesz, T. (2016). Astrogliopathy predominates the earliest stage of corticobasal degeneration pathology. *Brain, 139*(Pt 12), 3237-3252. doi:10.1093/brain/aww256

Litvan, I., Agid, Y., Calne, D., Campbell, G., Dubois, B., Duvoisin, R. C., . . . Zee, D. S. (1996). Clinical research criteria for the diagnosis of progressive supranuclear palsy (Steele-Richardson-Olszewski syndrome): report of the NINDS-SPSP international workshop. *Neurology, 47*(1), 1-9.

Litvan, I., Agid, Y., Jankovic, J., Goetz, C., Brandel, J. P., Lai, E. C., . . . Pearce, R. K. (1996). Accuracy of clinical criteria for the diagnosis of progressive supranuclear palsy (Steele-Richardson-Olszewski syndrome). *Neurology, 46*(4), 922-930. doi:10.1212/wnl.46.4.922

Mille, E., Levin, J., Brendel, M., Zach, C., Barthel, H., Sabri, O., . . . Rominger, A. (2017). Cerebral Glucose Metabolism and Dopaminergic Function in Patients with Corticobasal Syndrome. *J Neuroimaging, 27*(2), 255-261. doi:10.1111/jon.12391

Niethammer, M., Tang, C. C., Feigin, A., Allen, P. J., Heinen, L., Hellwig, S., . . . Eidelberg, D. (2014). A disease-specific metabolic brain network associated with corticobasal degeneration. *Brain, 137*(Pt 11), 3036-3046. doi:10.1093/brain/awu256

Otsuka, M., Ichiya, Y., Kuwabara, Y., Miyake, Y., Tahara, T., Masuda, K., . . . et al. (1989). Cerebral blood flow, oxygen and glucose metabolism with PET in progressive supranuclear palsy. *Ann Nucl Med, 3*(3), 111-118. doi:10.1007/BF03178296

Pardini, M., Huey, E. D., Spina, S., Kreisl, W. C., Morbelli, S., Wassermann, E. M., . . . Grafman, J. (2019). FDG-PET patterns associated with underlying pathology in corticobasal syndrome. *Neurology, 92*(10), e1121-e1135. doi:10.1212/WNL.0000000000007038

Pastor, P., Pastor, E., Carnero, C., Vela, R., García, T., Amer, G., . . . Oliva, R. (2001). Familial atypical progressive supranuclear palsy associated with homozigosity for the delN296 mutation in the tau gene. *Ann Neurol, 49*(2), 263-267. doi:10.1002/1531-8249(20010201)49:2<263::aid-ana50>3.0.co;2-k

Pinkhardt, E. H., & Kassubek, J. (2011). Ocular motor abnormalities in Parkinsonian syndromes. *Parkinsonism Relat Disord, 17*(4), 223-230. doi:10.1016/j.parkreldis.2010.08.004

Respondek, G., Grimm, M. J., Piot, I., Arzberger, T., Compta, Y., Englund, E., . . . Movement Disorder Society-Endorsed Progressive Supranuclear Palsy Study, G. (2020). Validation of the movement disorder society criteria for the diagnosis of 4-repeat tauopathies. *Mov Disord, 35*(1), 171-176. doi:10.1002/mds.27872

Respondek, G., Roeber, S., Kretzschmar, H., Troakes, C., Al-Sarraj, S., Gelpi, E., . . . Höglinger, G. U. (2013). Accuracy of the National Institute for Neurological Disorders and Stroke/Society for Progressive Supranuclear Palsy and neuroprotection and natural history in Parkinson plus syndromes criteria for the diagnosis of progressive supranuclear palsy. *Mov Disord, 28*(4), 504-509. doi:10.1002/mds.25327

Respondek, G., Stamelou, M., Kurz, C., Ferguson, L. W., Rajput, A., Chiu, W. Z., . . . Höglinger, G. U. (2014). The phenotypic spectrum of progressive supranuclear palsy: a retrospective multicenter study of 100 definite cases. *Mov Disord, 29*(14), 1758-1766. doi:10.1002/mds.26054

Rosler, T. W., Tayaranian Marvian, A., Brendel, M., Nykanen, N. P., Hollerhage, M., Schwarz, S. C., . . . Hoglinger, G. U. (2019). Four-repeat tauopathies. *Prog Neurobiol, 180*, 101644. doi:10.1016/j.pneurobio.2019.101644

Schonecker, S., Brendel, M., Palleis, C., Beyer, L., Hoglinger, G. U., Schuh, E., . . . Levin, J. (2019). PET Imaging of Astrogliosis and Tau Facilitates Diagnosis of Parkinsonian Syndromes. *Front Aging Neurosci, 11*, 249. doi:10.3389/fnagi.2019.00249

Schonhaut, D. R., McMillan, C. T., Spina, S., Dickerson, B. C., Siderowf, A., Devous, M. D., Sr., . . . Rabinovici, G. D. (2017). (18) F-flortaucipir tau positron emission tomography distinguishes established progressive supranuclear palsy from controls and Parkinson disease: A multicenter study. *Ann Neurol, 82*(4), 622-634. doi:10.1002/ana.25060

Schrag, A., Ben-Shlomo, Y., & Quinn, N. P. (1999). Prevalence of progressive supranuclear palsy and multiple system atrophy: a cross-sectional study. *Lancet, 354*(9192), 1771-1775. doi:10.1016/s0140-6736(99)04137-9

Smith, R., Scholl, M., Honer, M., Nilsson, C. F., Englund, E., & Hansson, O. (2017). Tau neuropathology correlates with FDG-PET, but not AV-1451-PET, in progressive supranuclear palsy. *Acta Neuropathologica, 133*(1), 149-151. doi:10.1007/s00401-016-1650-1

Soleimani-Meigooni, D. N., Iaccarino, L., La Joie, R., Baker, S., Bourakova, V., Boxer, A. L., . . . Rabinovici, G. D. (2020). 18F-flortaucipir PET to autopsy comparisons in Alzheimer's disease and other neurodegenerative diseases. *Brain, 143*(11), 3477-3494. doi:10.1093/brain/awaa276

Steele, J. C., Richardson, J. C., & Olszewski, J. (1964). Progressive Supranuclear Palsy. A Heterogeneous Degeneration Involving the Brain Stem, Basal Ganglia and Cerebellum with Vertical Gaze and Pseudobulbar Palsy, Nuchal Dystonia and Dementia. *Arch Neurol, 10*, 333-359.

Tang, C. C., Poston, K. L., Eckert, T., Feigin, A., Frucht, S., Gudesblatt, M., . . . Eidelberg, D. (2010). Differential diagnosis of parkinsonism: a metabolic imaging study using pattern analysis. *Lancet Neurol, 9*(2), 149-158. doi:10.1016/S1474-4422(10)70002-8

Volter, F., Beyer, L., Eckenweber, F., Scheifele, M., Bui, N., Patt, M., . . . Brendel, M. (2022). Assessment of perfusion deficit with early phases of [(18)F]PI-2620 tau-PET versus [(18)F]flutemetamol-amyloid-PET recordings. *Eur J Nucl Med Mol Imaging*. doi:10.1007/s00259-022-06087-y

Whitwell, J. L., Jack, C. R., Jr., Parisi, J. E., Gunter, J. L., Weigand, S. D., Boeve, B. F., . . . Josephs, K. A. (2013). Midbrain atrophy is not a biomarker of progressive supranuclear palsy pathology. *Eur J Neurol, 20*(10), 1417-1422. doi:10.1111/ene.12212

Whitwell, J. L., Lowe, V. J., Tosakulwong, N., Weigand, S. D., Senjem, M. L., Schwarz, C. G., . . . Josephs, K. A. (2017). [(18) F]AV-1451 tau positron emission tomography in progressive supranuclear palsy. *Mov Disord, 32*(1), 124-133. doi:10.1002/mds.26834

Williams, D. R., de Silva, R., Paviour, D. C., Pittman, A., Watt, H. C., Kilford, L., . . . Lees, A. J. (2005). Characteristics of two distinct clinical phenotypes in pathologically proven progressive supranuclear palsy: Richardson's syndrome and PSP-parkinsonism. *Brain, 128*(Pt 6), 1247-1258. doi:10.1093/brain/awh488

Williams, D. R., Holton, J. L., Strand, C., Pittman, A., de Silva, R., Lees, A. J., & Revesz, T. (2007). Pathological tau burden and distribution distinguishes progressive supranuclear palsy-parkinsonism from Richardson's syndrome. *Brain, 130*(Pt 6), 1566-1576. doi:10.1093/brain/awm104

Williams, D. R., Holton, J. L., Strand, K., Revesz, T., & Lees, A. J. (2007). Pure akinesia with gait freezing: a third clinical phenotype of progressive supranuclear palsy. *Mov Disord, 22*(15), 2235-2241. doi:10.1002/mds.21698

Yoshiyama, Y., Higuchi, M., Zhang, B., Huang, S. M., Iwata, N., Saido, T. C., . . . Lee, V. M. (2007). Synapse loss and microglial activation precede tangles in a P301S tauopathy mouse model. *Neuron, 53*(3), 337-351. doi:10.1016/j.neuron.2007.01.010

Zalewski, N., Botha, H., Whitwell, J. L., Lowe, V., Dickson, D. W., & Josephs, K. A. (2014). FDG-PET in pathologically confirmed spontaneous 4R-tauopathy variants. *J Neurol, 261*(4), 710-716. doi:10.1007/s00415-014-7256-4

Zhao, P., Zhang, B., & Gao, S. (2012). 18F-FDG PET study on the idiopathic Parkinson's disease from several parkinsonian-plus syndromes. *Parkinsonism Relat Disord, 18 Suppl 1*, S60-62. doi:10.1016/S1353-8020(11)70020-7

Danksagung

An erster Stelle möchte ich mich bei meinem Betreuer Herrn Prof. Dr. Peter Bartenstein, bedanken, der auch neben dieser Promotionsarbeit seit mehr als zehn Jahren als ein außerordentlich guter Mentor immer ein offenes Ohr hatte. Hierbei bedanke ich mich vor allem für die hervorragende Betreuung und die extrem detaillierte wissenschaftliche Beratung im Rahmen dieser Promotion. Mein besonderer Dank gilt auch den Kolleginnen und Kollegen der Grundlagenforschung am Deutschen Zentrum für Neurodegenerative Erkrankungen sowie den klinischen Kolleginnen und Kollegen in der Neurologie, Psychiatrie, Neuropathologie und dem Institut für Schlaganfall und Demenzforschung an der LMU München, deren wissenschaftlicher und klinischer Input maßgeblich zu dieser Arbeit beigetragen hat. Stellvertretend sind insbesondere Prof. Dr. Johannes Levin, Prof. Dr. Günter Höglinger, Prof. Christian Haass, Prof. Dr. Jochen Herms, und Prof. Dr. Robert Perneczky zu nennen. Meinen Kollegen der Klinik und Poliklinik für Nuklearmedizin möchte ich für die ausgezeichnete wissenschaftliche und auch klinische Zusammenarbeit danken. Ein großes Dankeschön möchte ich auch meiner Arbeitsgruppe für translationale molekulare Bildgebung neurodegenerativer Erkrankungen widmen, denn ohne die stetige Mitarbeit hätte auch dieses Projekt lange nicht so viel Spaß gemacht. Ferner gilt den nationalen und internationalen Kooperationspartnern mein großer Dank, denn ohne die hervorragende Kooperation wäre der multizentrische Datensatz dieser Arbeit nicht realisierbar gewesen. Abschließend möchte ich mich ganz besonders bei meiner Frau Eva und meinen Kindern Paulina, Antonia und Tim bedanken, ohne die auch das Forschen nur halb so schön wäre.